2012-03-14

Buckling Failure Boundary for Cylindrical Tubes in Pure Bending

Daniel Peter Miller
Brigham Young University - Provo

Buckling Failure Boundary for Cylindrical Tubes in Pure Bending

Daniel Peter Miller

A thesis submitted to the faculty of
Brigham Young University
in partial fulfillment of the requirements for the degree of

Master of Science

Kenneth L. Chase, Chair
Carl D. Sorenson
Brian D. Jensen

Department of Mechanical Engineering

Brigham Young University

April 2012

ABSTRACT

Buckling Failure Boundary for Cylindrical
Tubes in Pure Bending

Daniel Peter Miller
Department of Mechanical Engineering
Master of Science

Bending of thin-walled tubing to a prescribed bend radius is typically performed by bending it around a mandrel of the desired bend radius, corrected for spring back. By eliminating the mandrel, costly setup time would be reduced, permitting multiple change of radius during a production run, and even intermixing different products on the same line.

The principal challenge is to avoid buckling, as the mandrel and shoe are generally shaped to enclose the tube while bending. Without the shaped mandrel, buckling will likely occur sooner, that is, at larger bend radii.

A test apparatus has been built for arborless bending. It has been used to determine the limits of bend radius, wall thickness, material properties, etc. on buckling. Key to the process is a set of moveable clamps, which grip the tube and rotate to produce the bend. A complex control system moves the clamps radially to maintain pure bending, without superimposing tension or compression.

A series of tests were performed to document the safe region of operation to avoid buckling. Charts have been created to assist the operator, as well as the design engineer, in determining the minimum bend radius. Similar tests will be required for each additional tube size, thickness, material, etc.

Keywords: Daniel Miller, pure bending, tube bending, buckling, failure boundary

ACKNOWLEDGMENTS

This research project would not have been possible without the support of many wonderful people. The author wishes to express his deepest gratitude first to his supervisor, Dr. Kenneth Chase, who offered the time and resources and patience that allowed this project to happen. His support, guidance, and mentorship were an invaluable resource. Gratitude is also due to Dr. Carl Sorenson whose guidance through difficult concepts was essential. Thank you for stepping in without reservation and assuming the advisor role through the final steps of this project. The support given from Miriam Busch and the rest of the Mechanical Engineering department faculty and staff was crucial to the continuance of this project. Also thank you to the department for providing the financial means and the facilities necessary to complete the work required.

The author would like to convey a special thanks to Joel Blumer, who spent countless hours running tests and creating visuals essential to giving a clear description of the phenomenon.

Finally, none of this would have been possible without the support, long patience, and constant understanding offered by my beloved wife. Thank you for your consistently positive words of encouragement through the many late nights and long hours this project required.

TABLE OF CONTENTS

LIST OF TABLES

LIST OF FIGURES

1 INTRODUCTION

Conventional bending of round tubing requires a shaped fixture, called an arbor, around which the tube is bent, by means of a similarly shaped forming tool called a shoe. Both the arbor and shoe are shaped to enclose the tube, which assures that the tube retains its circular cross section throughout the bending process, preventing cross section ovalization and buckling.

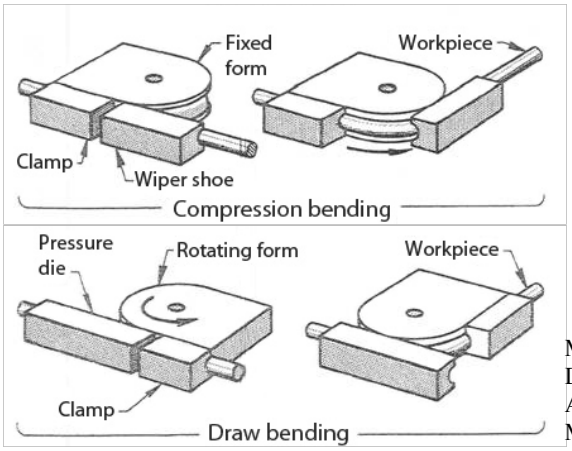

Metals Handbook
Desk Addition
American Society for Metals, 1985

Figure 1—1: Conventional methods of tube bending

Figure 1—1 illustrates two main types of conventional benders employing an arbor, with the main difference between them being the moving part. In compression bending, the clamp, arbor and end of tube are fixed and a part called a wiper shoe sweeps the tube around the form, sliding along it as it goes. In draw bending, the part is clamped to the arbor, and the clamp, arbor and end of the tube are pulled and rotated around the arbor's form. Both of these options require

the part to be clamped to the arbor and they require a die form that ensures the part is bending around the die.

Figure 1—2: Burr Oak's current coil forming machine

However, the arbor creates undesirable constraints on the process, preventing the conversion to modern, quick-changeover times, and flexible manufacturing. The arbor tooling and fixtures must be changed each time there is a change of tube size or bend radius. This is a major task, which shuts production down for an extended period of time. Large production runs are required in order to spread the cost of tooling changes over a large number of parts.

For specialty bends of finned tubes, such as refrigeration coils shown in Figure 1—3, the clamps do not make direct contact with the tubing due to the closely spaced fins supporting each tube. The arbor is therefore a smooth cylinder of the proper radius for the coil assembly. Without the formed mandrel and shoe, there is increased risk of the tube buckling. Although the fins provide some support to the tube cross section, buckling is still a critical issue. Bending forces must be applied through the fins, so there is also danger of deforming the fins, causing undesirable heat transfer properties.

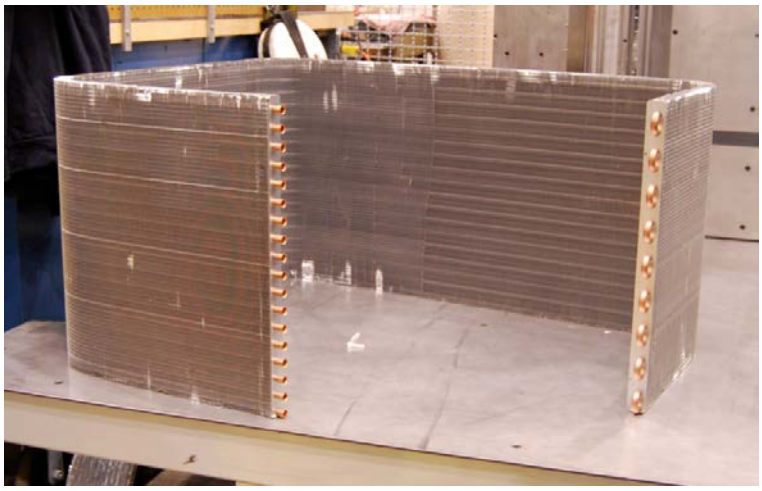

Figure 1—3: Bent refrigerator coils

To eliminate costly tooling changes for each tube size or bend radius, a process called arborless bending has been proposed. In contrast to conventional bending, an arborless bend is an air bend. An air bending process is shown conceptually in Figure 1—4. It is accomplished by clamping the ends of the tubing and leaving the center unsupported. A pure moment is applied to the tube by holding one clamp stationary, while rotating the other through the specified bend angle. Linear actuators attached to the clamps move each clamp axially to maintain a constant length of neutral axis. The clamps are the only hardware that must be changed, and they are only changed when a new outer diameter tube is bent. There are no parts that must be adjusted for different bend radius needs. For finned coils, the clamps are flat plates, capable of clamping any thickness coil. Arborless bending allows the bend to occur without any direct contact to the fins in the bend zone.

All of these features allow the user to take a single tube or coil and make multiple bends of multiple radii in succession without changing a single tool. The only change that is required is the input into the software interface that communicates to the machine what the final bend radius

will be. Lot size could then be reduced to a single part if required, or a single coil with multiple parallel bend radii.

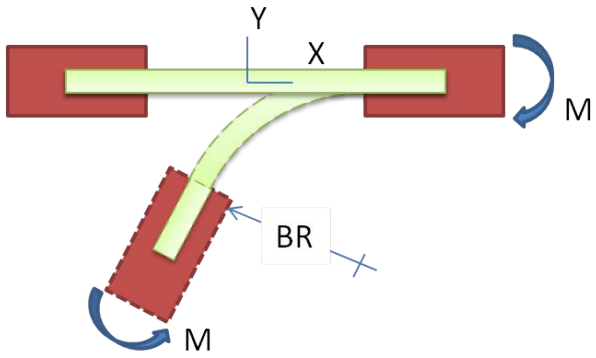

Figure 1—4: Air bending

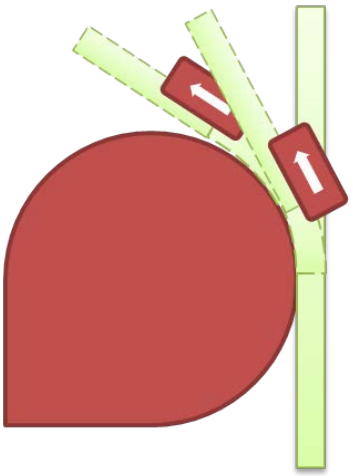

Figure 1—5: Arbor bending

1.1 Arbor Bending vs. Air Bending

In arbor bending, a single cross section is bent to the final radius, then the bend is advanced sequentially to the next cross section, as the shoe sweeps the length of the tube, as shown in

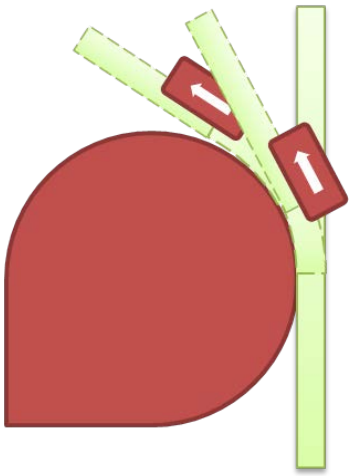

Figure 1—5. Arborless bending, on the other hand, maintains a uniform radius over the entire length between the clamps, smoothly decreasing the radius of all of the cross sections at once, until the final radius is reached over the full length simultaneously (see Figure 1—4: Air bending).

1.2 Brief History: How this Project Originated

This project began as a capstone design project in the mechanical engineering department at BYU. Originally it was intended to be finished in a school year through the work of a Senior Capstone design team. Their work was sponsored by Burr Oak Tools and was intended for production. Their goal was to produce a machine that would allow arborless bending of refrigerator coils, complete with fins, such as those shown in Figure 1—3, to be bent without damaging the coils or buckling the tubes. In addition, all deformation must be in the range

between initial plastic deformation and buckling failure. Working within known boundaries, users will be able to bend the tube as required, so understanding the failure boundary is essential.

By the end of the school year, the students had designed and built a functioning machine, but it experienced mechanical failure before any testing could be performed, which left work to be done in repairing and testing the machine, making the software user friendly, perfecting the control system, and understanding the mathematical models driving the deformation. The work of this thesis, funded by BYU, is essentially a continuation of their project, with the additional scholarly goal of understanding three-dimensional deformation of a thin-walled tube in pure bending and documenting the failure boundary.

In order to define a failure boundary, a laboratory apparatus has been assembled which places a pure bending load on a tube. With this system and the associated controls, a pure bending load is produced that will create the desired geometry. By bending the tube to a radius that buckles the tube, the critical factors associated with that buckling were determined.

1.3 Approach

Arborless bending has a number of positive features, including quick changeovers and lower invasive contact with the part. However, it permits ovalization of the cross-section, which leads to buckling. This buckling failure mode is a function of the tube size, wall thickness, bend radius, and material properties. In addition to designing a machine and a control system for air bending, the goal of this research is to establish a buckling failure boundary for hollow tubes in pure bending. In order to do this, empirical testing has been accomplished. Tubes of three different materials have been bent to buckling and the test results have been recorded. The three materials tested are aluminum, copper, and EMT steel. Three different dimensions of copper tubing have been tested. Two have the same outer diameter, but different wall thicknesses, and

the third has a similar wall thickness, but a larger outer diameter. The aluminum and EMT were only tested at one wall thickness and outer diameter. Overall, nearly 200 tests were performed allowing for a range of data to be analyzed.

Along with the empirical testing, a theoretical analysis of the strain that occurs in the tube is provided herein. This theoretical model, in combination with the empirical results, allows a failure boundary to be established as a function of tube diameter, wall thickness, bend radius, and material.

Throughout the following report, examples are given from the data. These examples all come from a single test, labeled Test #126, so that a detailed example can be used to demonstrate the whole testing process. The data on Test #126 is given in Table 1—1. The calculation example was given at 30° due to ovalization beginning at that time, which always preceded buckling.

Table 1—1: Data for Test #126

Test #	126
Tube ID #	Cu-5-90-08
Material	Copper, Alloy 122
Nominal Dimensions	¾" Type M
Tube Diameter	0.625"
Wall Thickness	0.027"
Buckling Angle (visual reading)	30° (shown as 60° on the protractor)

Angle	**Minor Axis (in)**	**Major Axis (in)**
10°	0.625	0.625

20°	0.624	0.627
30°	0.599	0.647
40°	0.409	0.770
50°-90°	Past buckling, Not recorded	Past buckling, Not recorded

1.4 Challenges

There were many challenges that stood in the way of understanding the failure boundary. Understanding one-dimensional column buckling was an important step, but studying three-dimensional effects on buckling was required in order to understand the effects of ovalization on tube buckling. This is due to the tri-axial strains that are applied to the tubing. Tri-axial strains are caused by the material deforming in three orthogonal directions: it deforms 1) axially, normal to the cross section, 2) transversely, within the cross-section, and 3) radially, through the wall thickness. These strains are shown Figure 1—6.

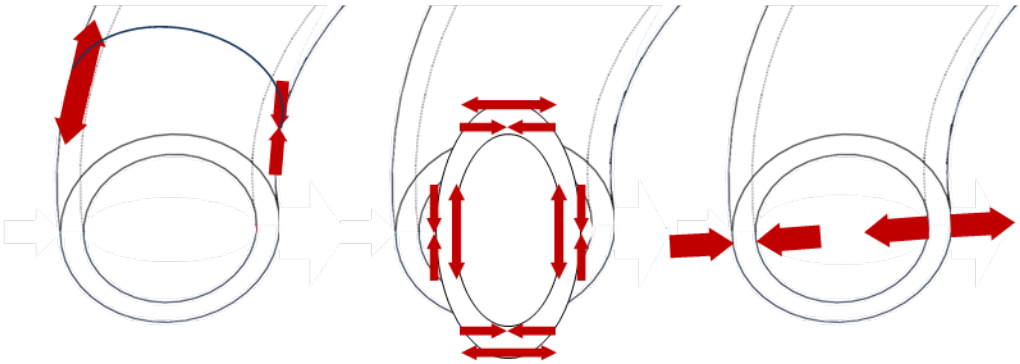

a) Axial **b) Cross Sectional** **c) Radial**

Figure 1—6: Tri-axial strain modes

Axial deformation is due to primary bending of the tube around an imaginary mandrel. The outer fibers are in tension and the inner are compressive, while the neutral axis experiences zero deformation. Cross sectional deformation results in the originally circular tube becoming

elliptical, which increases as the bend radius decreases. The third dimension of deformation is a change in the wall thickness due to biaxial strains of bending and ovalization. Each of these directions and their interactions need to be understood in order to know which will fail due to catastrophic buckling first. This is coupled with the fact that materials do not act linearly in the plastic range, so estimates were made to account for the nonlinearity.

Capturing and recording the data was difficult as well. Recording the strain throughout the bend would have been optimal, but because of the large deformations, strain gauges were not an option. Gathering load data from the voltage of the motor was considered, but the response data was too noisy to see any sort of trend. Because of these limitations, strain data was gathered through visual recording from above through the use of a web camera. The camera's limitations on focus, frames per second, and stability proved to be challenges when trying to record the point of buckling.

Ovalization data was recorded on a number of tests by pausing the bend process every ten degrees. Calipers were then used to measure the maximum and minimum axes of the ovalizing cross section.

1.5 Objective

The first objective of this thesis is to define the boundaries and necessary conditions to achieve an arborless bend with a pure bending moment load. The task includes providing the desired geometry of the specimen, while minimizing unnecessary ovalization and without causing buckling to occur. Process boundary limits were established by extensive testing to define the critical bend radius and bend angle combination where buckling occurs within the 90° final bend radius limit. A variety of tube diameters, wall thicknesses, and materials were tested.

This has all been done with a focus on industry needs. The failure boundary theory has been laid out in a form that is usable for a design engineer or manufacturing process personnel.

The secondary objective of this thesis is to prototype a machine that achieves arborless bending without buckling. The Capstone team previously provided a nearly functional machine, but much work was required to get the machine to function consistently and without mechanical failure. This work included creating clamps to fit the tubing, fixing software issues, and ensuring that the linear actuators drive at the appropriate rate at each stage of the bend test.

2 LITERATURE SEARCH

2.1 Standard Mechanics of Materials Equations

Standard buckling, pure bending, neutral axis theory, and curved beam analysis equations can be found in many standard text books, but are referenced herein from three common texts, namely Robert Norton's *Machine Design: An Integrated Approach* (Norton 2006), James Gere's *Mechanics of Materials* (Gere 2001), and Richard Budynas' *Mechanical Engineering Design.* They lay the foundation to the rest of the analysis approach presented.

2.2 Bending Tubing

Based on the basics of the mechanics of a material in pure bending set forth by Datsko (Datsko, 1966), a better understanding of the maximum strain to failure can be realized. Also from Datsko, it is established that the ultimate engineering strain ($\boldsymbol{\varepsilon_u}$) is equal to the exponent m in the true stress-strain Equation (2—1).

$$\sigma = \sigma_0 \varepsilon^m \qquad \textbf{(2—1)}$$

This allows us to calculate the maximum bend radius based on failure due to the ultimate strain. Datsko also dictates a more descriptive notation for the stresses and strains in a system where strain occurs in all three dimensions, clearing up some of the ambiguity in the system. (Datsko 1966)

Calladine's additions to the subject include establishing the equations for the critical buckling moment, curvature, and strain for a part, considering both the bifurcation point, which splits the tube at one main buckling point, versus corrugated buckling at multiple points, also called wrinkling. This reading is applicable in that our test follows the non-corrugated function, but helps us understand that the other exists. (Calladine 1974)

Brazier observed that buckling at a single location on a tube corresponds to a certain point on the moment-curvature plot. This behavior is called the Brazier Buckling phenomenon. He also established equations to predict the ovalization displacement along the cross section and the process of finding the maximum point on the moment-versus-curvature plot. This point defines the point where buckling occurs. (Brazier 1927)

Korol showed empirically that Brazier's work was valid by using a moment-curvature plot using original data to show where buckling occurred. (Korol 1978)

K. Pan and K. A. Stelson cite Von Karman's research in establishing that ovalization occurs due to a continual change of direction of the forces parallel to the center line or neutral axis, thus describing ovalization and what brings it about. (Pan and Stelson 1995)

Finally, P. Cheng of MIT published a thesis on pure bending and compression bending of tubes containing composite support structures within the outer shell of the tube. Her discussion of pure bending is invaluable for this project, as it not only brings much of the previous research together on tube bending and buckling, but she also corrects some of the ovalization equations and correcting some typographical errors in the equations set forth by Karam and Gibson and Calladine. (Cheng 1996)

Wang and Cao offer a buckling failure boundary theory for an arbor bend on a rotary draw bending machine. Their theory has been used as a pattern of a failure boundary. The failure

boundary shown herein for arborless buckling was created using a similar set of axes. (Wang et al. 2001, 430)

Although pure bending of hollow structures has been covered theoretically by Cheng and others, none of the research described above has been applied to an arborless bender designed for production. Empirical data must be established in order to know where the moment-curvature buckling condition occurs in relation to the arborless machine setup. Ovalization of the tube in this configuration needs to be understood along with moment-curvature values in relation to the bend angle. Through empirical data, as well as mathematical models, these relationships have been investigated and a theoretical and empirical failure boundary for arborless bending has been established. This data is useful to understand the details of the moment's effect of the buckling, although a different approach was taken here.

3 ANALYTICAL MODEL

3.1 Pure Bending Explained

Pure bending is defined as flexure of a beam under a pure bending moment. Pure bending only occurs in regions of a beam where the shear force is zero. This is because the shear force is defined as the derivative of the moment along the beam.

$$V = \frac{dM}{dx} = 0 \quad \text{If } M = \text{Constant} \qquad \textbf{(3—1)}$$

This is in contrast to non-uniform bending, which occurs in the presence of shear forces. When a beam is subject to a pure moment the longitudinal axis is deformed into a curve with a constant radius of curvature along the whole axis, causing it to form an arc of a circle. (Gere 2001)

Putting a beam in pure bending causes the beam to be in tension on its outer edge and compression on its inner edge. Cross sections of this beam are assumed to remain plane if the moment load is pure, and the cross sections are symmetric about the Y or Z-axis, so throughout the calculations that follow, this assumption will be held. In pure bending, plane cross sections rotate about an axis perpendicular to the XY plane as shown in Figure 3—1.

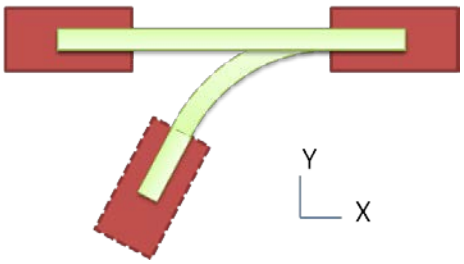

Figure 3—1: Bending coordinate axis

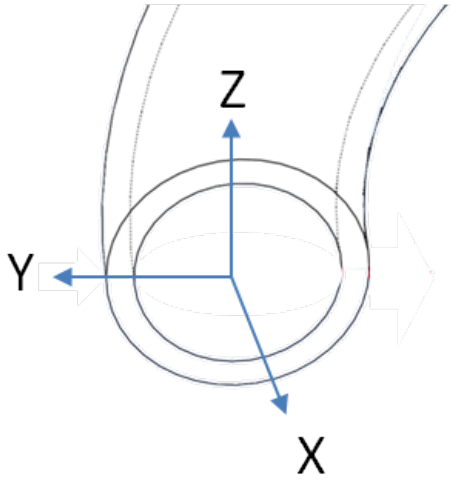

Figure 3—2: Coordinate axis on tube cross-section

This situation requires that a surface between the inner and outer curve of the bent material be free from loading. The load-free surface intersects the cross section, forming an axis called the Neutral Axis of the cross section. The bending strain occurring anywhere in the cross section is proportional to its distance from the neutral axis. For small strains, the value can be found through Equation (3—2),

$$\epsilon_x = -\frac{y}{\rho} \qquad \textbf{(3—2)}$$

where **y** is the distance from the neutral axis and **ρ** is the radius of curvature of the beam's neutral axis. This equation shows that the strain varies linearly with Y across the cross section, a theory that is central to the work that follows. This is the case regardless of the shape of the

stress-strain curve of the material. Finally, longitudinal strains in the beam also produce transverse strains due to Poisson's ratio.

3.2 Locating the Neutral Axis

The neutral axis of a beam is defined as the intersection of the no-load plane and the cross-section in question. For small strains, $y_{NA} = \bar{y}$, so the distance from the neutral axis is given in the following equations as $y - \bar{y}$. It can be found by setting the longitudinal force acting on the cross section to zero, or, where the strain is zero. This is shown through Equation (3—3).

$$\int_A \sigma_x dA = -\int_A \frac{E\,y}{\rho} dA = 0 \qquad \textbf{(3—3)}$$

By dividing out the constants **E** and **ρ**, Equation (3—3) can be simplified to: (Gere 2001)

$$\int (y - \bar{y}) dA = 0$$

$$\int_A y\, dA = \bar{y} A$$

$$\bar{y} = \frac{\int y dA}{A} \qquad \textbf{(3—4)}$$

3.3 Curved Beam Theory

Most structural applications employ straight beams, for which the deflections are kept small to avoid exceeding the elastic limit, causing permanent deformation. If the beam has initial curvature under no load, or if a forming operation is performed to produce permanent deformation, then curved beam analysis must be applied.

Understanding the strains in a curved beam requires a similar process to understanding strains in a straight beam. In order to do this analysis, six conditions must be maintained (Budynas et al. 2011):

1. The applied load is distant from the segment analyzed
2. Loading occurs along a plane of symmetry
3. Plane sections remain plane and perpendicular to the neutral axis
4. The material is homogeneous and obeys Hooke's law
5. Stresses remain below the elastic limit and the deflection analyzed is small
6. Pure bending is applied to the beam with no axial or shear loads

The key differences with the process given herein are that the neutral axis will no longer be coincident with the centroidal axis, as it is with straight beams, and strains will no longer be below the elastic limit. The neutral axis is initially shifted toward the center of curvature by a distance $\boldsymbol{e}$ from the centroidal radius of curvature. The neutral axis can be found through Equation (3—5)

$$R_{NA} = \frac{A}{\int \frac{dA}{r}} \qquad \textbf{(3—5)}$$

where $\boldsymbol{r}$ is the radius of curvature of the differential area $\boldsymbol{dA}$. The evaluation of this integral for our circular beam cross section is found in 0.

3.4 Standard Buckling Model: Euler's vs. J.B. Johnson's Equations

Standard buckling is a failure mode that occurs commonly in long slender beams subjected to a compression load along the axis of the beam. Buckling causes an axially loaded beam to collapse, damaging the supported structure. A similar behavior applies to our tube-bending process in that a localized buckle occurs when the tube is bent beyond a limiting

compressive strain. Here, classical column buckling is described in order to increase understanding of the failure modes of the tube.

(Gere 2001) Buckling of a column occurs when long, slender structural members are loaded axially. Column buckling can also occur locally, any time a load path is concentrated in compression along a section of a surface. Although the bending machine used does not apply an axial load, due to the nature of pure bending, there are areas where compression results in a concentrated load line, which can cause buckling. Buckling can be better understood by looking at an idealized beam, shown in Figure 3—3.

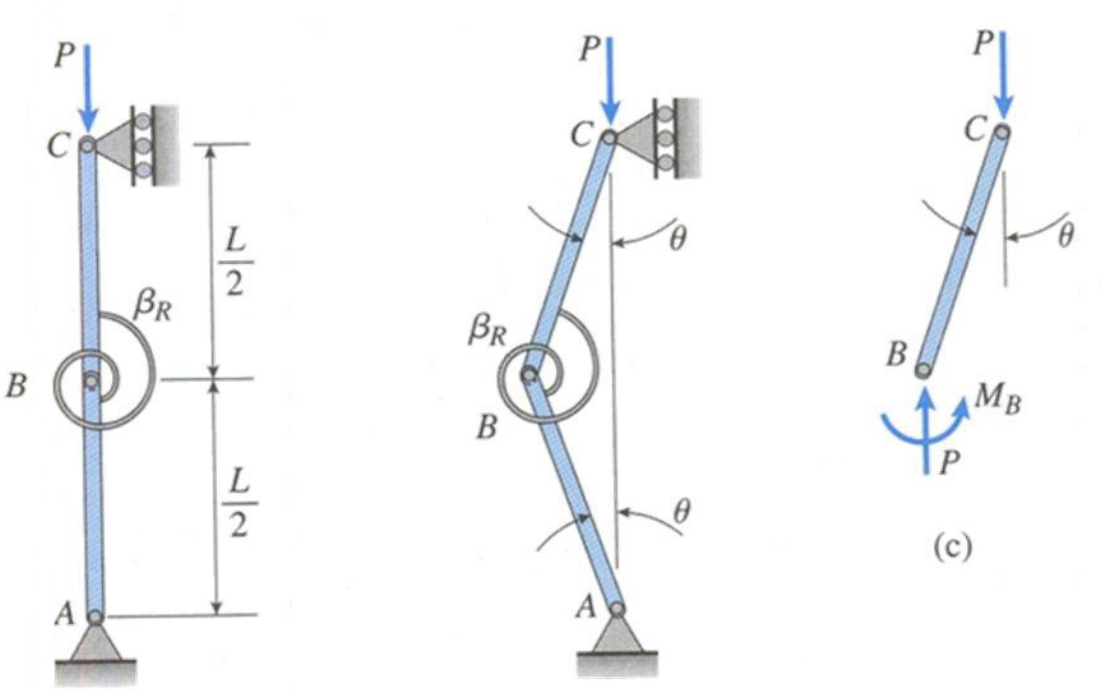

Figure courtesy of Gere text (Gere 2001)

Figure 3—3: Idealized column with buckling loads

If the axial force ***P*** is relatively small, the action of a restoring moment will cause the structure to return to its initial straight position. If the axial force reaches a crucial point, it will overcome the

restoring moment and render the structure unstable, causing it to collapse by lateral buckling. This critical load is found by considering the entire structure as a free body.

An ideal column is one with no impurities and a constant cross section of a material that follows Hooke's law. Using an ideal column, as shown in Figure 3—4, we see that the only stresses are the uniform compressive stresses.

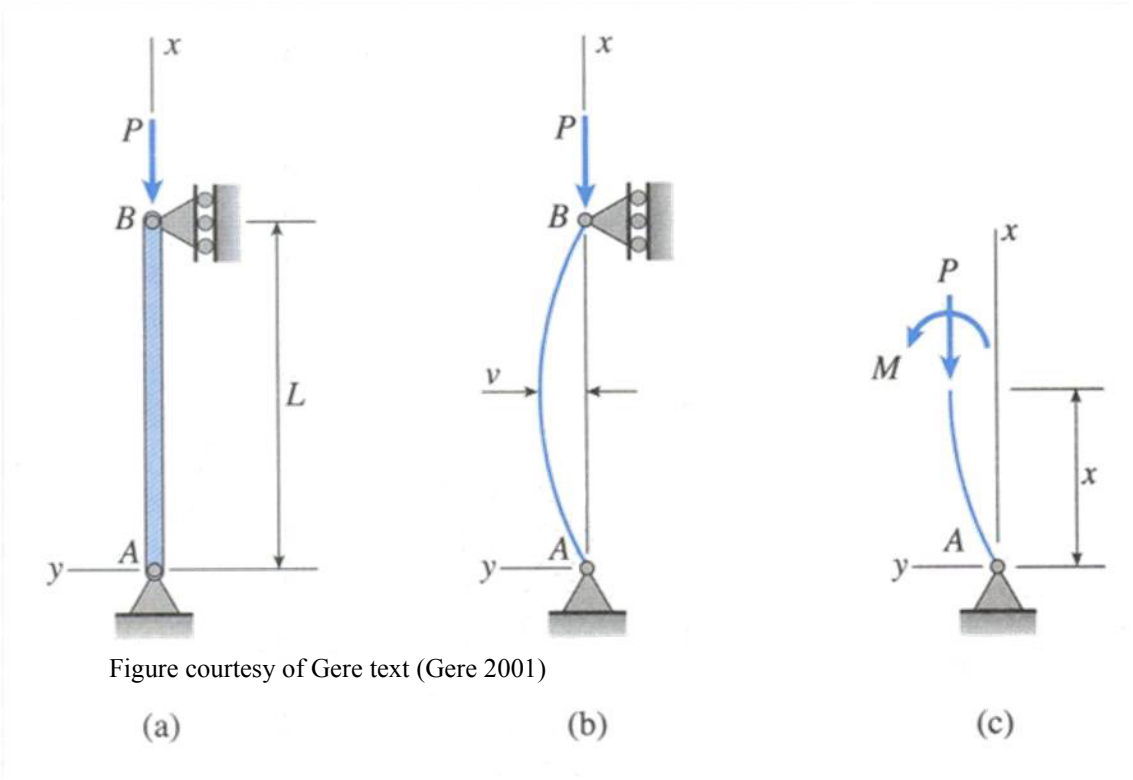

Figure courtesy of Gere text (Gere 2001)

Figure 3—4: Idealized column with compressive load

If this is the case, the column is in stable equilibrium: it will return to the straight position after a disturbance. If the load **P** is increased, eventually a critical load will be reached in which the column becomes unstable. As this case occurs, any side load or deformity in material on the column will allow the beam to fail by buckling. For a column with pinned ends, the predicted critical load is found through Equation (3—6) (Gere 2001).

$$P_{cr} = \frac{\pi^2 EI}{L^2} n \qquad \textbf{(3—6)}$$

where **n** is a correction factor, between 0.25 and 4, which accounts for different end supports. This mode of buckling is called "Euler buckling" and occurs under idealized elastic conditions. A non-dimensional ratio related to this mode of buckling is called the slenderness ratio. The slenderness ratio is defined as

$$Slenderness\ ratio = L/r \qquad \textbf{(3—7)}$$

where **L** is the axial length of the column. The variable **r** is the radius of gyration, defined as

$$r = \sqrt{\frac{I}{A}} \qquad \textbf{(3—8)}$$

where **I** is the moment of inertia for the principal axis about which buckling occurs. The slenderness ratio depends only on the dimensions of the column. A long slender column will have a high slenderness ratio, and a short stocky column will have a low slenderness ratio.

There is another mode of buckling that occurs under plastic stress conditions, which follows the J.B. Johnson buckling curve. This curve is used when the slenderness ratio is less than the slenderness ratio found by solving Equation (3—9). This condition occurs when the column is on the shorter end of the spectrum with a larger diameter.

$$(S_r)_1 = \pi \sqrt{\frac{2E}{S_{yc}} n} \qquad \textbf{(3—9)}$$

$$If\ S_r > (S_r)_1 \quad Then\ Euler\ curve$$

$$If\ S_r < (S_r)_1 \quad Then\ J.B.Johnson\ curve$$

where S_{yc} is the compressive yield strength of the column's material and n denotes the end condition of the column.

At the point where the slenderness ratio is exactly equal to $(S_r)_1$ in Equation (3—9), the Euler curve and the J.B. Johnson curve are tangent, creating the continuous curve shown in

Figure 3—5.

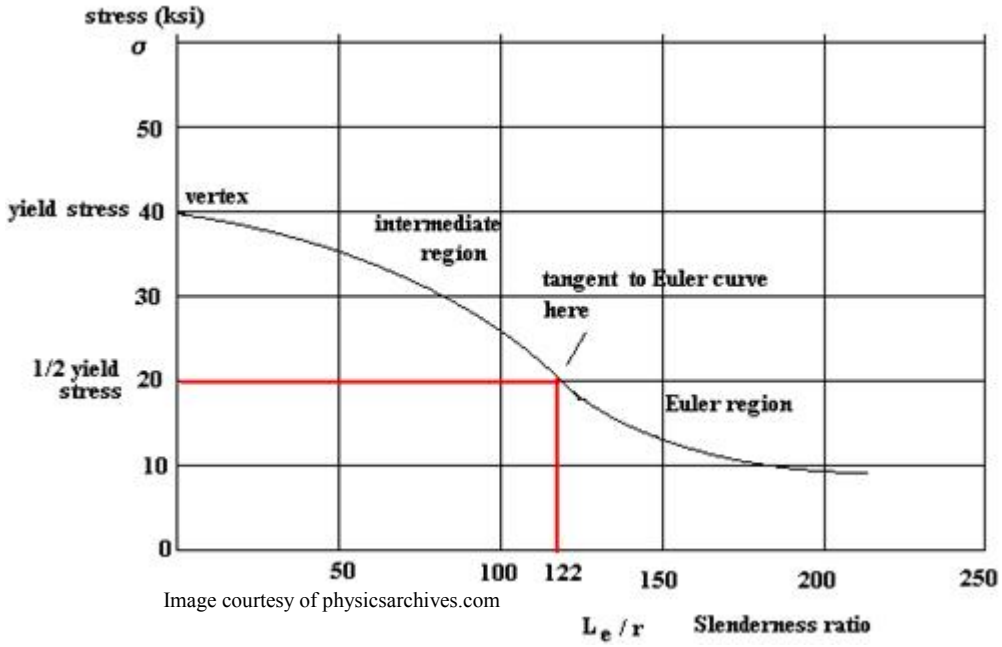

Figure 3—5: Euler and J.B. Johnson curve

The critical buckling load based on a cross sectional area with a slenderness ratio less than the limit can be found using the J.B. Johnson equation, Equation (3—10).

$$\frac{P_{cr}}{A} = S_{yc} - \frac{1}{E}\left(\frac{S_{yc}S_r}{2\pi}\right)^2 \qquad \textbf{(3—10)}$$

3.5 Ovalization Generally

Ovalization is the term given to the cross section deformation a tube goes through as it is bent into an arc. The cross section has been shown to change from a circular shape to a noticeable oval, whose minor axis is contracting continuously until buckling occurs. It is caused by the tri-axial forces applied to the material due to its geometry. Buckling, in the case of a

tubular member, results in the inside portion of the cross section collapsing inward, causing the member to fold in a sharp bend.

3.6 Strain Equations

In order to orient the reader, several color-coded visuals have been created. The specimen is shown with a blue outer and inner surface and a red material that can be seen when a cross section view is taken (Section A-A). The tubular test specimen is made of one type of material with consistent properties throughout. The specimen is shown in these visuals without the clamps attached, but it is important to note that the bend radius used in the calculations is measured to the inner edge of the clamp. This can be seen best in Figure 3—6.

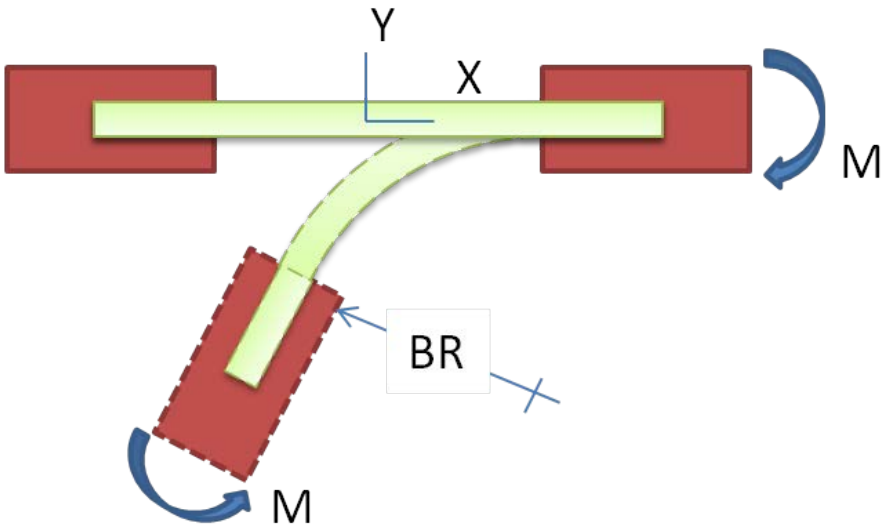

Figure 3—6: Bend radius measured to the inner edge of the clamp

The rest of the images show the bend radius as the South point on the tube. This is a close estimate, and will keep the images simpler for the reader allowing orientation to be clear. This specimen is depicted in Figure 3—7 and others with this adjustment.

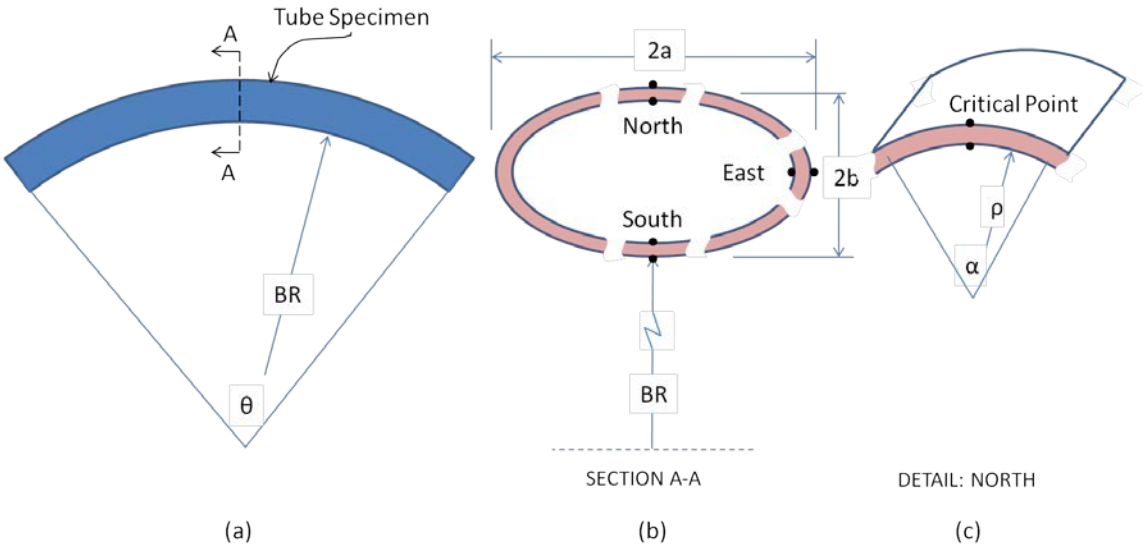

a)Bending plane **b)Cross-section plane A-A** **c) Detail view of critical point**

Figure 3—7: Tube in bending

The goal of the analysis is to accurately determine and ultimately predict the failure location of a tube bent by a pure bending moment. This is accomplished through a study of the geometry of the bend and the cross section and correlating it to the instantaneous bend radius. This information is then used to determine the principal strains at the inner and outer walls of three critical points on the tube, shown in Figure 3—7, which will be defined as North, East and South, the fourth, or West, being a mirrored case and equivalent to East. This section will lay out the process for calculating the strain and safety factor of the load case from information taken from a bend test.

3.6.1 Axial Bending

This process is described as if the process is stopped and the analysis completed ,while the specimen sits in the machine. Cross section measurements are taken during a pause of the test, and used to calculate the strains during analysis of the data after the test.

To find the strains that occur due to axial bending, the intended final bend angle and bend radius are input into the machine and separately recorded. This is to determine the proper length specimen to achive the desired angle and radius. Also, the wall thickness and outer diameter of the tubing are recorded. This information is then used to find the inner and outer radius of the undeformed cross section of the tubing. These dimensions are noted as R_1 and R_2 in Figure 3—8.

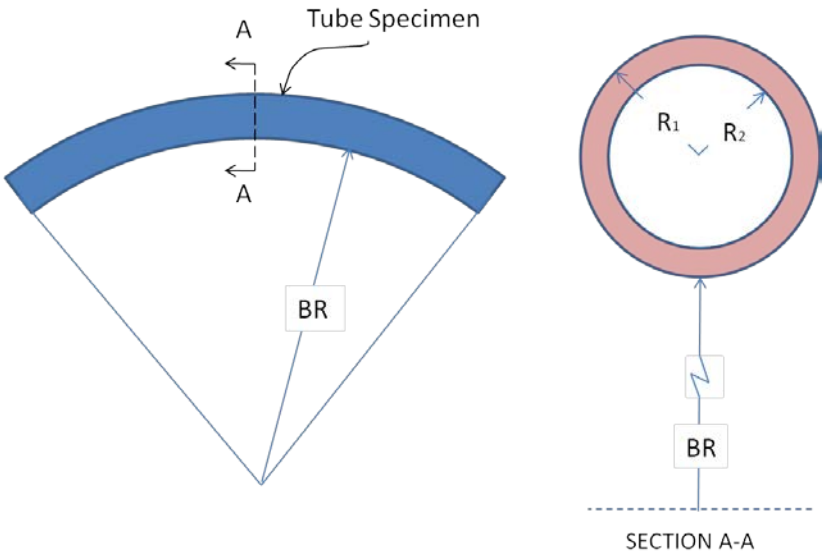

Figure 3—8: Bend radius and cross-section inner and outer radii

As the test is performed, the apparatus is paused every ten degrees. Calipers are used during each pause to measure the major and minor axes of the elliptical cross-section of the tube,(**2a** and **2b,** respectively) near the expected buckling point and the instantanious bend angle **θ** is recorded. The major and minor axes are visualized in the section view of Figure 3—9. The inner bend radius of the tube, BR, is shown in both views without the clamps. It is important to remember that the bend radius, for calculation purposes, is measured to the inside of the clamps, as mentioned above and shown in Figure 3—6.

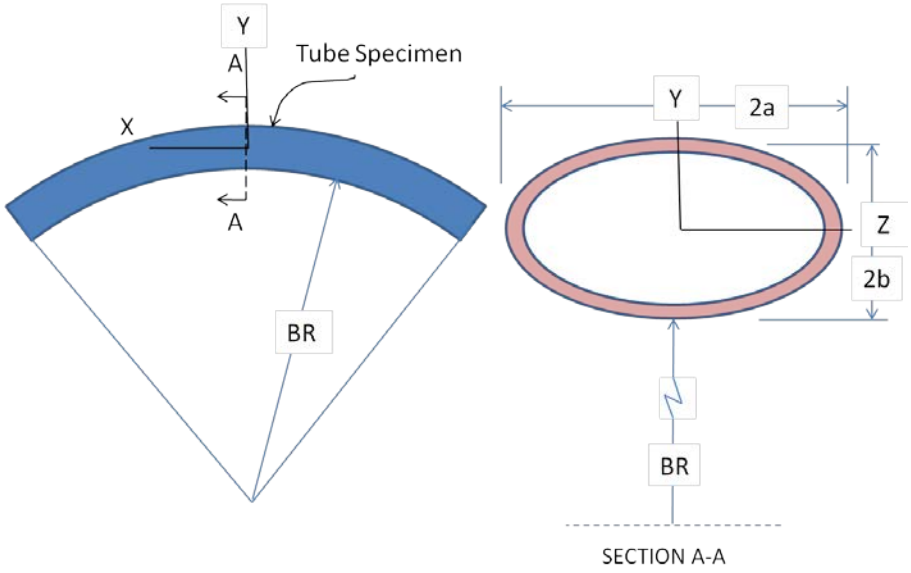

Figure 3—9 : Bend radius and cross-section oval dimensions a and b

Note that the offset, **U**, between the axis of the rotational motor and the centroidal axis of the tubing is recorded before the test is run. This is done by measuring half the distance between the clamp jaws, because the inner side of the clamp jaw is aligned with the axis of the rotational motor as shown in Figure 3—10. The choise of bend axis was selected as a well defined reference surface. Since tubes of different sizes are to be tested, it would be inconvenient to adjust the test apparatus to align with the centerline of each specimen. The offset, **U**, was accounted for in the calculations and included in the clamp motions to keep the neutral axis length constant during the test. When a fixture is used, the inside bend radius is difficult to measure. Alternatively, it is convenient to use the inside edge of the fixture as the reference point, instead of the tube.

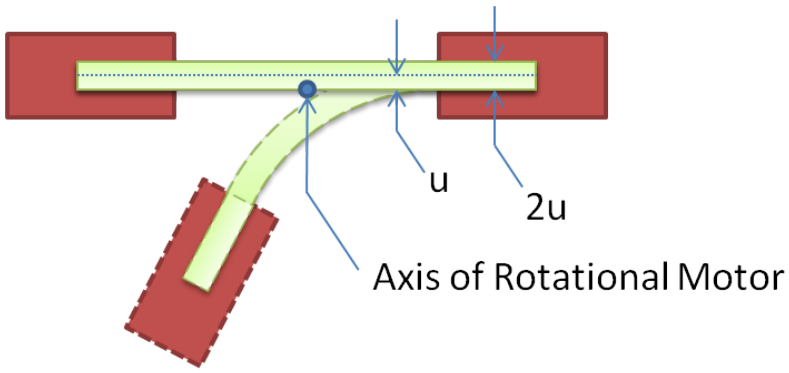

Figure 3—10: Rotational axis offset (u)

The final centroidal radius, the axis of the tube, is then found based on the final desired bend radius. This is simply done by adding the fixture offset, **U**, to the desired final bend radius BR_f. Equation (3—11) can be used for calculating all the centroidal radii throughout the test.

$$\bar{r}_i = BR_i + u \tag{3—11}$$

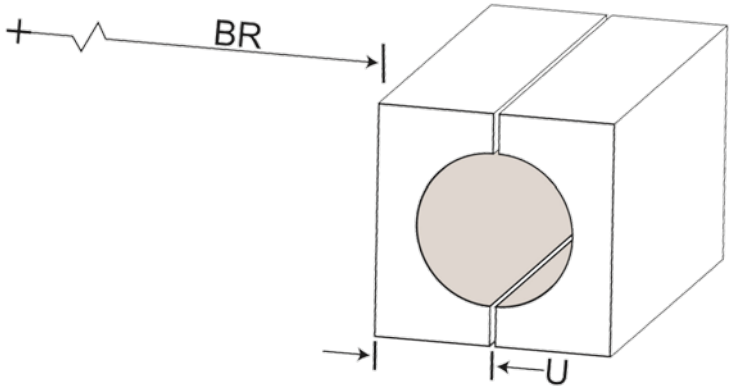

Figure 3—11: Centroidal radius, based off the fixture

Once this data is recorded, the radius of the neutral axis at the final step of the test is calculated using Equation (3—12). The derivation of the equation governing this shift has been included in 0.

$$R_{NA_f} = \frac{R_1^2 - R_2^2}{2\left(\sqrt{\left(\bar{r}_f^2 - R_2^2\right)} - \sqrt{\left(\bar{r}_f^2 - R_1^2\right)}\right)} \tag{3—12}$$

Due to ovalization being a local phenomenon, and minor prior to the onset of buckling, the equation above assumes that the cross section is circular at the final bend angle. This simplification will give adequate results, but future work may be done in this area.

Using the final angle and the final neutral axis radius, the length of the neutral axis at its final intended postion can be found using the arclength equation. This length is set as the initial length between the clamps and should be held constant throughout the test.

$$L_{NA_f} = R_{NA_f} * \theta_f \qquad \textbf{(3—13)}$$

The initial length between the clamp and the center of rotation is half the length of the final neutral axis. This dimension is shown as distance ***a*** in Figure 3—12

$$a = \frac{L_{NA_f}}{2} \qquad \textbf{(3—14)}$$

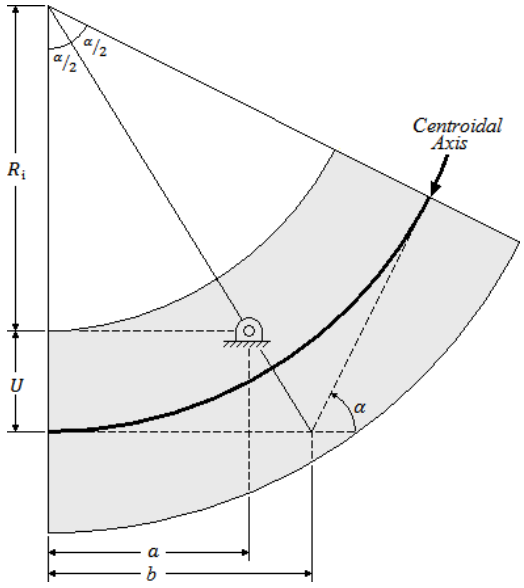

Figure 3—12: Distance from clamp to center of rotation

In order to find the bend radius for the intermediate steps of the test, the new distance between the rotational axis and the clamp must be found. To find this distance, it is first assumed

that there is no clamp adjustment. Using the geometry in Figure 3—12, a new value for the bend radius is found.

$$\mathrm{BR}_i = \frac{\mathrm{a}}{\mathrm{Tan}\left(\frac{\theta_i}{2}\right)} \quad \textbf{(3—15)}$$

Using this bend radius, a new centroidal radius is calculated using Equation (3—11). This new centroidal radius is used in Equation (3—12) to find a candidate neutral axis radius. This neutral axis radius is too long, as can be shown by finding the arclength of this neutral axis with the angle θ_i. This length will be different from the initially calculated length of the neutral axis, and so the clamps must be adjusted. This adjustment, Δa, is simply half the difference between what the neutral axis radius is calculated as, and what it should be.

$$\Delta\mathrm{a} = \frac{\mathrm{L}_{NA,f} - L_{NA,candidate}}{2} \quad \textbf{(3—16)}$$

This Δa is the clamp adjustment, and is added to the origional distance between the rotation point and the clamp.

$$\mathrm{a}_i = \mathrm{a} + \Delta\mathrm{a}_i \quad \textbf{(3—17)}$$

Using this new value, a new bend radius is calculated for the given angle using Equation (3—15), which is then used to find a new centroidal radius from Equation (3—11). This new centroidal radius is used to calculated a new neutral axis radius using Equation (3—12). This new neutral axis radius forms an arc with the angle being analyzed whose arclength is equal to the length of the final angle neutral axis.

To check this solution, the constant arclength is compared at two known points using Equation (3—18). This neutral axis length can be shown to be very close, within 0.004” at 30° with an intended bend radius of 5”. If a more precise value is desired, an interative solution can be used.

$$R_{NA_i} = \frac{R_{NA_f}\theta_f}{\theta_i} \tag{3—18}$$

By taking the difference of this newly calculated neutral axis radius and the centroidal radius at each pausing angle the neutral axis shift, **e**, is found.

$$e_i = \bar{r}_i - R_{NA_i} \tag{3—19}$$

Next the distance, **y**, between the the neutral axis and the point of maximum bending stress is found. For example, the point on the outer sides of the bend are shown below with Equation (3—20) and Figure 3—13.

$$y_{North} = b_i + e_i$$
$$y_{South} = b_i - e_i \tag{3—20}$$

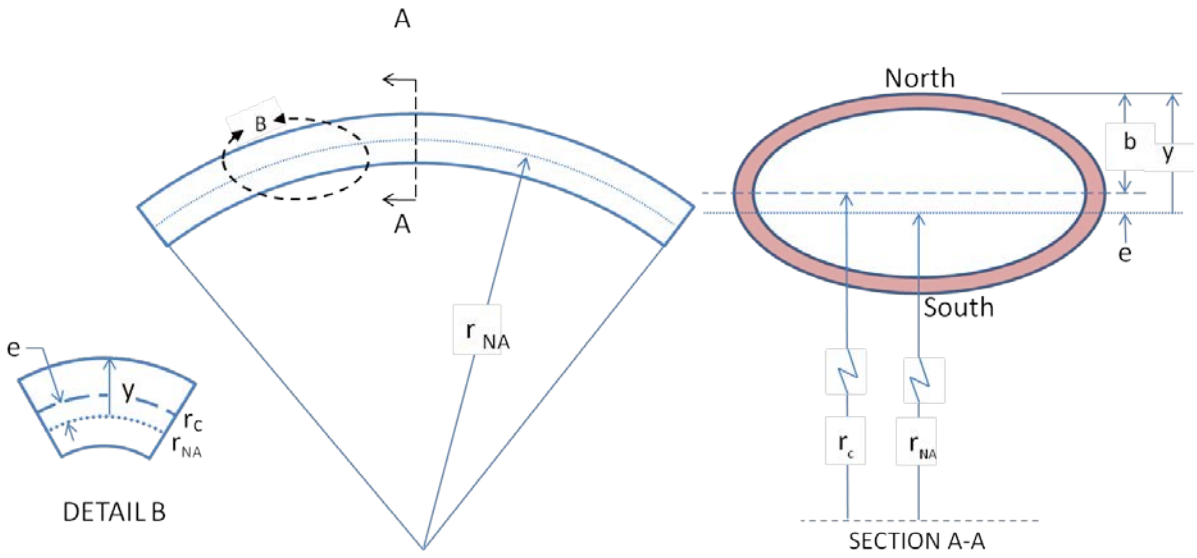

Figure 3—13: Dimensions within the cross section

The change in axial strain in the tube is then calculated using the change of angle, since the last measurement was taken.

$$\Delta\epsilon = \frac{y * \Delta\theta}{(r_{NA} + y) * \theta_i} \tag{3—21}$$

An example of this process is given for the South point of Test #126 as it reaches a 30° bend angle. The first step is to find the inner and outer radii of the cross-section. These values can be found using the wall thickness and measured outer diameter as shown:

$$R_1 = \frac{OD}{2} = \frac{0.625}{2} = 0.3125$$

$$R_2 = R_1 - t = 0.3125 - 0.0270 = 0.2855$$

Using the intended bend radius of 5 inches, the final centroidal radius is found using Equation (3—11)

$$\bar{r}_f = 5 + 0.7155 = 5.7155$$

The final expected neutral axis can then be found using Equation (3—12)

$$R_{NA_f} = \frac{0.3125^2 - 0.2855^2}{2\left(\sqrt{(5.7155^2 - 0.2855^2)} - \sqrt{(5.7155^2 - 0.3125\text{^}2)}\right)} = 5.7077$$

This radius, at 90°, gives the length of the neutral axis that is intended to stay constant throughout the bend.

$$L_{NA_f} = 5.7077 * \left(90° * \frac{\pi}{180°}\right) = 8.9656$$

and the distance between the point of rotation and the clamp at the starting position is

$$a = \frac{8.9656}{2} = 4.4828$$

This value is used to find the candidate bend radius using Equation (3—15)

$$BR_{30°} = \frac{4.4828}{Tan\left(\frac{30°}{2}\right)} = 16.7300$$

Using Equation (3—11), a candidate centroidal radius is found

$$\bar{r}_i = 16.7300 + 0.7155 = 17.4455$$

This centroidal radius candidate is used to find a candidate neutral axis radius

$$R_{NA,30^\circ} = \frac{0.3125^2 - 0.2855^2}{2\left(\sqrt{(17.4455^2 - 0.2855^2)} - \sqrt{(17.4455^2 - 0.3125\text{^}2)}\right)} = 17.4429$$

At 30°, this neutral axis radius creates a length of the neutral axis that is longer than the neutral axis length at the final point, which is supposed to be unchanging.

$$L_{NA,30^\circ} = 17.4429 * \left(30^\circ * \frac{\pi}{180^\circ}\right) = 9.1331 > 8.9656$$

This means that the clamps must be moved to adjust for this difference. The distance they must move is found using Equation (3—16)

$$\Delta a = \frac{8.9656 - 9.1331}{2} = 0.08376$$

This change in distance must be added to the intial distance between the clamp and the axis of rotation.

$$a_i = 4.4828 + 0.08376 = 4.3990$$

Plugging this value into Equation (3—15), a more accurate bend radius is calculated.

$$BR_{30^\circ} = \frac{4.3990}{\text{Tan}\left(\frac{30^\circ}{2}\right)} = 16.4174$$

This bend radius allows a more accurate centroidal radius to be calculated using Equation (3—11).

$$\bar{r}_i = 16.4174 + 0.7155 = 17.1329$$

This centroidal radius, applied to the neutral axis radius equation, Equation (3—12), results in a more accurate netural axis radius.

$$R_{NA,30^\circ} = \frac{0.3125^2 - 0.2855^2}{2\left(\sqrt{(17.1329^2 - 0.2855^2)} - \sqrt{(17.1329^2 - 0.3125\text{^}2)}\right)} = 17.1303$$

This neutral axis radius results in an arclength, which can be found using Equation (3—13)

$$L_{NA,30^\circ} = 17.1303 * \left(30^\circ * \frac{\pi}{180^\circ}\right) = 8.9694$$

This neutral axis radius is approximately three times the final neutral axis radius calculated, which is as expected. This can be proven by comparing the neutral axis length at 30° and at 90°.

$$L_{NA} = R_{NA_f} * \theta_f \approx R_{30^\circ} * \theta_{30^\circ}$$

$$L_{NA} = 8.96557 \approx 8.96938$$

$$error = 8.96557 - 8.96938 = .00382$$

The neutral axis shift can be found at this point by taking the difference of the radius of the neutral axis and the centroidal radius.

$$e = \bar{r}_{30^\circ} - \mathrm{R}_{\mathrm{NA}_{30^\circ}} = 17.1329 - 17.1303 = 0.002615$$

At the South point, the Y values are as follows:

$$Y_{South,outer} = -b - e = -0.3235 - 0.002615 = -0.3261$$

$$Y_{South,inner} = Y_{South,outer} + t = -0.3264 + 0.0270 = -0.2991$$

The change in strain can then be found as shown

$$\Delta\epsilon_{South,outer,30^\circ} = \frac{y_{South,outer} * \Delta\theta}{(r_{NA,30^\circ} + y_{South,outer}) * \theta_{20^\circ}} = \frac{-0.3261 * 10^\circ}{(17.1303 - 0.3261) * 20^\circ} = -0.00635$$

$$\Delta\epsilon_{South,inner,30^\circ} = \frac{y_{South,inner} * \Delta\theta}{(r_{NA,30^\circ} + y_{South,inner}) * \theta_{20^\circ}} = \frac{-0.2991 * 10^\circ}{(17.1303 - 0.2991) * 20^\circ} = -0.00582$$

This change in strain is then added to all the previous strains to get the following total strain at the location.

$$\epsilon_{South,outer,30^\circ} = \sum_{0^\circ}^{30^\circ} \Delta\epsilon$$

To simplify this process, below is a step-by-step simplified guide through this process:

1.	Set $\boldsymbol{BR_f}$ and $\boldsymbol{\theta_f}$	
2.	Measure the tube OD and ID in order to gather $\boldsymbol{R_1}$and $\boldsymbol{R_2}$	
3.	$\bar{\mathbf{r}}_\mathbf{i}$ for the final step (Eq. (3—11))	$\bar{r}_f = BR_f + u$
4.	$\mathbf{R_{NA}}$ for the final step (Eq. (3—12))	$R_{NA} = \frac{R_1^2 - R_2^2}{2\left(\sqrt{(\bar{r}^2 - R_2^2)} - \sqrt{(\bar{r}^2 - R_1^2)}\right)}$
Assume no clamp adjustment		
5	Final neutral axis length (Eq. (3—13))	$L_{NA_f} = R_{NA_f} * \theta_f$
6	Distance from axis of rotation to clamp edge (Eq. (3—14))	$a = \frac{L_{NA_f}}{2}$
7	Candidate bend radius (Eq. (3—15))	$BR_i = \frac{a}{\mathrm{Tan}\left(\frac{\theta_i}{2}\right)}$
8	Candidate centroidal radius (Eq. (3—11))	$\bar{r}_i = BR_i + u$
9	Candidate neutral axis radius (Eq. (3—12))	$R_{NA,i} = \frac{R_1^2 - R_2^2}{2\left(\sqrt{(\bar{r}_i^2 - R_2^2)} - \sqrt{(\bar{r}_i^2 - R_1^2)}\right)}$
10	Candidate neutral axis length (Eq. (3—13))	$L_{NA,candidate} = R_{NA_i} * \theta_i$
Use clamp adjustment		
11	Clamp adjustment (Eq. (3—16))	$\Delta a = \frac{L_{NA,f} - L_{NA,candidate}}{2}$
12	New distance from axis of rotation to clamp edge (Eq. (3—17))	$a_i = a + \Delta a_i$
13	New bend radius (Eq. (3—15))	$BR_i = \frac{a_i}{\mathrm{Tan}\left(\frac{\theta_i}{2}\right)}$
14	New centroidal radius (Eq. (3—11))	$\bar{r}_i = BR_i + u$
15	New neutral axis radius (Eq. (3—12))	$R_{NA,i} = \frac{R_1^2 - R_2^2}{2\left(\sqrt{(\bar{r}_i^2 - R_2^2)} - \sqrt{(\bar{r}_i^2 - R_1^2)}\right)}$
16	Calculate **e** for all angles (Eq. (3—19))	$e_i = \bar{r}_i - R_{NA_i}$

17	Find **y** at each point of interest (Eq. (3—20))	$y_{i,south} = b_i - e_i$
18	Find $\Delta\epsilon$ at each point of interest (Eq. (3—21))	$\Delta\epsilon = \frac{y * \Delta\theta}{(r_{NA} + y) * \theta_i}$

The calculations shown above have been applied to Test #126. Figure 3—14, Figure 3—15, and Figure 3—16 show the axial strain for each point calculated throughout the bend using these calculations. Due to the small neutral axis shift, and the East point laying on the centroidal axis, it can be seen in Figure 3—16 that the East point's axial strain is minimal.

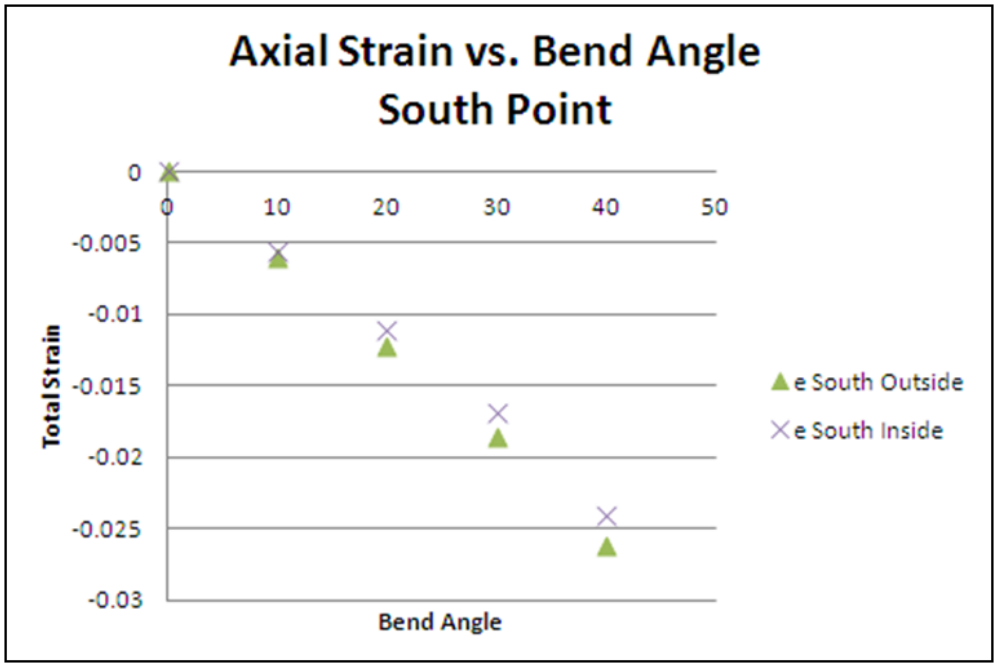

Figure 3—14: Axial strain versus the bend angle for the South point

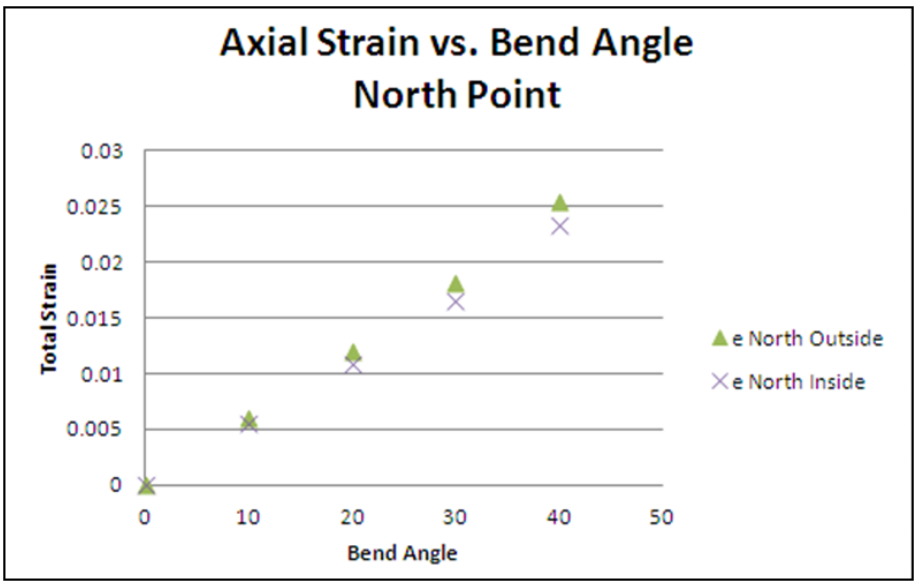

Figure 3—15: Axial strain versus the bend angle for the North point

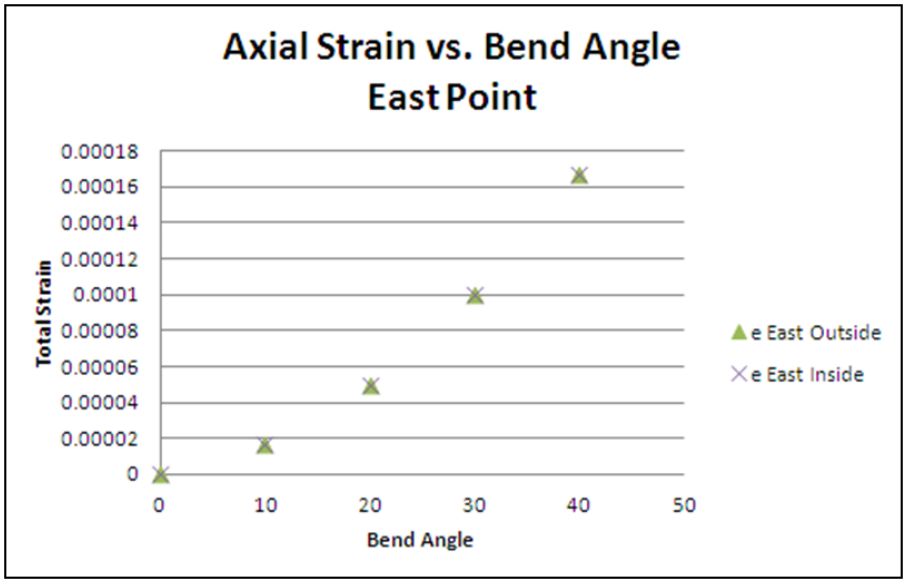

Figure 3—16: Axial strain versus the bend angle for the East point

3.6.2 Cross Sectional Strain

There are two orthogonal planes in which curved beam bending occurs. The first is the main bending plain, in which the tube is being bent to its desired bend radius. This is shown in Figure 3—17a. Orthogonal to this, is the cross section of the tube, which starts out as a circular thin walled cylinder and then deforms locally to an oval as shown enlarged in Figure 3—17b.

In order to orient the reader, Figure 3—17c shows a three dimensional view of the critical point of cross-section analyzed in the process below. Each critical point on the cross section is analyzed independently as if the section of the beam around the critical point was a curved plate in bending due to ovalization. The North and South points of this oval are flattening out and the East point is becoming more curved due to this ovalization. The critical points occur locally, near the cross-section where buckling occurs.

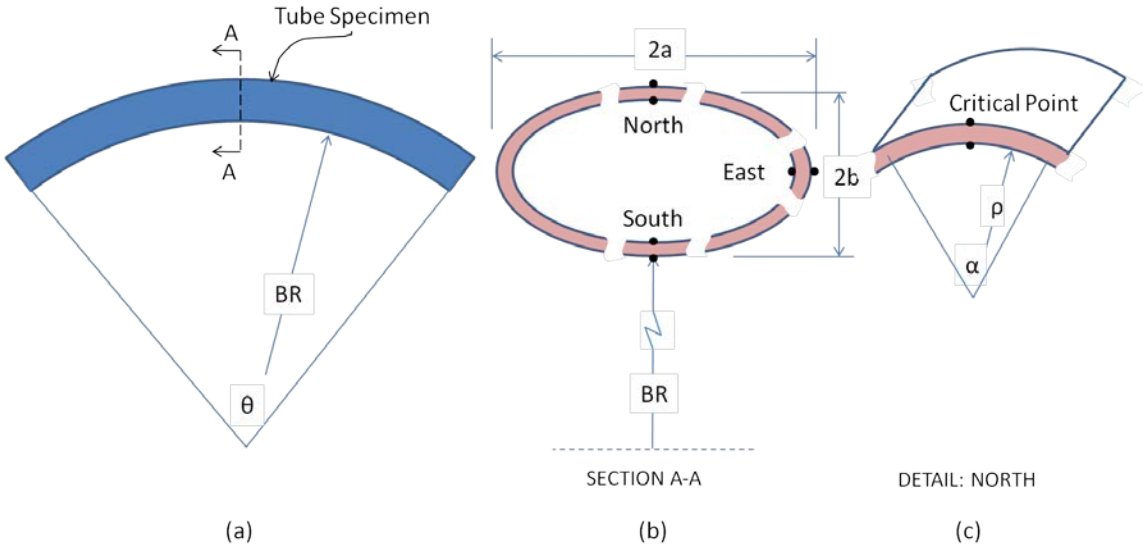

Figure 3—17: Tube in bending

a)Bending plane b)Cross-section plane A-A c) Detail view of critical point

As mentioned in the last section, it is important to remember that the bend radius is measured to the inner edge of the clamp, not the inner edge of the tube. This can be seen clearly in Figure 3—6

In order to determine the strain in the cross sectional direction, the radius of curvature for the critical points must be determined. Note that the radius of curvature of the cross section is not the same as the bend radius. Figure 3—17 shows the two orthogonal planes of a tube in bending: a) shows the axis of the tube being bent to a constant radius in the bending plane; b) shows the

elliptical cross section, which is perpendicular to the tube axis and has a varying radius of curvature in the plane of the cross section; and c) shows a detail of a critical point on the cross-section. The radius of curvature for the cross sectional ellipse is given in Equation (3—22)

$$\rho = \left(\frac{a^2 \sin^2 s + b^2 \cos^2 s}{a * b}\right)^{3/2} \qquad \textbf{(3—22)}$$

where (a) and (b) are half of the major and minor diameters of the ellipse and **s** is a parametric variable that can be determined by Equation (3—23)

$$s = \begin{Bmatrix} y \geq 0 & cos^{-1}\left(\frac{x}{a}\right) \\ y < 0 & 2\pi cos^{-1}\left(\frac{x}{a}\right) \end{Bmatrix} \qquad \textbf{(3—23)}$$

using the coordinate axis, where X follows the axis of the tube, YZ is the plane of the bend, and Y is positive away from the bend radius center as shown in Figure 3—18.

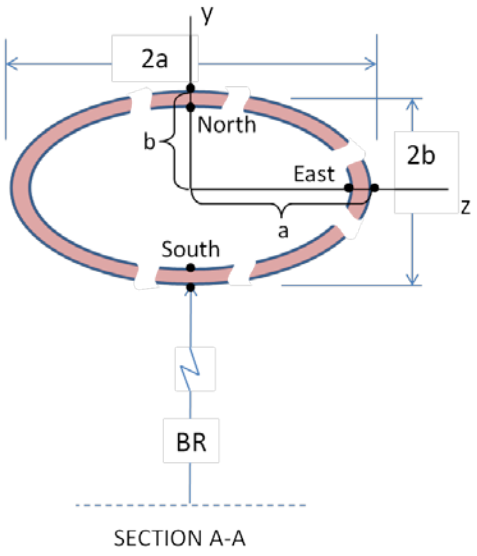

Figure 3—18: Coordinate axis on tube cross-section

Therefore, the values at the critical points for the variable **s** are

$$s_{North} = \frac{\pi}{2}$$

$$s_{East} = 0 \qquad \textbf{(3—24)}$$

$$s_{South} = -\frac{\pi}{2}$$

Inputting these values into Equation (3—22) quickly simplifies the solution. For the initial conditions, the radius of curvature is the outer radius of the un-deformed specimen. After ovalization, the curvature at the end of a minor axis, the South point in our example, is given as:

$$\rho_{North} = \rho_{South} = \frac{a^2}{b} \qquad \textbf{(3—25)}$$

At the end of a major axis, the East point in our example, the radius of curvature is given as

$$\rho_{East} = \frac{b^2}{a} \qquad \textbf{(3—26)}$$

From that radius of curvature, we assume that a slice is taken out of the wall and the radius of the inner wall, $\boldsymbol{\rho_i}$**,** and the centroidal radius of curvature, $\boldsymbol{\bar{\rho}}$**,** are concentric with the outer radius of curvature, $\boldsymbol{\rho_i}$. This allows us to calculate the radius of curvature for the inner wall and the centroidal axis using Equations (3—27) and (3—28).

$$\bar{\rho} = \rho_o - \frac{t}{2} \qquad \textbf{(3—27)}$$

$$\rho_i = \rho_o - t \qquad \textbf{(3—28)}$$

The radius of the neutral axis can then be determined using Equation (3—29)

$$\rho_{NA} = \frac{t}{\ln\left(\frac{\rho_o}{\rho_i}\right)} \qquad \textbf{(3—29)}$$

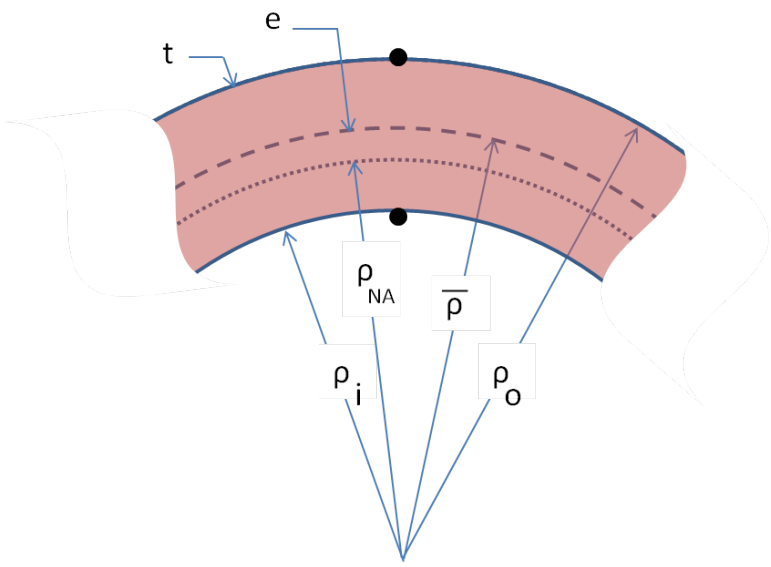

Figure 3—19: Detail of critical point

The difference can then be found between the neutral axis and the centroidal axis. This is listed as the variable **e** and is called the neutral axis shift.

$$e = \bar{\rho} - \rho_{NA} \qquad \textbf{(3—30)}$$

The distance in the Y direction from the neutral axis to the point being analyzed is found next. The points on the outer and inner surfaces of the tube wall are given in Equations (3—31) and (3—32).

$$y_o = \rho_o - \rho_{NA} \qquad \textbf{(3—31)}$$

$$y_i = \rho_{NA} - \rho_i \qquad \textbf{(3—32)}$$

At this point the segment of the specimen is analyzed by examining a small section with an assumed angle of 10° across the bend. This small section is the focus of the analysis.

The arc length,$\boldsymbol{L_{NA}}$, of the neutral axis is found using the radius of the neutral axis and the assumed angle. This is done using Equation (3—33) and is shown in Figure 3—20:

$$L_{NA} = \rho_{NA} * \alpha \qquad \textbf{(3—33)}$$

At this point the specimen is bent to a new bend angle and paused again. The process is repeated the same as above, where the new bend angle and the major and minor axes are recorded. The new bend radius, centroidal radius, and neutral axis are found using the same equations as above. Using the new neutral axis and the minor axis measurement the new distance to the point in question, referred to as **y**, is found.

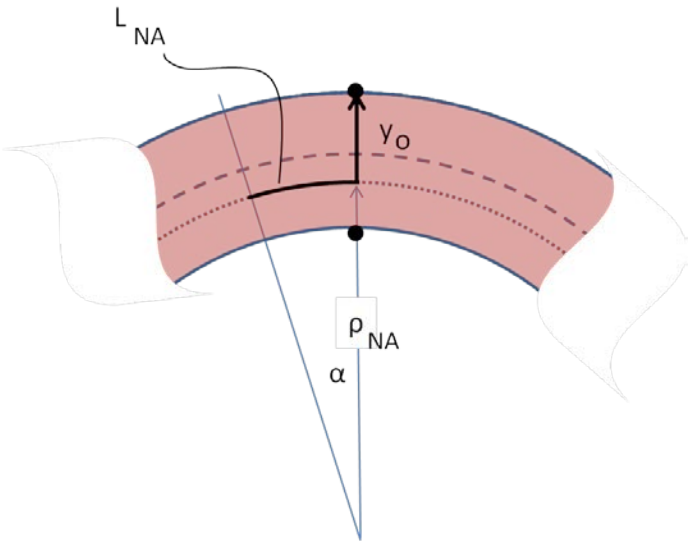

Figure 3—20: Length of the neutral axis at a critical point

Because the material at the neutral axis has no strain, it can be assumed that the length, $\boldsymbol{L_{NA}}$, of the neutral axis, that we focused on above, has not changed length. Using this length, and the new neutral axis radius, the change of angle is found that corresponds to a change of length at the point of interest. This angle change is determined with Equation (3—35) and can be seen in Figure 3—21.

$$L_{NA} = \rho_{NA} * a = \rho_{NA,new} * \alpha_{new} \quad \textbf{(3—34)}$$

$$\alpha_{new} = \frac{L_{NA}}{\rho_{NA,new}} = \frac{\rho_{NA} * \alpha}{\rho_{NA,new}} \quad \textbf{(3—35)}$$

Once this new angle is known the old length, found by the swept previous angle **α** is related to the new length swept using the new angle using Equation (3—36)

$$\Delta\epsilon = \frac{\Delta L}{L} = \frac{y * \Delta\alpha}{(\rho_{NA} + y) * \alpha_{i-1}} \quad \textbf{(3—36)}$$

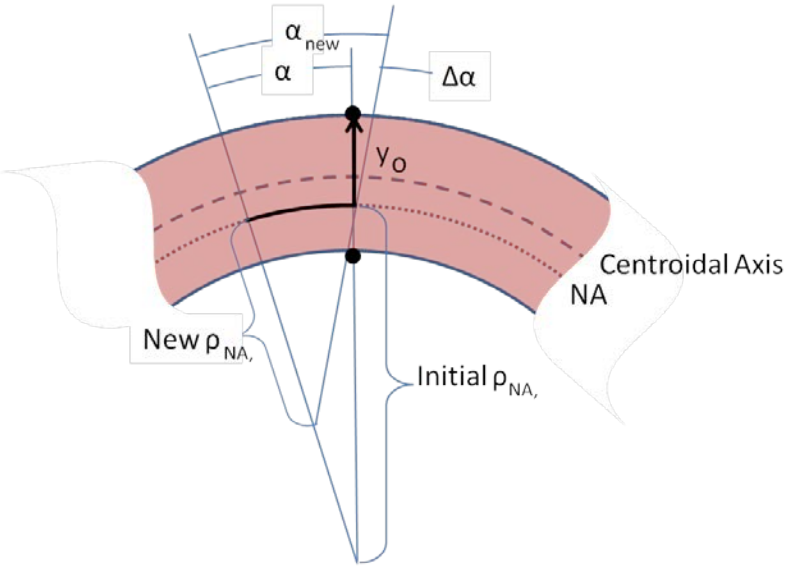

Figure 3—21: Detail of angle change if curvature increases

On the outer surface, this is equal to

$$\Delta\epsilon = \frac{(\rho_o - \rho_{NA})d\alpha_1}{\rho_o\alpha_1} = \frac{\left(\frac{t}{2} + e\right)d\alpha_1}{\rho_o\alpha_1} \quad \textbf{(3—37)}$$

and on the inner edge it becomes

$$\Delta\epsilon = \frac{(\rho_{NA} - \rho_i)d\alpha_1}{\rho_i\alpha_1} = \frac{\left(e - \frac{t}{2}\right)d\alpha_1}{\rho_i\alpha_1} \quad \textbf{(3—38)}$$

At this point, the tubing is bent another 10 degrees and new measurements for the major and minor axes are made, which can be repeated above.

It is important to note that the sign change between the points analyzed should always be checked. Y values on the inside of the curve should be negative due to the positive Y vector pointing away from the center of curvature. Also, if a radius of curvature is decreasing, the angle

change will be negative. In the case of the tube in pure bending, this relates to the North and South points on the cross section.

To illustrate these calculations, the following investigates the South point of Test #126 as it is bent from a 20° to a 30° bend angle. The final form of the tube is expected to reach a 90° bend with a 5 inch radius. Calculations have already been made for the initial conditions and the 10° and 20° bend angles. Measurements were taken of the major and minor axes, when the tube was bent to 30° and 20° bend angles and their half diameter values and thickness are as follows:

$$t = 0.0270\ in$$

$$a_{30^\circ} = 0.2993\ in$$

$$b_{30^\circ} = 0.3235\ in$$

$$a_{20^\circ} = 0.3118\ in$$

$$b_{20^\circ} = 0.3138\ in$$

From these values we can find the radius of curvature at the outer surface of the South point in the plane of the cross section.

$$\rho_{30^\circ,outer\ wall} = \frac{a^2}{b} = \frac{0.2993^2}{0.3235} = 0.2769$$

The radius of curvature for the inner wall and centroidal neutral axis are then calculated as follows

$$\bar{\rho}_{30^\circ} = \rho_{30^\circ,outer\ wall} - \frac{t}{2} = 0.2769 - \frac{0.0270}{2} = 0.2634$$

$$\rho_{30^\circ,inner\ wall} = \rho_{30^\circ,outer\ wall} - t = 0.2769 - 0.0270 = 0.2499$$

The radius of the Neutral Axis is

$$\rho_{30^\circ,NA} = \frac{t}{\ln\left(\frac{\rho_{30^\circ,outer}}{\rho_{30^\circ,inner}}\right)} = \frac{0.0270}{\ln\left(\frac{0.2769}{0.2499}\right)} = 0.2632$$

The neutral axis shift, given as the variable e is found to be

$$e_{30^\circ} = \bar{\rho}_{30^\circ} - \rho_{30^\circ,NA} = 0.2634 - 0.2632 = 0.002$$

The angle change that is applied to the cross section at the point of interest is found using the arc length formula and the value of the radius of curvature at the chosen angle, 10° ($\rho_{10^\circ,\mathrm{NA}} = 0.2988$ in), as follows:

$$\alpha_{30^\circ} = \frac{L_{original}}{\rho_{30^\circ,NA}} = \frac{\rho_{10^\circ,NA} * 10^\circ * \left(\frac{\pi}{180^\circ}\right)}{\rho_{30^\circ,NA}} = \frac{0.2988 * 0.1745}{0.2632} = 0.1981$$

Following the same process, $\alpha_{20^\circ} = 0.1761$. This allows the change in angle to be found:

$$d\alpha_{30^\circ} = \alpha_{20^\circ} - \alpha_{30^\circ} = 0.1761 - 0.1981 = -0.0220$$

This gives us all the information needed to find the strain change due to the bend angle change for both the outer and inner wall of the tube, as shown below.

$$\Delta\epsilon_{30^\circ,outer\ wall} = \frac{\left(\frac{t}{2} + e_{30^\circ}\right) d\alpha_{30^o}}{\rho_{30^\circ,outer\ wall} * \alpha_{20^o}} = \frac{\left(\frac{0.0270}{2} + 0.0002\right) * -0.0220}{0.2769 * 0.1761} = -0.0062$$

$$\Delta\epsilon_{30^\circ,inner\ wall} = \frac{\left(\frac{t}{2} - e_{30^\circ}\right) d\alpha_{30^o}}{\rho_{inner\ wall} * \alpha_{20^o}} = \frac{\left(0.0002 - \frac{0.0270}{2}\right) * -0.0220}{0.2769 * 0.1761} = 0.0059$$

To summarize the procedure, the following numbered list has been given. The subscript character s refers to the initial condition, i refers to the inner surface of the tube and o refers to the outer surface of the tube.

Initial Conditions

1.	Initial arbitrary angle		$\alpha_s = 10° = 0.01745\ rad$
2.	Outer radius of curvature	Equation (3—25)	$\rho_o = OD/2$
3.	Centroidal radius of curvature	Equation (3—27)	$\bar{\rho} = \rho_o - \frac{t}{2}$
4.	Inner radius of curvature	Equation (3—28)	$\rho_i = \rho_o - t$
5.	Neutral Axis radius of curvature	Equation (3—29)	$\rho_{NA} = \frac{t}{\ln\left(\frac{OD/2}{(OD/2-t)}\right)}$
6.	Length of Neutral Axis	Equation (3—33)	$L_s = \rho_{NA,s} * \alpha_s$
7.	Neutral Axis Shift	Equation (3—30)	$e = \bar{\rho} - \rho_{NA}$
8.	Initial strain change, outer point		$\Delta\epsilon_o = 0$
9.	Initial strain change, inner point		$\Delta\epsilon_i = 0$

Iteration Steps

10.	Outer radius of curvature	Equation (3—25)	$\rho_{o,North\ or\ South} = \frac{a_1^2}{b_1}$ $\rho_{o,East} = \frac{b_1^2}{a_1}$
11.	Centroidal radius of curvature	Equation (3—27)	$\bar{\rho} = \rho_o - \frac{t}{2}$
12.	Inner radius of curvature	Equation (3—28)	$\rho_i = \rho_o - t$
13.	Neutral axis's radius of curvature	Equation (3—29)	$\rho_{NA} = \frac{t}{\ln\left(\frac{\rho_o}{\rho_i}\right)}$
14.	Neutral axis shift	Equation (3—30)	$e = \bar{\rho} - \rho_{NA}$
15.	New angle	Equation (3—35)	$\alpha_{new} = \frac{L_s}{\rho_{NA,new}}$ $= \frac{\rho_{NA,s} * \alpha_s}{\rho_{NA,new}}$
16.	Angle change		$\Delta\alpha = \alpha_{new} - \alpha_s$
17.	Strain change, outer surface	Equation (3—37)	$\Delta\epsilon_o = \frac{\left(\left(\frac{t}{2} + e\right) * \Delta\alpha\right)}{\rho_o * \alpha_{new}}$
18.	Strain change, inner surface	Equation (3—38)	$\Delta\epsilon_i = \frac{\left(\left(e - \frac{t}{2}\right) * \Delta\alpha\right)}{\rho_i * \alpha_{new}}$
19.	Iterate steps 10 through 19		
20.	Sum the strain changes for the total strain		$\epsilon_{Total} = \sum \Delta\epsilon$

Figure 3—22 and Figure 3—23 show the cross-sectional strain calculated for each angle increment throughout the bend. Due to the curvature increasing at the East point, and decreasing at the North and South points, it can be seen that the direction of the strain is switched between the plots. It is important to note that ovalization mainly occurs just prior to buckling. Most of the cross sectional strain occurs at this time as well.

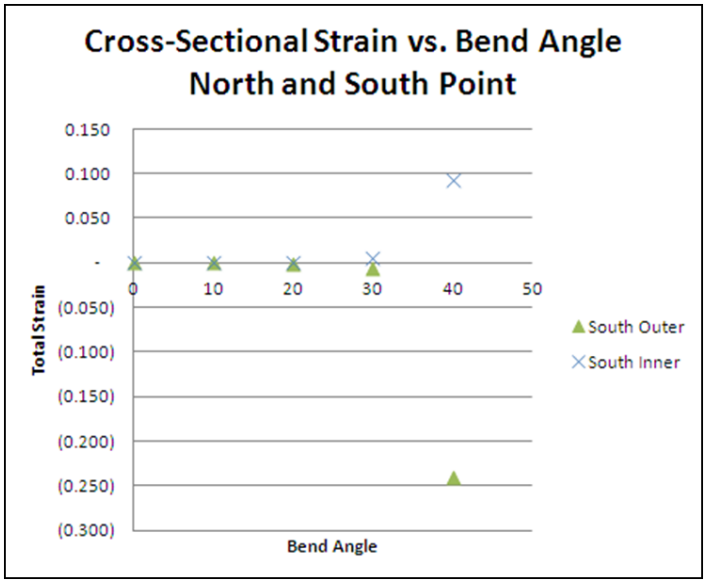

Figure 3—22: Cross-sectional strain versus the bend angle for the North and South points

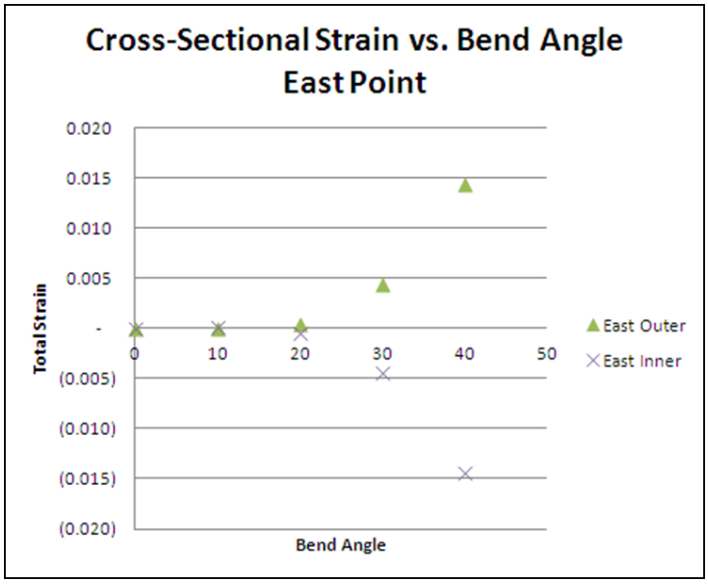

Figure 3—23: Cross-sectional strain versus the bend angle for the East point

3.6.3 Radial Strain

As mentioned above, radial strain is a function of the other two strains and is driven by the assumption that the sum of the strains must equal zero for post yield, constant volume behavior:

$$\epsilon_{Axial} + \epsilon_{Cross-Sectional} + \epsilon_{Radial} = 0 \quad \textbf{(3—39)}$$

The radial strains are then used to determine the new thickness of the material. This is done by taking the average of the inner and outer strain percentages and then multiplying the previous thickness to that percentage. This simple assumption is used as an approximation, because the middle of the material will be deforming at a non-linear rate.

This calculation has been applied to Test #126. Figure 3—24, Figure 3—25, and Figure 3—26 show the radial strain for each point calculated throughout the bend. Due to the summing effect of the two strains (axial and cross sectional) both being in compression on the outer wall of the South point, the maximum strain will occur at this point and be shown in Figure 3—24.

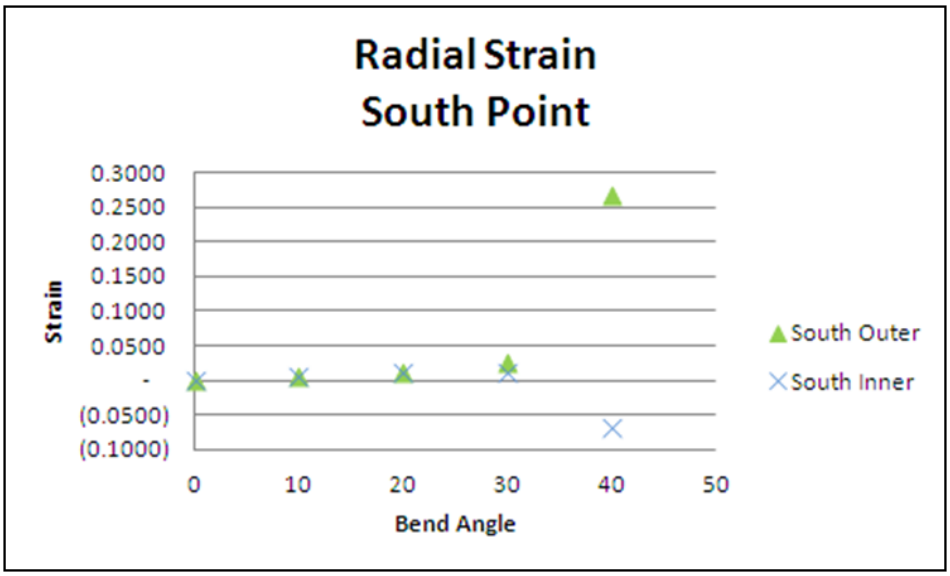

Figure 3—24: Radial strain versus bend angle for the South point

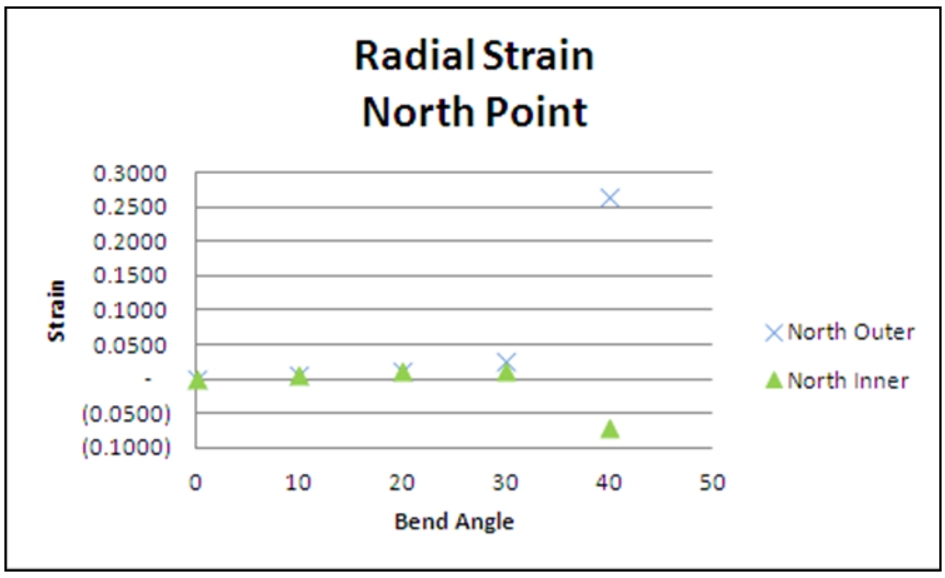

Figure 3—25: Radial strain versus the bend angle for the North point

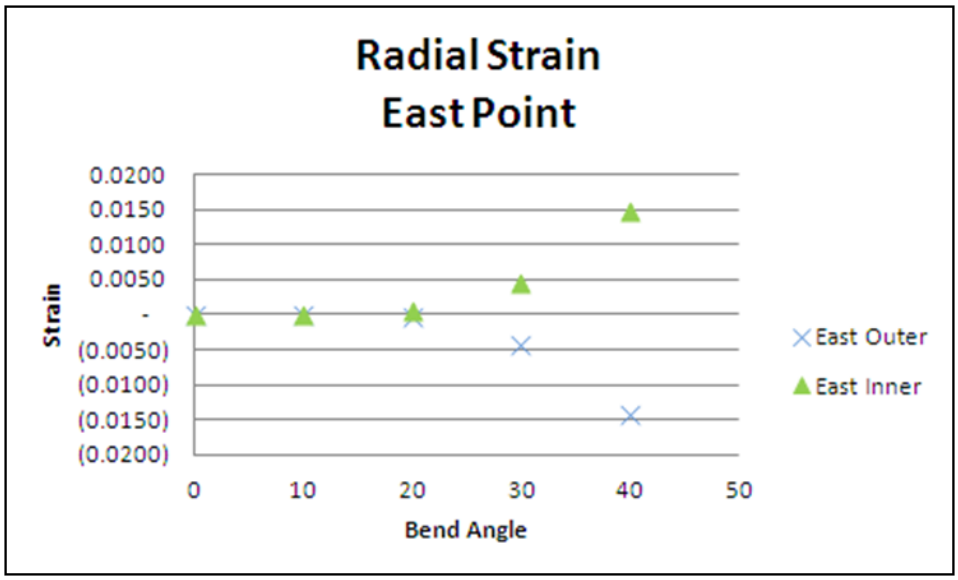

Figure 3—26: Radial strain versus the bend angle for the East point

3.7 Discussion

3.7.1 Failure Boundary

In order for the tube bending machine to be useful in industry it is crucial that a failure boundary be established. With the current set of calculations, a failure boundary cannot be predicted prior to testing due to the inputs needed. Specifically, the major and minor diameters of the ovalized section cannot be predicted, but, rather, are only observed. Once a set of tests has been run and an empirical failure boundary is proposed it can be used by the machinist to know if the bend they need to make is possible on an arborless tube bender or if the bend must be created on a standard tube bender.

3.7.2 Results

These equations have been validated using data from the empirical tests. For example, a test was done on ½" M alloy 122 copper with the intended bend radius of 5." Measurements of the major and minor axis were taken every 10° and buckling visually occurred at 30°. Using the equations described herein, the incremental tri-axial strain on the tubing was calculated to be as follows:

Table 3—1: Calculated incremental strains predicted at a 30° bend.

Configuration: ½ x M alloy 122 copper, free length: 7.85"

	Axial Strain	Cross Sectional Strain	Radial Strain
South, inner surface	-0.582%	0.561%	0.020%
South, outer surface	-0.635%	-0.622%	1.257%

Total strains for this same test specimen are shown in Table 3—2. This expected strain is near the 2.74% yield strain for alloy 122 copper discussed in Section 5.2.

Table 3—2: Calculated total strains predicted at a 30° bend.

Configuration: ½ x M alloy 122 copper, free length: 7.85”

	Axial Strain	Cross Sectional Strain	Radial Strain
South, inner surface	-1.693%	0.602%	1.091%
South, outer surface	-1.852%	-0.663%	2.515%

Strain calculations were run for all the tests of copper tubing for which data on the major and minor axes was recorded throughout the bend. The maximum strain was found to occur in the South Outer surface in the radial, or thickness, direction. This is due to the axial and cross sectional strains occurring in the same sign, in orthogonal planes, so that transverse strains in the radial direction are additive. The maximum strain calculated for each copper test is shown plotted in Figure 3—27.

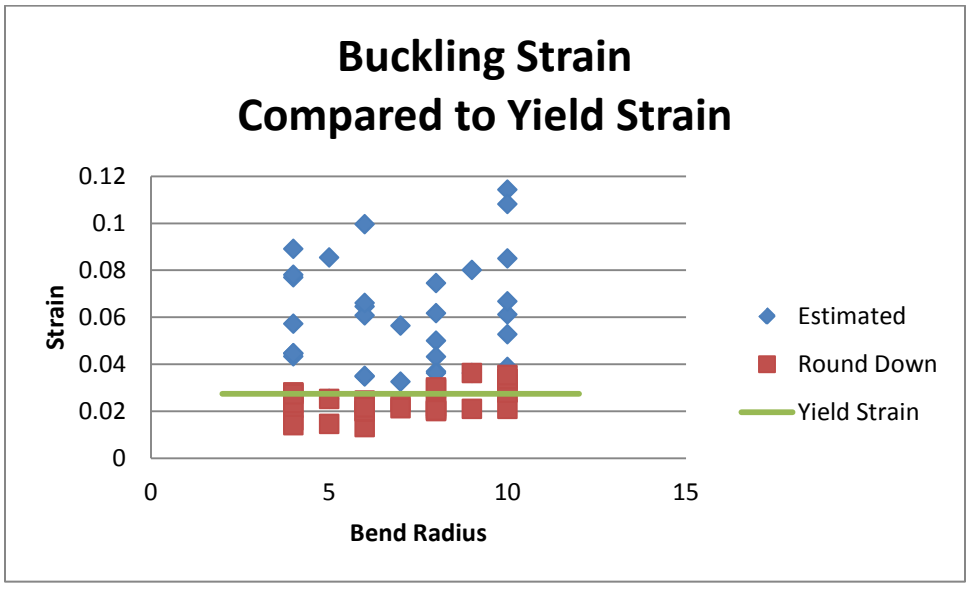

Figure 3—27: Buckling strain compared to yield strain

This data was found by calculating the strain, as shown in Section 3.6, in each of the three directions, at each bend angle throughout the test process. The buckling angle was determined visually as described in Section 4.4, and this angle frequently fell between two of the 10° increments of the test. Because cross section strain calculations can only be run if the ovalization data is recorded, the radial strain at the buckling point was estimated by linear interpolation, from the bend angle immediately preceding and after the buckling occurred. The bend angle at which buckling occurred is recorded on video to within 1°. Assuming approximately linear behavior, the buckling strain may be estimated by the ratio

$$\epsilon_{radial\ at\ Buckling} = \frac{\theta_{Buckling} - \theta_{30^\circ}}{\theta_{40^\circ} - \theta_{30^\circ}} * (\epsilon_{40^\circ} - \epsilon_{30^\circ}) \qquad \textbf{(3—40)}$$

This corresponds to the buckling angle visually recorded which gives an estimate of the actual strain at buckling. This can be shown in Figure 3—28. This estimate will always be higher than the predicted strain, due to the function being concave, unless buckling occurred right at one of the 10° increments, where ovalization was measured.

The data presented in Figure 3—28 comes from Test #126 and is a repeat of the data shown in Figure 3—24. For this test, buckling was seen first occurring at 30°, but for illustrative purposes the buckling angle has been exaggerated to 35°. This data would show a strain at the data point taken just before buckling occurred, or "rounded down" data point of approximately 0.024, or 2.4% strain, which is close to the yield strain. The strain at the data point just after buckling would be approximately 0.26, or 26%. The line fit estimate using these two points would give an estimated buckling strain at 35° of 0.15, or 15%, but if a curve was fit to this data the buckling strain would be estimated at closer to 0.05, or 5%. This is due to the rapid change of the strain after buckling. The line fit approximation will always be higher than the curve fit strain, but it gives a quickly estimated value.

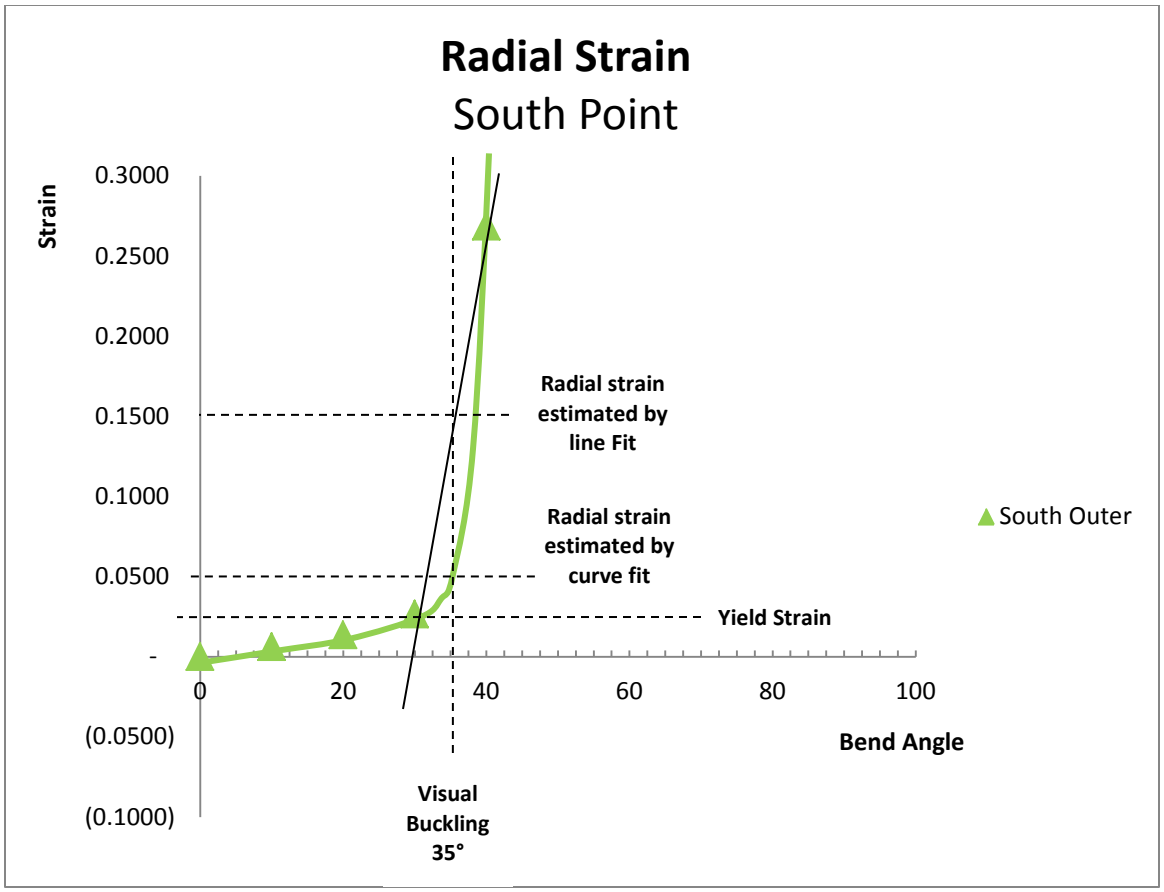

Figure 3—28: Estimating the maximum buckling strain

It is important to note that the strains at the rounded down point (the last measured value before buckling,) shown in Figure 3—27 are mostly all near, and typically below, the expected yield strain of alloy 122 copper. Also, the estimated buckling strains are all above the yield strain of alloy 122 copper. This shows that the failure occurred just after the yield point was reached. Copper is shown here to fail quickly after it reaches yielding, just as the published data predicts, which will be discussed in more detail in Section 5.2

4 APPARATUS AND TEST SET UP

4.1 Components of the Machine

4.1.1 Hardware Description

An arborless tube bending machine has been provided by the BYU capstone program and their sponsor, Burr Oak Tool Inc. The control system was built and programmed by Kevin Cole. The machine is controlled by a feedback control loop using a Compact RIO controller by National Instruments, which is run with LabView and a desktop computer. The system controls three motors: two linear actuators and a central rotary drive motor. The central motor is an AC gear motor, which drives the angular displacement of the bender arm. Two linear actuators attached to the movable clamps, which grip the ends of the tubing, make up the rest of the control system. One of the actuators is fixed to the table and the other is on the rotating arm, whose angle is controlled by the central motor. The arm rotates about its pivot, and the clamp grips one end of the tube as it moves through the bend angle. The control system simultaneously changes the position of the linear actuators in an attempt to keep the neutral axis of the tube at its original length. The continuous position adjustments of the clamps keep axial pressure from developing in the tube's neutral axis and allow the system to apply only a pure bending moment.

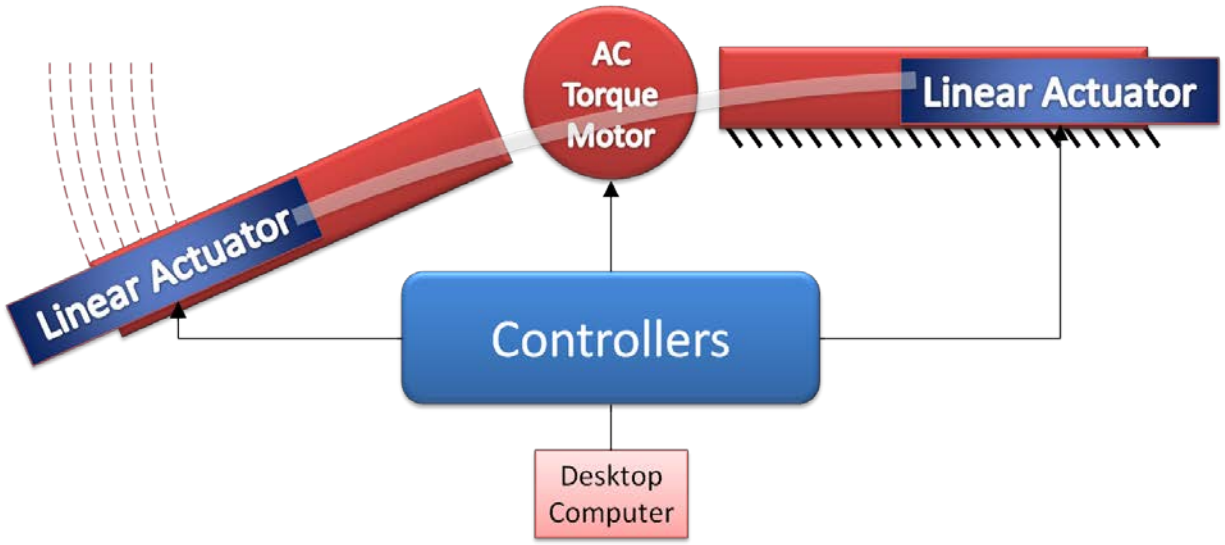

Figure 4—1: Bending machine controls schematic

Views of the bend site from above are recorded by the computer through a web camera, which allows the operator to see when buckling occurs. The critical instant when the tube begins to collapse is detected, and, after the test when the video recording is being reviewed, it may be paused to record the angle. The bend specifications and the buckling angle are then recorded on a spreadsheet.

The individual components of the machine are described in detail in the Capstone report. These components include the clamping mechanism, the sliders, the fixed structural arm, and the structural arm that swings through the bend, the linear actuators, and the torque motor. A description of the specifications for each part is located with its description in the report.

4.1.2 Control System

In order for the apparatus to meet the required functional specification of applying only a pure moment to the tube, a Data Acquisition System (DAQ) is required. This system precisely controls the amount of movement in the linear actuators in relation to the bend angle. It is able to start and stop the machine manually at any time in order to collect data, as well as know when

the bend is complete and stop the bend at that point. It is directed by the program LabView, which allows the user to easily see and manipulate the configuration of the system parameters.

Using the equations in Section 3.6.1, the computer can find the expected radius of curvature for the tube at every given angle throughout the bend. By inputting the expected final bend radius and bend angle, the user is specifying the final, and constant, length of the neutral axis. Using this information, the offset value **u**, and the neutral axis shift **e**, the control system can calculate the change needed in the length of the centroidal axis that would keep the neutral axis constant.

This formula has been programmed into the LabView program and governs the linear actuator position. This equation has been set up to keep the neutral axis length unchanging throughout the bend, which will make the applied axial pressure negligible. This is what maintains the pure bending moment. The equation as it was coded into the program is shown in Equation (4—1). The derivation for this equation can be found in 0.

$$a = \left(\frac{R_f \alpha_f}{\alpha} - U\right) \tan\left(\frac{\alpha}{2}\right) \qquad \textbf{(4—1)}$$

A computer interface and display has been designed which allows technicians to enter test parameters and monitor the process to assure the bend is properly controlled. Through this system they are able to see the expected location of both linear actuators, compared to their actual position, as read by means of potentiometers, and plotted together on one graph. They also are able to manually start and stop the machine at any time. When the bend has gone to its pre-programmed position, the DAQ automatically stops the machine, and the technician can then remove the specimen from the clamps. To repeat the test, the technician resets the clamps to the initial position, based on inputs that were put into the user interface, by simply pressing the reset

button. This system has been designed with the user in mind and attempts to be simple for a technician to run. A user manual has been included in 0.

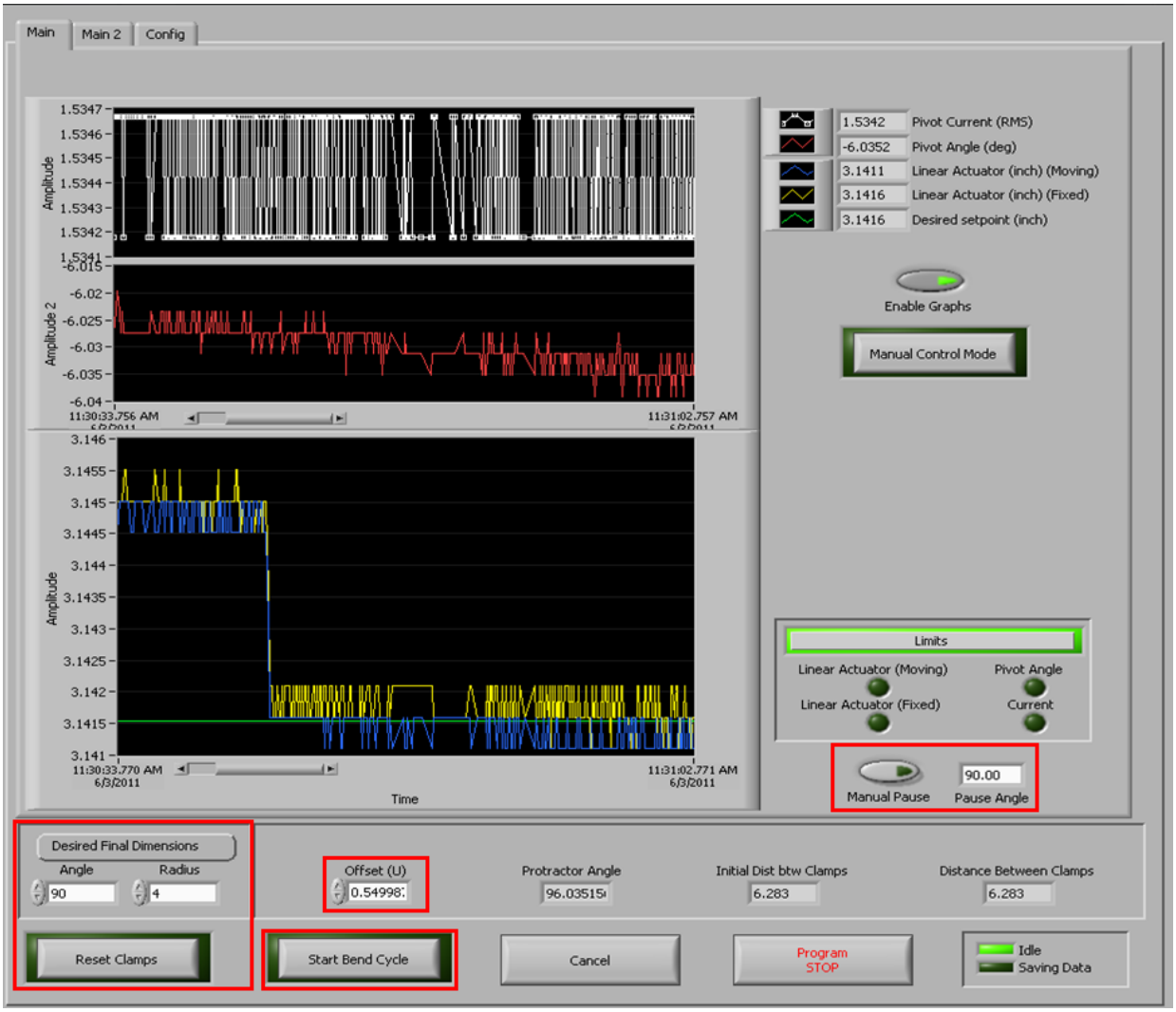

Figure 4—2: Screen shot of bending machine control systems in LabView

4.1.3 Instrumentation

The feedback data that is used in the control system comes from a set of three potentiometers located on the linear actuators and the rotary motor. This data controls the action of the motors through a set of relays, which allow the power to be turned on or off or which switches the direction of the current to reverse the motor as needed. In case of a failure, limit

switches have been included at 0 and 90 degrees that will shut off the power to the rotary motor if they are triggered. Specifications on each of these components have been listed in the Capstone report.

4.2 Machine Limits

The machine is limited in the angle in which it can bend a specimen. Limit switches have been installed at locations on the table corresponding to approximately -10° and 95° which stop the program if tripped. When deemed necessary, the limit switches may be removed and bends larger than 90° may be reached.

The clamps on the machine have fixtures that are shaped specifically to match the outer diameter of the tubing. They are replaced with each change of tubing size to keep the grip area consistent. Currently, there are two different grip fixtures matching the two tubing diameters which have been tested. If a different diameter is to be tested new clamps will have to be made. Finned coils or other flat-sided material have been bent by removing the fixtures and holding the material directly in the clamp jaws.

4.3 Recording Methods

Many of the challenges relating to correlating the bend angle with the buckling load are centered on the method of recording the exact instant of buckling and corresponding bend angle. Potential concepts were tried that each had their difficulties and benefits. The three concepts that were tried were 1) a visual reading from a web camera, 2) an attached elastomer strain gauge, and 3) measuring the current drawn by the motor. The following examines why the visual reading was chosen and the others discarded.

4.3.1 Concept Generation and Selection

Visual reading

Buckling on a tube is obvious once the whole tube has failed, but it is much harder to detect when it actually begins. By recording the instant when buckling becomes visible, it was possible to get a consistent and repeatable data point that could be used for comparison to the theoretical equations. The difficulties involved with this were based around the ability of the operator to find the buckling point consistently, but it was found that, through training, this could be done. After the test, the operator would playback the video, watching it to see when the inner edge of the tubing no longer formed an arch with a constant radius along the whole bend. When this frame in the video was found, the user paused the video and recorded the angle, based on the protractor, which is also visible in the screen. This method allows the data to be recorded without interference. The data could then be reviewed after the test to find the critical point.

An in-depth description of this method, with examples of when the technician marked the buckling point is found in the User Manual supplied in 0

Elastomer Strain Gauge

Concurrent with this project was a project headed by Dr. Fullwood of BYU, where elastomer strain gauges were being tested. These strain gauges consisted of a strip of rubber-like material which, when formed, had been infused with conductive carbon shavings. They had the capability to read strains in the range that we were interested in, but were still experimental. Unfortunately, we were not able to get a good reading from them due to adhesion issues between the strain gauge and the metal. The gauge would detach itself midway through the bend causing the key data to be lost.

Current Reading from Motor

Another technique for detecting buckling was based upon reading the current supplied to the motor. It was based on the motor current being proportional to the torque load on the motor, which would equal the bending moment on the tubing. The moment applied was expected to drop suddenly when buckling occurred due to the tube walls no longer resisting the moment and this should produce a sudden change in the motor current.

In order to read the current supplied to the motor, the wire connecting the motor was wrapped around a current transformer, which produced a signal. In the end, this signal was much too weak. Even with filtering and amplification, a reliable buckling point could not be detected.

Manual Caliper Readings

Prior to buckling, the cross section surrounding the buckling point begins to deform from circular to oval. The major axis of the oval is normal to the bending plane and the minor axis parallel to the bending plane. In order to quantify this ovalization, measurements were taken at 10° intervals throughout the bend of the major and minor axes at the buckling point along the tube.

Unfortunately, the gear system had enough play between the gears to allow the tube to spring back a degree or so while the measurement was being taken, but this did not seem to affect the final buckling angle and so it is assumed that the test was not critically different. The spring back also had a negligible effect on the major/minor axis measurements. These readings were carried out on a smaller number of tubes because of the time required to stop and start the machine. The ovalization measurements turned out to be a valuable metric for the transverse strain calculations.

4.3.2 Running the Machine

The machine is monitored by a computer, on which LabView is installed. Within LabView, the technician runs the custom program, FlexTech. Once the program is running, the technician enters the desired final position to the computer in terms of final bend angle and final bend radius as well as the offset. They also may input the angle increment at which to pause in order to take measurements during the test. Each input allows the technician to control an aspect of the bend.

The initial length of the specimen is determined from the specified final bend angle and final bend radius. The initial grip position is then calculated through the arc length formula

$$L_{arc} = R_f \theta_f = Distance\ between\ grips \qquad \textbf{(4—2)}$$

where the initial distance between the grips is equal to the final neutral axis arc length. This is the value to which the neutral axis will be maintained, using the linear actuators, as it proceeds through the bend.

In order to maintain a constant length neutral axis, it is important to know its precise length throughout the bend process. The offset is input into the program in order to define the initial position of the neutral axis. It is defined as the distance between the axis of rotation for the rotary motor and the neutral axis in the plane of bending. The offset is labeled **U** in the figure below. Calculations for the neutral axis location versus the bend angle are derived in 0. The addition of the effect made the neutral axis shift calculations much more complex.

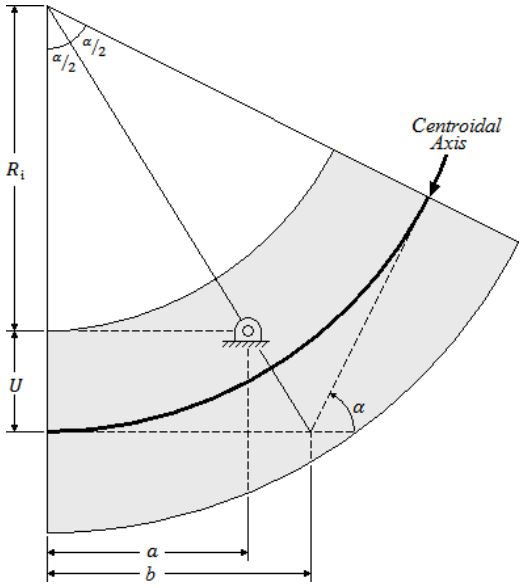

Figure 4—3: Tube in bending

4.3.3 Recording Video

During the bend tests, a video is recorded that allows the technician to collect the raw data. A webcam is placed above the table at approximately the rotational motor's axis. This camera captures the center section of the specimen throughout the bend.

Once the test specimen is prepared for a test, the camera is turned on and controlled through Windows Movie Maker or equivalent video capturing software. The camera is kept running through the full bend regardless of pauses or failed tests. This allows the technician to concentrate fully on the test apparatus. At the end of the test, the video recording is stopped, and the video is reviewed in order to determine the buckling angle based on the profile of the specimen.

4.3.4 Recording Major/Minor Axes Measurements

For many tests, the technician paused the machine at every 10° of the bend cycle and took measurements of the major and minor axis of the tubing cross section. This measurement, taken manually via calipers, was recorded on the same spreadsheet as the buckling angle. Other tests were run without stopping the machine, and the results show that stopping the process had no significant effect on the buckling angle.

The program allows the user to choose any interval for the distance travelled before the manual pause is reached, based on the pause angle input. For the purposes of this test, the pause angle has been every ten degrees. After the pause, the test is resumed right where it left off, recovering the small spring back that occurred during the pause. The sudden increase in ovalization measurements are another clear indication that buckling has occurred.

4.3.5 Interpreting Results

Once the test has been run and the video has been captured, the technician reviewed the video and recorded the buckling angle of the tubing. They did this through visually watching the video, frame-by-frame near the point when buckling was expected, and stopping the video when they saw buckling occur. They specifically watched the inner edge of the specimen for the uniform radius of curvature to become non-uniform. At the point they were able to see the radius of curvature change from a smooth curve, constant throughout, to a point failure, they then read the protractor which has been installed below the clamps, right over the rotary motor axis. The angle was then recorded in a spreadsheet, along with the test number and material specifications.

This process is obviously easier and more valid for materials that fail suddenly, like copper, than with materials that fail subtly, like aluminum. For both those that fail suddenly, and those that are more subtle, this process has proven to be valid when compared to tests where the

major and minor axes are measured. When these measurements are taken, it is clear when the failure occurs due to the rapid decrease in minor diameter and increase of major diameter, which are clear signs that the ovalization is changing rapidly, which is when buckling occurs. This relationship can be seen below in Figure 4—4.

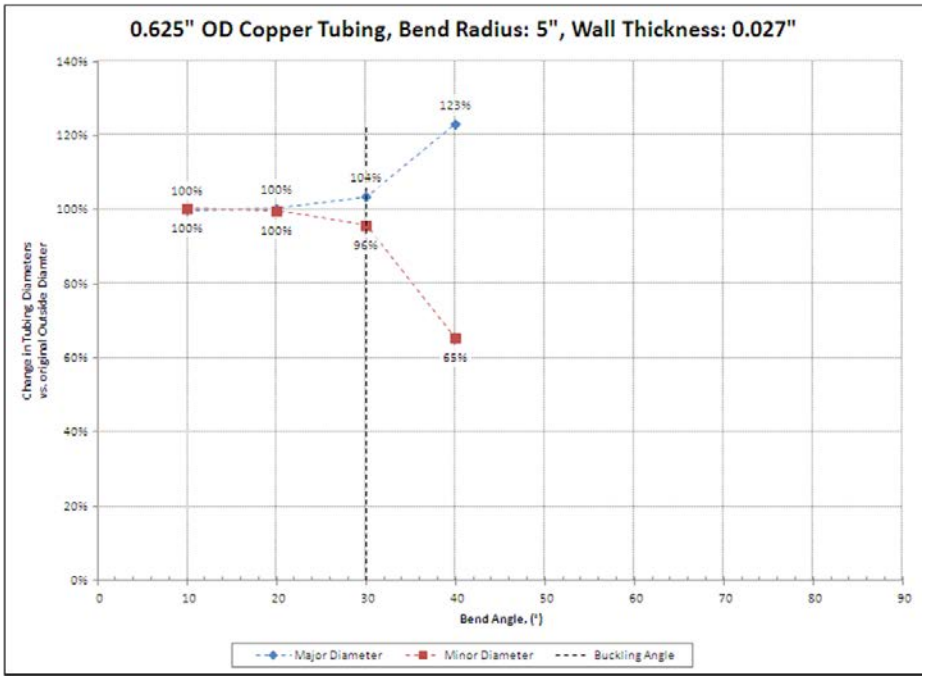

Figure 4—4: Ovalization of ½" x M copper tubing

The point of buckling recorded through this system of measurement is repeatable with a standard deviation of approximately 1.5° for copper, and 5° for aluminum and EMT steel, off the expected buckling angle. This is shown in more detail in the linearity analysis in Section 5.4. This is not a large variation considering the unstable nature of this mode of failure. It is sensitive to small surface variations, grain orientation, local hardening variations, etc.

4.4 Raw Data

Two forms of raw data have been recorded: Video recordings of the tests and manual measurements of the major and minor axes. Each adds some insight into the buckling failure and

where it occurred. Below, each form of raw data is shown and the spreadsheet showing the analysis is described.

4.4.1 Video Data

Figure 4—5 is a series of screen shots that show what the technician sees frame-by-frame. They use the frame-by-frame view to see more precisely where the radius of curvature becomes non-uniform along the inner edge of the specimen.

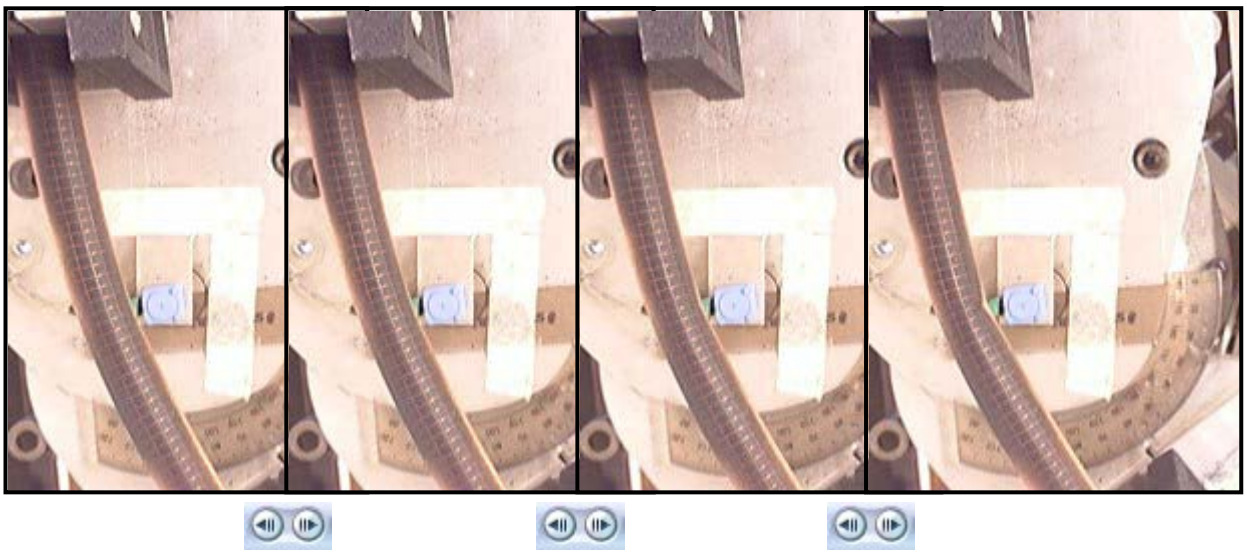

Figure 4—5: Determining the buckling angle by viewing footage frame-

Using the frame-by-frame viewing available in Windows Movie Maker allows comparison of the sample at 62°, 61°, 60°, and 59° protractor angles, as shown in Figure 4—5 above. Buckling has clearly occurred by 60°, but may be beginning at 61°. This specimen's buckling angle has been recorded as 61°. The test shown in the figure is not the Test #126 used throughout the rest of this report, but is an EMT sample. Test #126 buckled at 60° as shown on the spreadsheet shown in Figure 4—6. The compliment of this angle, 30°, is the value used in the theoretical analysis.

	A	B	C	D	E	F	G	H
1	Test Order	Tube ID#	Buckling Angle (visual, °)	Material	Bend Radius (in)	Tube Diam. (in)	Wall Thickness (in)	Notes
124	124	Cu-10-90-10	46	Copper	10	0.625	0.042	Home Depot Pipe
125	125	Cu-4-90-12	62	Copper	4	0.625	0.027	Home Depot Pipe
126	126	Cu-5-90-08	60	Copper	5	0.625	0.027	Home Depot Pipe
127	127	Cu-6-90-10	58	Copper	6	0.625	0.027	Home Depot Pipe
128	128	Cu-7-90-07	55	Copper	7	0.625	0.027	Home Depot Pipe
129	129	Cu-8-90-10	53	Copper	8	0.625	0.027	Home Depot Pipe

Figure 4—6: Table for recording buckling angle data

4.4.2 Hand Measurement Data

Hand calculations taken with calipers at the buckling point every 10° are recorded in the following spreadsheet. Not all tests were recorded this way due to the time intensive nature of the process. This process was used to validate the data recorded visually. Figure 4—7 shows how this data was recorded.

	A	B	C	D	E	F	G	H	I	J	K	L	M	N	O	P	Q	R	S	T
1	Test Order	Tube ID#	Buckling Angle (visual, °)	Material	Bend Radius (in)	Tube Diam. (in)	Wall Thickness (in)	Notes	0° Minor Diameter	0° Major Diameter	10° Minor Diameter	10° Major Diameter	20° Minor Diameter	20° Major Diameter	30° Minor Diameter	30° Major Diameter	40° Minor Diameter	40° Major Diameter	50° Minor Diameter	50° Major Diameter
124	124	Cu-10-90-10	46	Copper	10	0.625	0.042	Home Depot Pipe												
125	125	Cu-4-90-12	62	Copper	4	0.625	0.027	Home Depot Pipe			0.6	0.6	0.6	0.6	0.5	0.7	0.4	0.8		
126	126	Cu-5-90-08	60	Copper	5	0.625	0.027	Home Depot Pipe			0.6	0.6	0.6	0.6	0.6	0.6	0.4	0.8		
127	127	Cu-6-90-10	58	Copper	6	0.625	0.027	Home Depot Pipe			0.6	0.6	0.6	0.6	0.6	0.6	0.4	0.8		
128	128	Cu-7-90-07	55	Copper	7	0.625	0.027	Home Depot Pipe			0.6	0.6	0.6	0.6	0.6	0.6	0.6	0.7	0.4	0.8
129	129	Cu-8-90-10	53	Copper	8	0.625	0.027	Home Depot Pipe			0.6	0.6	0.6	0.6	0.6	0.6	0.5	0.7	0.4	0.8

Figure 4—7: Table for recording raw ovalization data

This data has been plotted along with the buckling angle recorded via the video. An example of this data as it is plotted is shown in Figure 4—4 which is repeated below for convenience. The graph includes the percentage change in the major and minor axis diameters versus the original tubing diameter. It also confirms that the buckling point recorded from the frame-by-frame video method was measured at the same point at which the major and minor axis deformation begins to increase dramatically, as shown by the inflection of the plot.

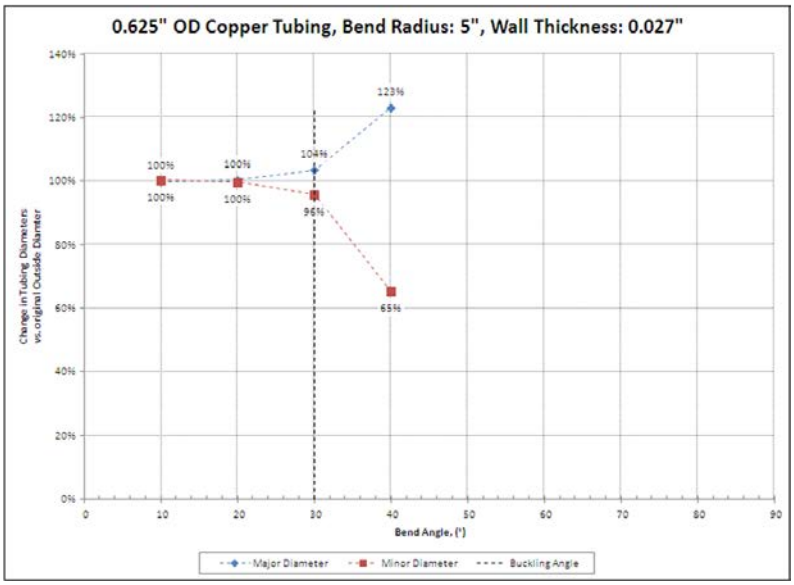

Figure 4—4: Ovalization of ½" x M copper tubing

5 TEST RESULTS

5.1 Introduction

The tests runs were analyzed in two different ways. One was to determine the reliability of the tests and to see if failures occurred at the same angle with respect to the bend radius. The second was to determine the failure boundary for a single material, alloy 122 copper. This material was varied by wall thickness and outer diameter, but material properties and the intended bend radius at 90° was held constant. This section describes this analysis and the results.

5.2 Materials Used

Tests were run using three different materials: aluminum, steel, and copper. Each of these materials were kept constant in alloy, but varied in tube diameter and wall thickness. The aluminum and steel were only tested in a single set of dimensions, but the copper, due to its clear buckling reaction, was tested in a range of dimensions in order to observe and present the failure boundary surface.

The aluminum was only tested with a 0.75” diameter and a 0.065” wall thickness. It acted more elastic and ductile than the other materials. Results were more difficult to read and buckling occurred with less repeatability, yet the standard deviation of the data was only 4.7° off the expected angle as shown by the trend line. (See Appendix A.1)

The steel specimens were EMT (*Electrical metallic tubing)* conduit. This tubing is used as electrical conduit and is readily available. This steel tubing had an outer diameter of 0.7" and a wall thickness of 0.045". The results from tests using steel showed less ductility than aluminum, but were still more variable than the failures for copper. The standard deviation in this data was only 5.75° off the expected angle as shown by the trend line. (See Appendix A.2)

Copper tubing buckles quickly and repeatedly, so it was used to test the buckling failure boundary. It came in a selection of wall thicknesses and outer diameters as well. The copper specimens were common water line pipe, which have standard dimension call-outs. All copper specimens were copper alloy 122. The standard deviation in their data was, on average, only 1.33° off the expected angle as shown by the trend line. (See Appendix A.3)

Alloy 122 has a published Young's modulus of 18,900 psi and tensile strength of 51,800 psi. It can be expected to reach its elastic limit at 2.74% strain. Published studies are purposefully conservative about their values, so the actual expected elastic limit would be higher than this value. Because the tubes are being deformed in the plastic, rather than the elastic range, buckling, and plastic deformation, should occur after the elastic strain limit, but before the ultimate strain. According to the stress-strain curve shown in Figure 5—1, final failure in tension doesn't occur until after 17% strain (295˚K test, approximately 71˚F).

It is noteworthy that in Figure 5—1, the stress-strain curve reaches the elastic limit and immediately drops off due to necking. This may be why we are seeing strains around the yield strain at buckling for copper tubes.

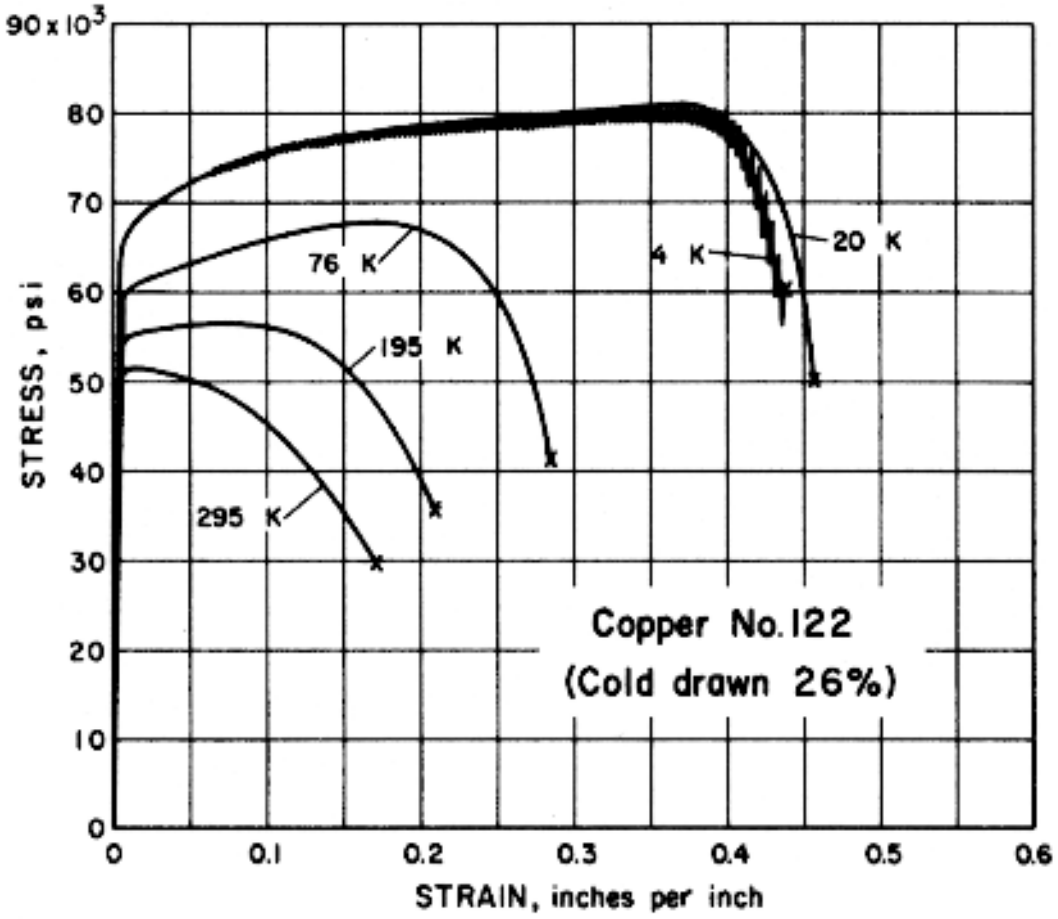

Figure 5—1: Stress strain curve for alloy 122 copper at cold temperatures

Source: http://www.copper.org

According to the ASTM B88 standard, copper pipe comes in three varieties: M, L, and K, which refer to the wall thickness. Type M has the thinnest, and type K has the thickest walls. This notation does not intentionally imply that each type M has the same wall thickness; just that Type M has a thinner wall than type K. The diameter call out is given by a nominal size.

Tests were run on four different sizes of tubing. The specimens included type M and type L wall thickness, and nominal diameters of ½" and ¾". Although the nominal size refers to the inner diameter, accurate measurements could only be taken of the outer surface during testing. The actual dimensions of the specimen are shown in Table 5—1 and Figure 5—2.

Table 5—1: Copper specimen dimensions

Nominal Size	Type	OD	Wall thickness Nominal	Tolerance
3/4	M	0.875	0.032	0.003
1/2	M	0.625	0.028	0.003
3/4	L	0.875	0.045	0.004
1/2	L	0.625	0.04	0.004

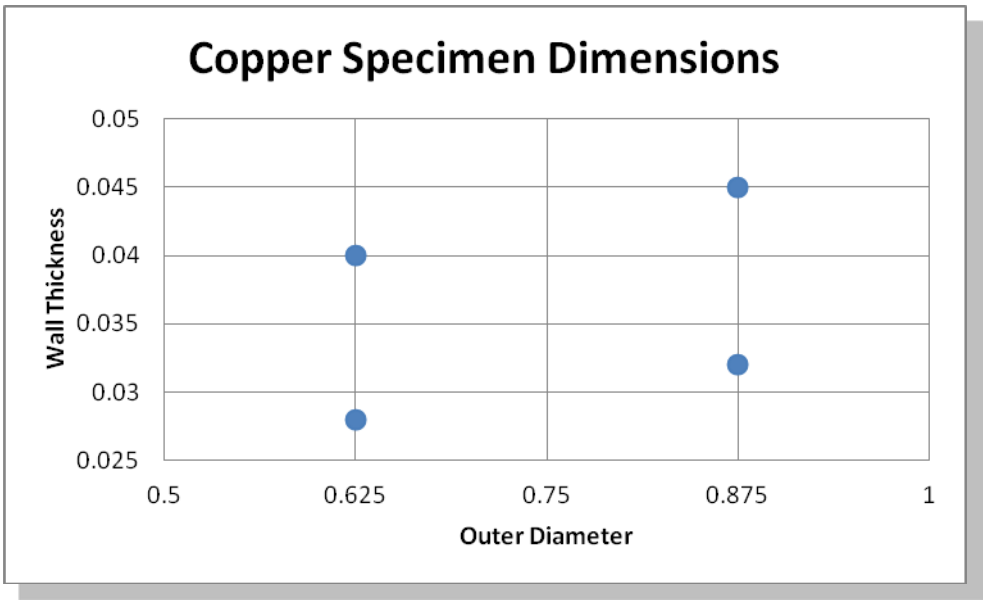

Figure 5—2: Copper specimen dimensions

5.3 Number of Tests Run

The number of runs varied, based on the availability of the material and the type of analysis desired. For the reliability analysis, multiple runs were performed for each material at each expected bend radius. For the failure boundary analysis, two to three runs were performed for each configuration.

There were 48 tests run with the aluminum material, testing at 4”, 6”, 8”, and 10” expected final bend radii. 36 of these tests were run at the 4” final bend radii with the intent to

gather some statistically significant data. Each of the other three final bend radii were tested 4 times each in order to get a range for the results.

Table 5—2: Number of tests run in aluminum

Aluminum	
Final Expected Bend Radius	Number of Runs
4	36
6	4
8	4
10	4
Total	48

EMT steel was tested in 37 runs at one inch intervals in bend radii between the 4" and 10" expected final bend radii. An expected final bend radius of 3.5" was also tested, but only once. The rest of the number of runs were mostly between a final bend radius of 4", 6", and 8", with a few scattered tests between in order to check for linearity of the test results.

Table 5—3: Number of tests run in EMT steel

EMT Steel	
Final Expected Bend Radius	Number of Runs
3.5	1
4	13
5	2
6	35
7	2
8	11
9	2
10	2
Total	68

Copper was tested for the linearity analysis and then some of the tests were used as part of the empirical data that helped build the failure boundary. For the linearity analysis, the copper

was tested over the same range as the EMT steel, with expected final bend radii between 3.5" and 10", with every inch represented between 4" and 10". Table 5—4 shows the number of runs for each expected final bend radius for each of the configurations of copper.

Table 5—4: Number of tests run in alloy 122 copper tubing

Copper
½" Type M

Final Expected Bend Radius	Number of Runs
3.5	2
4	5
5	5
6	5
7	5
8	5
9	5
10	5
Total	37

Copper
½" Type L

Final Expected Bend Radius	Number of Runs
4	5
5.5	1
6	3
8	3
10	4
Total	16

Copper
¾" Type M

Final Expected Bend Radius	Number of Runs
4	2
5	2
6	2
7	2
8	2
9	2
10	2
Total	14

Copper
¾" Type L

Final Expected Bend Radius	Number of Runs
4	4
6	3
8	3
10	4
Total	14

5.4 Linearity Analysis

The first analysis was intended to show the linearity of the results as the machine is used and materials are tested. The tests were grouped by material specifications and dimensions and results were plotted as the observed buckling angle against the expected final bend radius. The results are shown in Figure 5—3, which shows each material's results and includes a trend line for each. This trend line was used as an expected value when analyzing the normal probability.

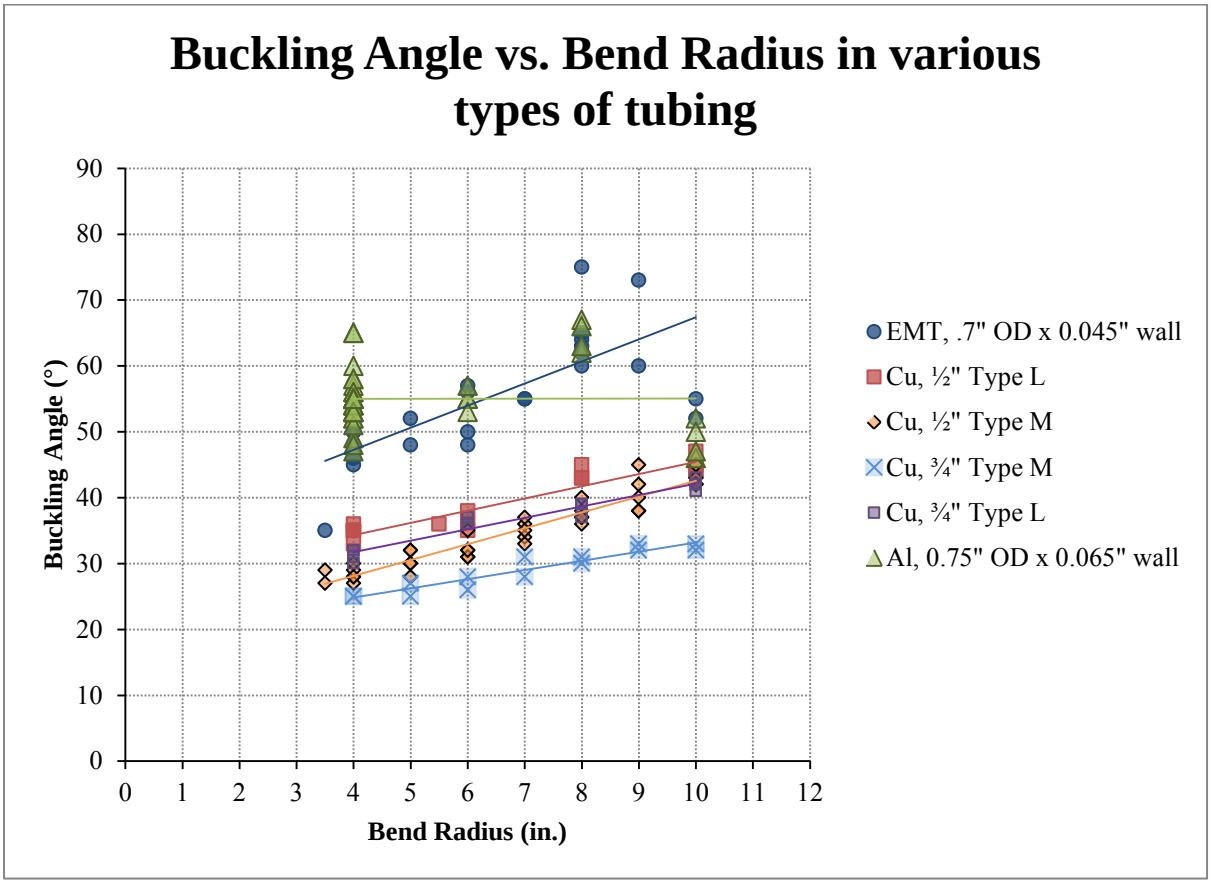

Figure 5—3: Buckling angle vs. bend radius for each material configuration

From the linearity analysis, it is shown that the buckling angle is approximately linearly proportional to the free length being bent. For copper this relationship is very clear. For aluminum and EMT, this data is clear, yet a larger spread is seen in the data. A trend line was taken and residuals were plotted for each material. These residuals were then analyzed through a

normal probability plot and their data appears to describe a normal distribution around the trend line. The residuals show whether there is a good fit between the data and the curve fit line. The normal probability plot shows how well the data can be described with a normal probability curve about the curve fit line. The data from the copper tests show that the curve fit line accurately predicts the data and that the data falls in an approximately normal distribution about this line. This indicates that the tests that were done were reliable over the range of specimen dimensions and that the material and machine function in a reliable manner. The plots corresponding to this analysis can be found in 0. An example is shown here for 3/4" Type M Copper.

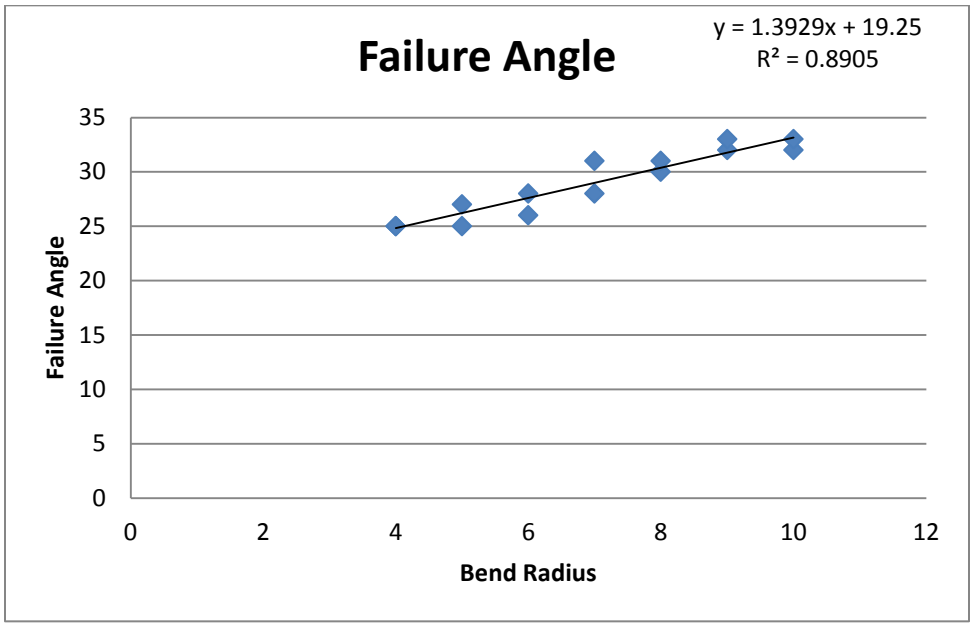

Figure 5—4:Failure angle data for ½" x L copper tubing

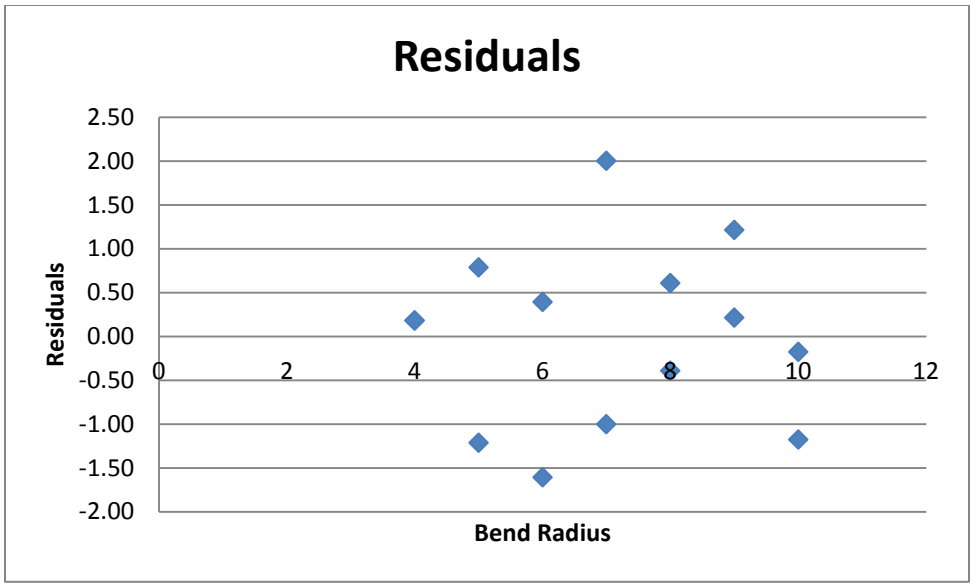

Figure 5—4a:Statistical analysis of residuals for ½" x L copper tubing

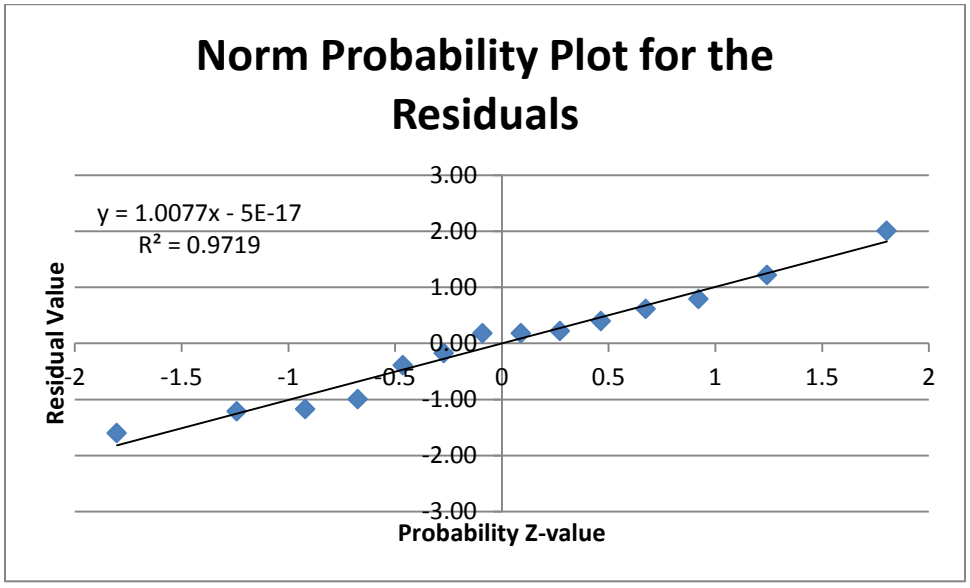

Figure 5—4b: Normal probability plot of the residuals for ½" x L copper tubing

5.5 Buckling Failure Boundary Analysis

The results from the copper tests were used to find the buckling failure boundary empirically. Copper was used because, as is shown, copper acted the most predictably at each

bend radius. As mentioned above, the standard deviation in its buckling angles was only 1.33° compared to 5° for the other materials. Materials other than copper can be tested in the same way, although more data will need to be gathered in order to produce a statistically significant result.

The copper was tested at four configurations of outer diameter and wall thickness, as mentioned above. Each of these configurations was tested at an expected final bend radius of 4", 6", 8", and 10" and at least two times in order to show repeatability. The number of runs for each final bend radius can be seen above in Table 5—4. This data is plotted in Figure 5—5 showing each individual specimen's expected bend versus its buckling angle.

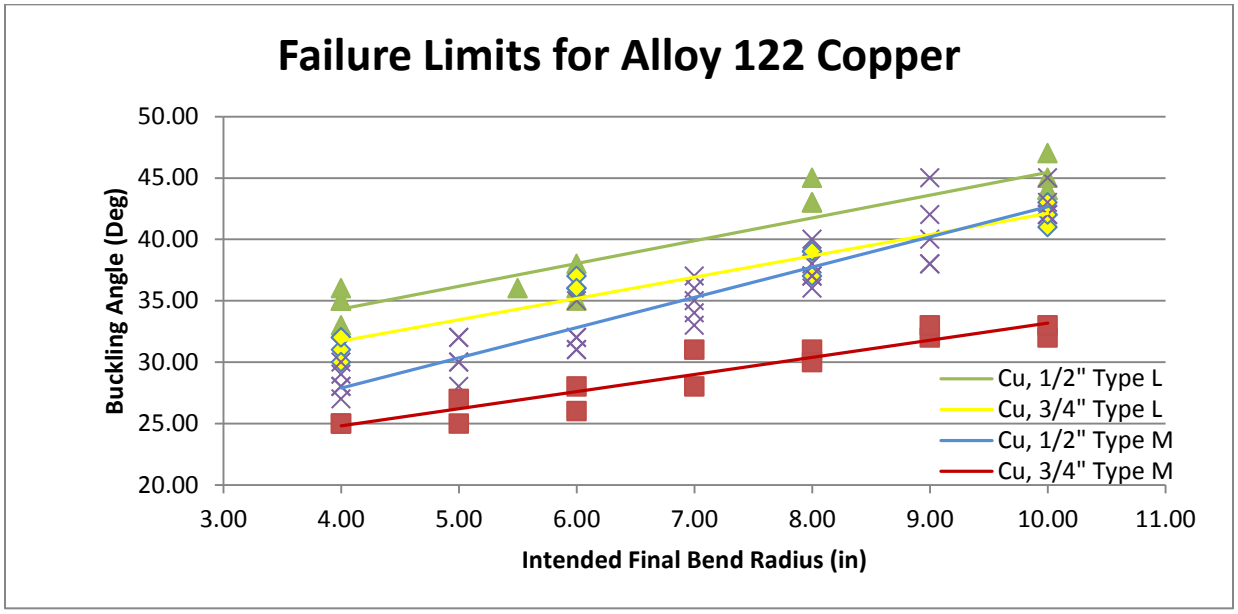

Figure 5—5: Failure limits for alloy 122 copper tubing

This data was analyzed in a surface plot with the values of the intended final bend radius and the thickness divided by the outer diameter forming the XY plane and the buckling failure angle forming the Z axis. The thickness divided by the outer diameter was used as an axis in order to relate the specimen shape to the failure angle. As can be seen in Figure 5—6, the data shows an upward trend where the larger the intended bend radius, the higher the failure angle.

Also the data shows a similar upward trend with respect to the thickness divided by outer diameter, although this relationship does not hold true for larger intended bend radii.

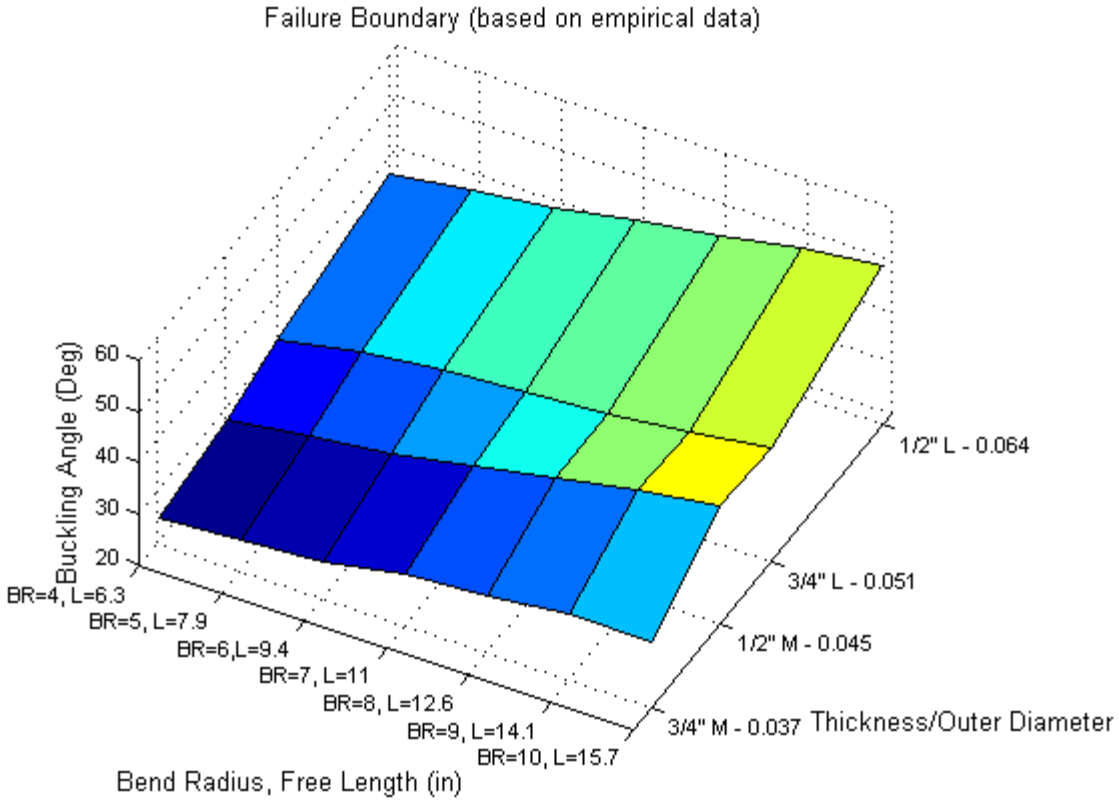

Figure 5—6: 3D plot of the surface failure boundary for copper tubing.

Due to the lack of a clear relationship between the buckling angle and the specimen dimensions, the initial two dimensional plot was preferred (Figure 5—7). To create this plot the trend lines were then plotted with the Y axis charting the failure limit and the X axis giving the way the specimen was held. This was done in two ways. First, the buckling angle was plotted with respect to the radius the machine was trying to reach at 90°. The data was plotted in a way that shows the information as it was given to and read from the machine. At setup, the machine asks for the final expected bend radius. Then, as the user observes buckling, they record the buckling angle off the protractor.

A second plot is made using data the design engineer or the technician would use. When the expected final bend radius is put into the machine it is converted into a free length by multiplying by the final expected bend angle, 90° ($\pi/2$ radians) in these tests. The final buckling angle can be converted into a final buckling radius by dividing the free length by the buckling angle. In the second plot the free length has been plotted versus the buckling radius.

These two plots are therefore essentially equivalent. The final expected bend radius and the free length are essentially the same term due to the final expected bend angle always being 90°. The buckling angle and the buckling radius both describe the buckling phenomenon, but show it in somewhat opposite ways. As the angle increases, the bend radius decreases, therefore, they are inversely related. The results from this test are shown plotted in Figure 5—7. The plotted points form a limit where any bend angle configuration above the buckling limit is expected to fail.

The buckling failure boundary analysis for the copper materials shows the relationship between bend radius, or free length, and the failure angle, or the failure radius. The angle, or radius, at which the material will fail increases as the bend radius, or free length, is increased. Also, there is a relationship between the dimensions (thickness and outer diameter) of the cross-section of the tube that affects the expected buckle angle. This can be seen in Figure 5—5 above where the thinner wall tubes buckle sooner (lower buckling limit).

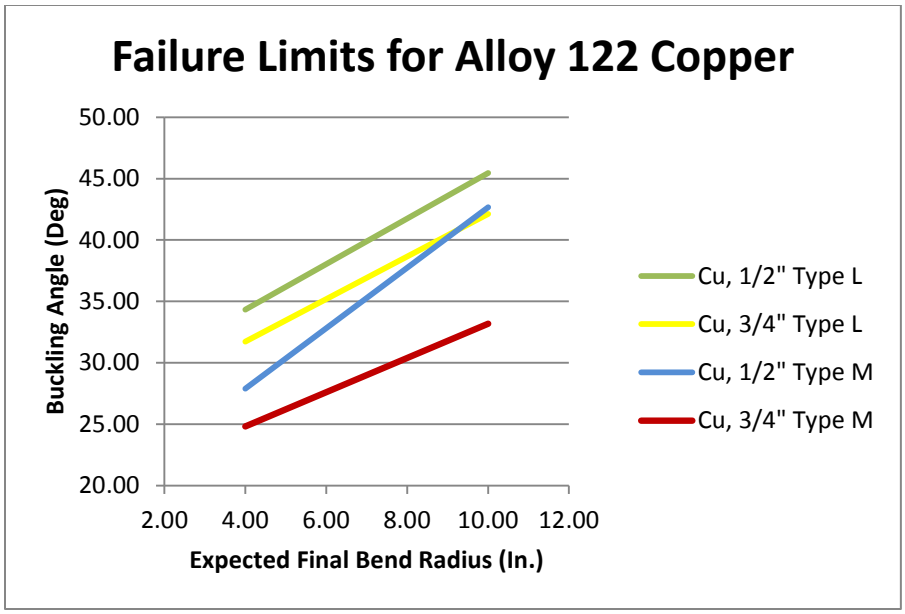

a) Buckling angle vs. expected final bend radius

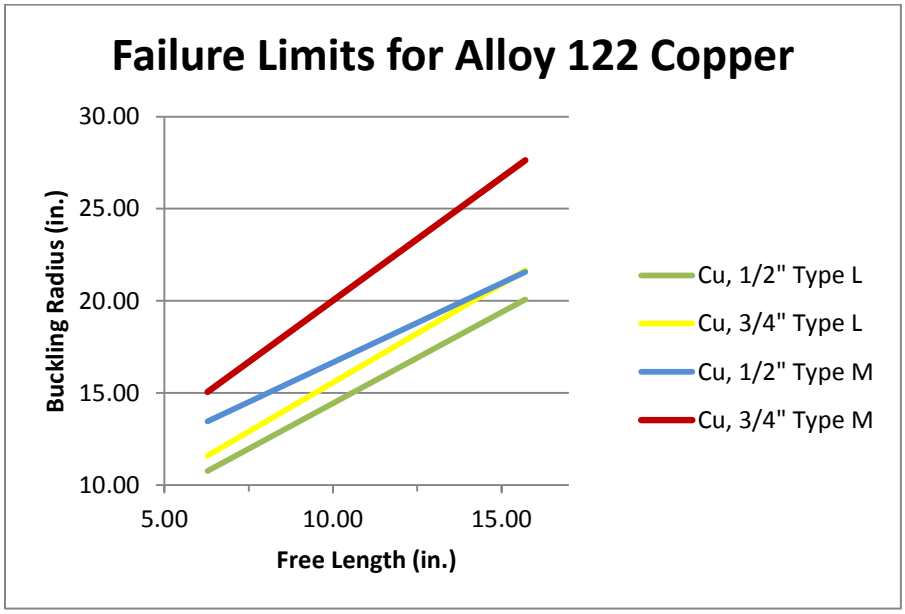

b) Buckling radius vs. free length

Figure 5—7: Failure limits for alloy 122 copper

5.6 Discussion

The air bending process is shown here to be a reliable process for bending a tube and failure happens at the expected parameters. Due to this information a machine operator can be

confident that if the parameters can be plotted below the surface shown in Figure 5—7, the tube will not be expected to buckle. If a material other than alloy 122 copper is intended to be bent, a similar plot can be created.

6 CONCLUSIONS

6.1 Summary of Work

The work performed by this thesis includes modifying a prototype for an arborless bending machine and improving its practical use as a tube bending apparatus, developing a sophisticated control system, testing the repeatability of the system, and creating a failure boundary for buckling, which has been validated through testing and analysis. Although the prototype was nearly usable at the start of the project, much work was done to test the control systems, improve the instrumentation, and make the software more user-friendly and the apparatus more reliable. Once a usable prototype was established, tests were performed to determine the repeatability of the system on a number of different materials, for a range of sizes and bend radii.

A buckling failure boundary was empirically created through testing a variety of dimensional configurations of copper tubes. This empirical study has been examined through an analytical model, which has shown the viability of the empirical tests. It has been demonstrated that bending tubing is possible without the use of an arbor, as long as a pure bending moment is applied and the neutral axis of the tubing is held at a constant length. The free length and dimensions of the tubing turned out to be the driving factors in predicting the buckling angle.

The scope of work included running nearly 200 tests on a variety of sizes and materials of tubes, over a range of bend radii, in order to validate the test apparatus' repeatability. Alloy 122

copper was tested in enough configurations and free lengths that an empirical failure boundary was able to be completed. Also included in the scope of the project, was an analysis of the tri-axial strains that are applied to the material as it bends and ovalizes.

6.2 Discussion Comparing Analytical and Empirical Results

Data calculated from the empirical tests using the analytical study was predictably close to the data expected from published stress-strain data. The example given in the discussion at the end of the analytical study was of a test specimen that had a maximum strain of 2.67% occurring in the radial direction (thickness change) at the south outer point at the time of buckling. According to the data reference in the empirical section, the total strain should reach about 2.74% at the elastic limit, but then fall off quickly after that. Because failure occurred near the yield value for all of the copper tests, we can confirm that the equations can be used to validate the empirical study. Any discrepancy is most likely due to unintentionally applied axial loads applied to the material. Compressive axial strain data was not accessible for this material.

6.3 Observed Results

From the tests and discussion, it is shown that bending a tube without the use of an arbor is possible with the right configuration of the apparatus. In order to accomplish this, it is important to keep the length of the neutral axis of the tubing constant throughout the bend and apply a pure bending moment. There is some room for error in this area, but if the calculated neutral axis is not close to its original length, an axial load will be applied to the tubing and will result in a non-pure bending moment. In a bend where a 5 inch bend radius is desired at 90°, the neutral axis is shifted by 0.008624” toward the center of curvature, resulting in an increase in arc length, and consequential clamp adjustment, of approximately 0.5” required in order to avoid

applying the axial load. This was accounted for by moving the clamps as described in Section 4.1.1. Without this adjustment, pure bending could not be achieved.

It was observed that failure typically occurred directly centered between the two clamps, and that the typical mode of failure was ovalization, followed by buckling at that center point. Occasionally, a wrinkle buckling failure would occur near the clamp, but it was a rare occurrence. The main buckling failure occurred inside the bend, at the South point, where the bending strain and cross-section strain are compressive, when the tube reached the buckling point due to the bending moment applied. Failure would also, in part, occur due to the non-uniformity of the material and possible failure of the linear actuators to keep up with the desired motion.

It was also shown that the angle at which a tube will buckle depends directly on the length of the unsupported section as well as the physical dimensions of the specimen. This was shown through an empirical failure boundary, consisting of a three-dimensional surface plotted with the axis being the unsupported length, the dimensions of the tube, and the dependent variable being the angle at which a specimen exhibited the onset of buckling. This boundary is limited due to the low number of actual tests at each point, but the test was shown to be repeatable.

6.3.1 Contributions

The work contained herein is significant due to its contribution to a new kind of tube bending apparatus. The ability to form a tube without the use of an arbor has the potential to improve the change-over time in manufacturing procedures, as well as to allow finned coils to be bent predictably without buckling the coils. In order to accomplish this arborless bend, a set of movable clamps have been analyzed, which keep the moment pure throughout the forming

process. No finned coils were tested, but as the tubes within the finned coils are copper the failure boundary created for the tubes is informative. This research was done with the intent to gather understanding of the buckling phenomenon that could then be applied to finned tubes.

The work is not exhaustive, but a variety of types and dimensions of tubes have been tested in order to validate the system. A failure boundary model has been offered as a basis to build failure boundaries for other materials, within which would allow the machine operator to avoid buckling on any material they are interested in working with.

6.4 Future Work

In order for this work to be more comprehensive, an extensive study of different materials should be done with different diameters and wall thicknesses. Specifically, materials such as aluminum and the EMT steel studied have high variability due to their slow buckling failures. A higher number of tests of these could be done that would allow for a more statistically significant failure boundary to be created.

Initially, this project was given to a Capstone team with the intent to be able to bend finned coils without damaging the fins or the coils. Tests of finned coils under pure bending will be necessary to determine how much the close-fitting fins reinforce the tubes, resisting ovalization and buckling. The fins are expected to support the tubing and delay buckling, however, the foregoing analysis only approximates their behavior by testing copper tubing without the fins. The analysis here looks at the fundamental behavior of a tube in pure bending, and from there, assumptions may be made that would aid in predicting buckling in a finned coil assembly.

The analysis and data presented here provide an opportunity for future work in the fields of the post-yield behavior and flow law associated with buckling. The comparison of the analysis

results to the empirical data should be studied to understand how the material behaves under post-yielding. Providing a flow law for this behavior would be beneficial as well. The successful development of a model for tri-axial strains in a tube bending process could provide a well-defined strain field for development of a tri-axial flow law. Further tests to determine the associated tri-axial stresses are under investigation.

REFERENCES

Brazier, L. G."The flexure of thin cylindrical shells and other 'thin' sections." Proc. Royal Society Series A no. 116 (1927): 104-114.

Budynas, R. G. *Advanced Strength and Applied Stress Analysis first edition*. New York: McGraw-Hill, 1977.

Budynas, R. G., and Keith Nisbett. *Mechanical Engineering Design, Shigle'ys 9th Ed*. New York: McGraw-Hill, 2011.

Calladine, C. R. "Limit analysis of curved tubes." *Journal of Mechanical Engineering Science* 16 (1974): 85-87.

Cheng, P. "Weight Optimization of Cylindrical Shells with Cellular Cores." Cambridge, MA: MIT, 1996.

Copper.org. http://www.copper.org/resources/properties/144_8/144_8.html (accessed February 1, 2012).

Datsko, J. *Materials in Design and Manufacturing*. Ann Arbor, MI: Malloy Inc., 1977.

Datsko, J. *Material Properties and Manufacturing Processes*. New York, NY: John Wiley and Sons Inc., 1966.

Gere, J. M. *Mechanics of Materials 5th ed.*. Pacific Grove, CA: Brooks/Cole, 2001.

Korol, R. M. "Buckling of circular tubes in bending." *Journal of Engineering Mechanics* ASCE 104 no. 4 (1978): 289-290, 939+.

Norton, R. L. *Machine Design: an Integrated Approach 3rd ed.* Upper Saddle River, NJ: Pearson Education, 2006.

Pan, K., K. A. Stelson. "On the Plastic Deformation of a Tube during Bending." Transactions of the ASME 117 (1995): 494-500.

Young, W. C, and R. G. Budynas. *Roark's Formulas for Stress and Strain 7th Ed*. New York, NY: McGraw-Hill, 2002.

Wang, X. and J. Cao. "Wrinkling Limit in Tube Buckling." *Journal of Engineering Materials and Technology* 123 (2001): 430-435

APPENDIX A: User Manual

The following pages contain a user manual that was developed by Joel Bloomer throughout the project. It includes a user manual for the machine as well as instructions on how to create a new clamp that aligns properly with the machine and will not cause unintentional loads.

Contents

Table of Figures

Running the machine

Opening LabView and starting the program.

The bending machine is run by a LabView program. On the computer currently in use, this program can be found on the desktop, in the "Flextech v16" folder as shown below in Figure 1.

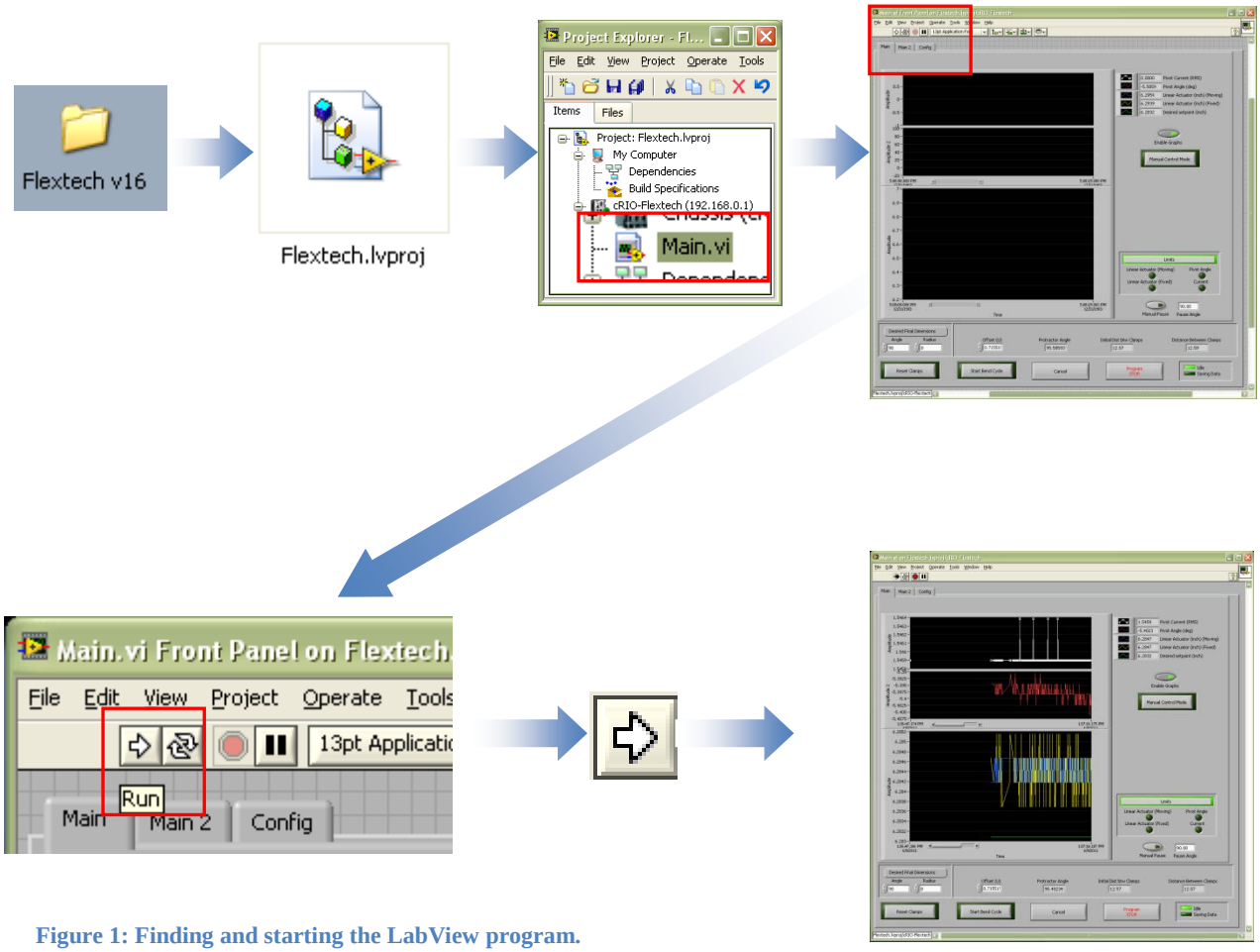

Figure 1: Finding and starting the LabView program.

From the *Flextech* folder, go to "Flextech.lvproj," "Main.vi," and then hit the "Run" button. Save all changes suggested by the program.

Using LabView to operate the machine

Once the program is running, the basic process for using the machine is as shown in Figure 2.

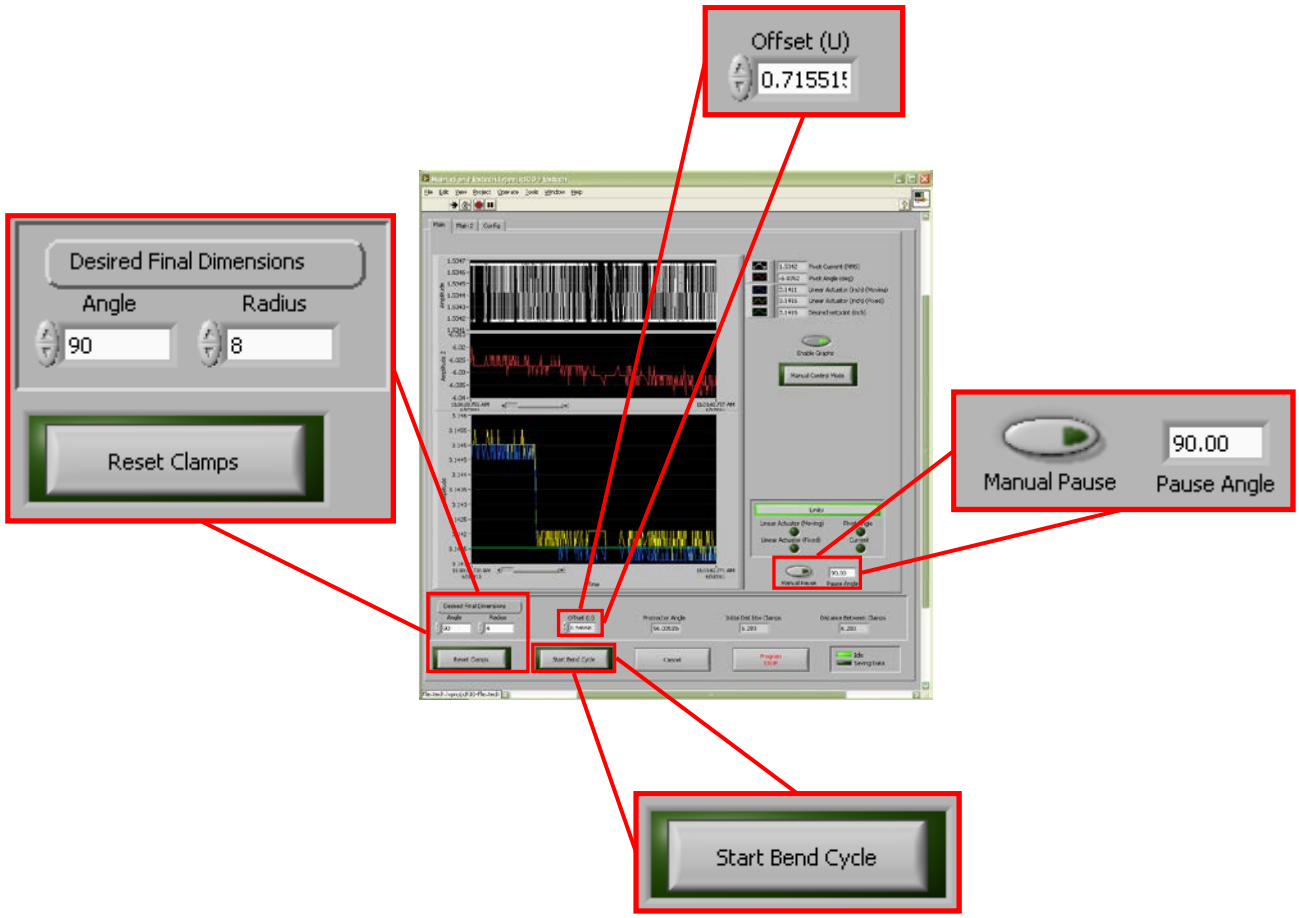

Figure 2: Running the LabView program, clockwise from the left:

1. Set the desired final dimensions, and then hit "Reset" to position the clamps. It is sometimes necessary to hit "Reset" a second time after the clamps have stopped moving in order to get them to the proper position.
2. After the pipe specimen has been cut (if desired—see Figure 3) and then secured in the clamps, measure the offset (see Figure 6) and enter its value.
3. Verify that the pause angle is correct.
4. Hit "Start Bend Cycle" to run the machine.

NOTE: Lengths are given in inches, angles in degrees.

Preparing and securing samples

In order to prepare to run a bend test, it will be necessary to cut a piece of tubing to fit the bending machine. The length of this sample should be just barely longer than the distance from the far edges of the vise jaw inserts, as shown in Figure 3. If it is any shorter than that distance and there is a burr on the outside of the cut edge, it may interfere with the clamping action and cause inconsistent bend behavior. This can be avoided by de-burring the tubing before clamping it. It can also be avoided by using a cutting method that does not leave a burr on the outside of the tubing, such as a rotating pipe-cutter.

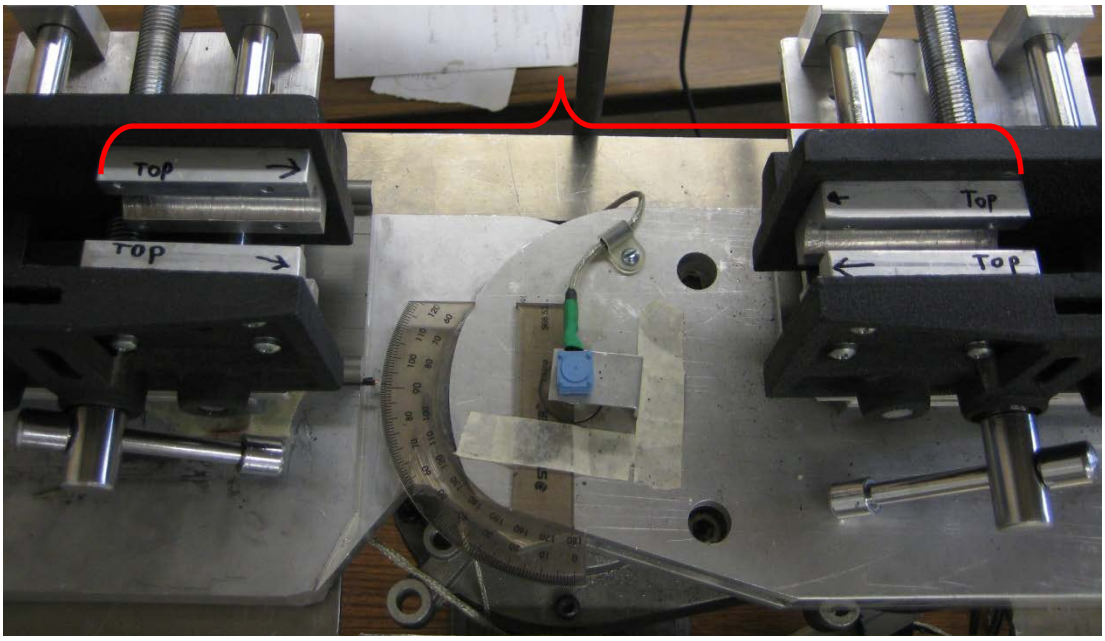

Figure 3: Determining the length to cut tubing for bending tests.
Tubing samples for bend tests should be cut to this length *after* the clamps' positions have been reset in the LabView program.

In order to ensure that the vise jaws are uniformly gripping the tubing, the spacer in each set of jaws must be adjusted. A poorly adjusted spacer will either prevent the vise from gripping the tubing, or will cause the vise to pinch one point of the tube while leaving the rest of it unsupported. **A poorly adjusted vise spacer will result in inconsistent bend behavior.** The vise jaw spacer can be adjusted as shown in Figure 4.

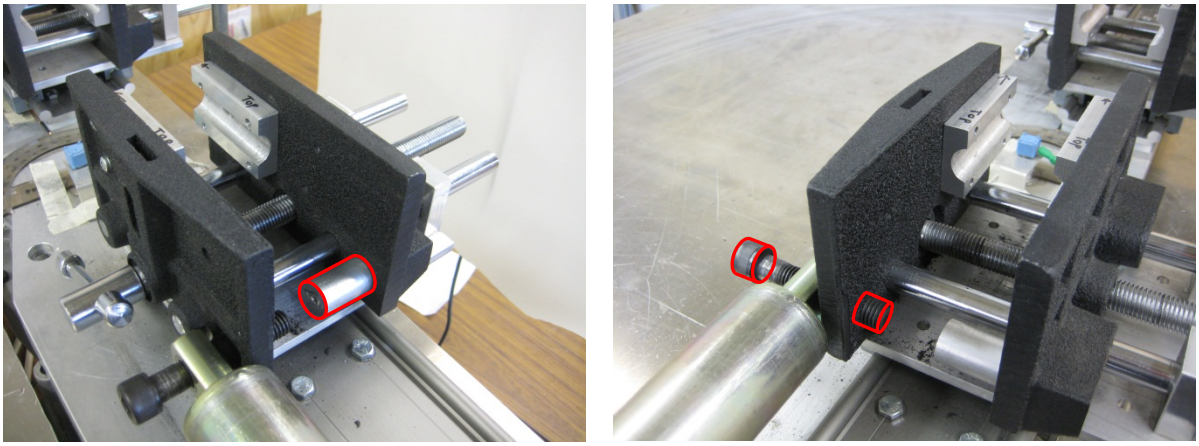

Figure 4: Adjusting the vise jaw spacers.
The spacer is located diagonally opposite the clamping point and is intended to ensure that the vise jaws remain aligned while clamping the tubing. The fixed spacer is highlighted in the picture on the left. It can be removed if necessary to accommodate smaller tubing or thinner vise jaws. The spacing can also be adjusted using the bolt highlighted in the picture on the right.

The vises themselves are low quality and very finicky; however, if the tubing is not clamped tightly enough, then it will cause problems in finding a consistent buckling angle. I have used a 5" long piece of EMT as a handle extension on the vise in order to get a sufficient clamping force. Once the specimen has completed a bend cycle, it takes a somewhat longer handle extension to get the vises to release the specimen. This will probably break the vises eventually, but seems to be necessary to make the current equipment work.

Determining the offset

The motion of the clamps during a bend cycle is calculated to allow the tubing to bend without buckling for as long as possible. Correctly calculating this motion depends on knowing the distance between the neutral axis of the tubing and the central pivot point of the bending machine. This is called the "Offset." The inside face of the fixed jaw of each vise is lined up with the machine's pivot point, so the offset for a given tubing specimen is simply the distance from the fixed clamp jaw face to the center of the tube in question. This is illustrated in Figure 5.

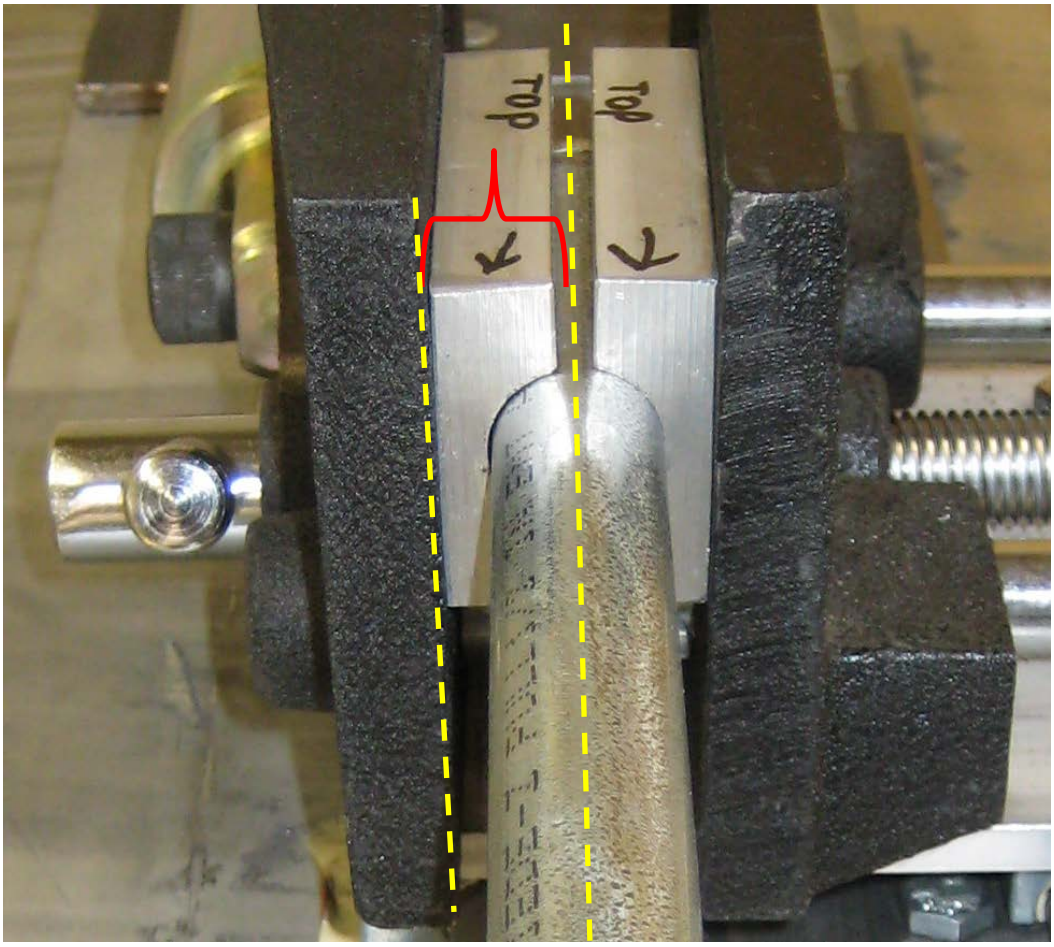

Figure 5: Measuring the offset
The offset is the distance from the fixed face of the clamp to the center of the clamped tubing.

Pausing the machine

During the bending process, it may be necessary to stop the machine—usually to take extra measurements, but perhaps for other reasons, too. While the "Cancel" button will stop the machine, it will also make it impossible to complete the bend cycle you have started. A better option is to use the "Manual Pause" button, which will pause the bend cycle until you hit the button a second time.

The best option is to plan ahead and use the “Pause Angle” setting. If, for instance, you need to pause the bend cycle every 10° so that you can measure the changing cross section then you can follow these steps:

1. Before you start the bend cycle, set the “Pause Angle” to 10°
2. Start the bend cycle. It will automatically run until it hits 10°, and then it will automatically stop and wait for further input.
3. When you are ready to go on another 10°, enter 20° in the “Pause Angle” field; the machine will not go on until you either hit “Enter” or click outside of the “Pause Angle” field.
4. Repeat as necessary.

The machine then uses the rotational potentiometer to track its angle and will pause the machine at 10°. One special case requires the combination of an input "Pause Angle" as well as the use of the "Manual Pause" button. Some very springy materials may reach the preset pause angle and then spring back far enough that the machine will turn on again in order to bring them back to the pause angle. This can result in an oscillation that makes taking any measurements next to impossible. "Manual Pause" will stop the oscillations, and a new pause angle can be input while the machine is stopped.

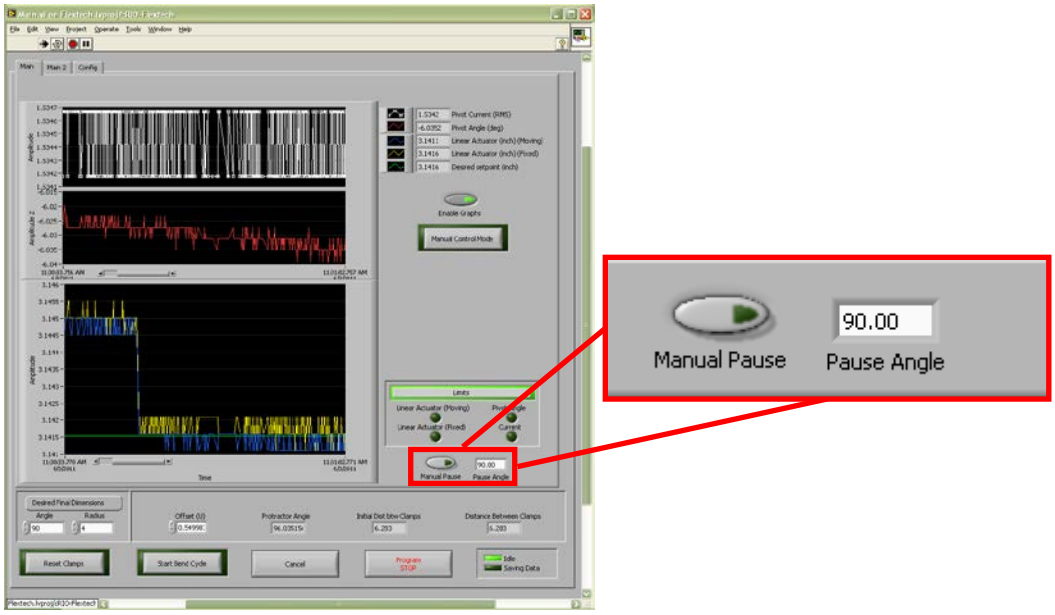

Figure 6: The "Manual Pause" button and the "Pause Angle" setting.
The “Manual Pause” button and the “Pause Angle” setting. “Manual Pause” pauses the bend cycle with one click and lets it continue with a second click. The “Pause Angle” setting allows you to stop the machine at a specific point. Entering a new “Pause Angle” after it has reached the first one allows the machine to continue from its current position to the new angle specified.

Recording Video and Interpreting Results

While LabView runs the actual bending of the samples, it does not take any data. The operator must either simultaneously watch the sample for buckling and the angle of the machine, or he/she can record the sample bend cycle on video for later review. This latter route is much more reliable, especially because determining the precise buckling angle can be very subjective. If all of the experimental runs are recorded, they can later be compared to one another in order to ensure consistent measurements.

Capturing Video with Windows Movie Maker

All of the bend samples that have been run so far have been recorded using Windows Movie Maker. While the program is capable of far more advanced operations, capturing video with the program is fairly simple. The basic program startup is shown in Figure 7, and the settings used for video capture in the tests so far are shown in Figure 8.

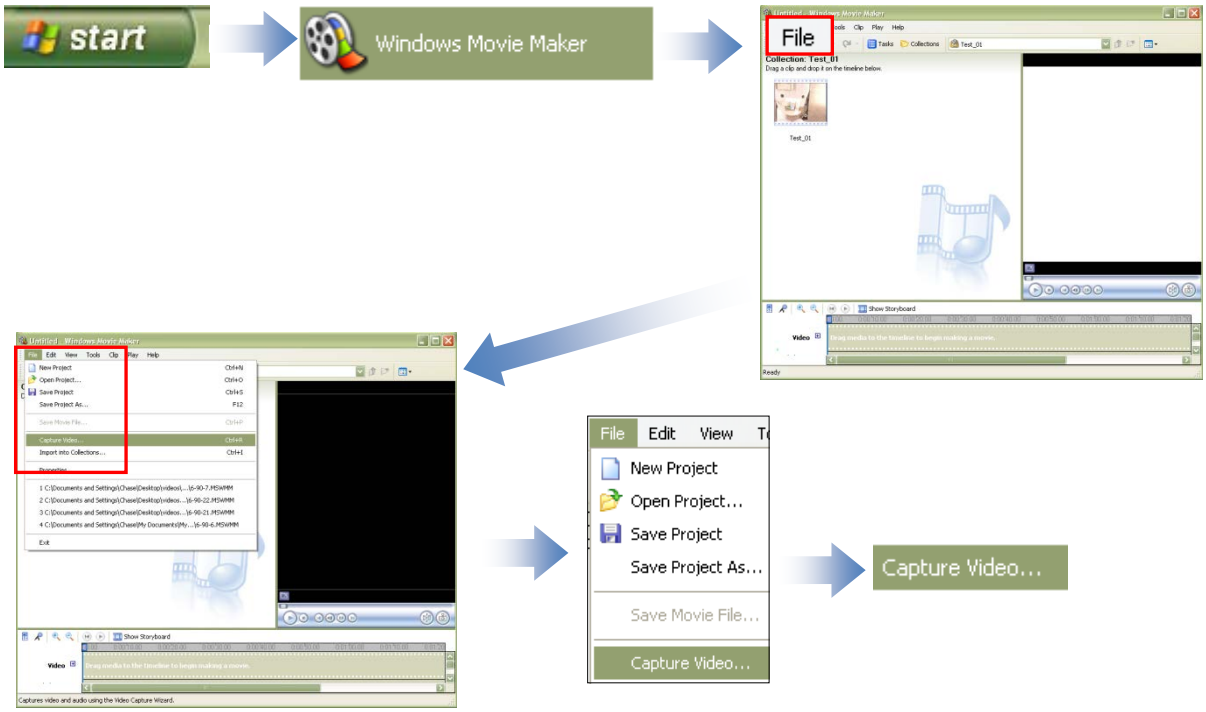

Figure 7: Finding Windows Movie Maker and initiating a video capture

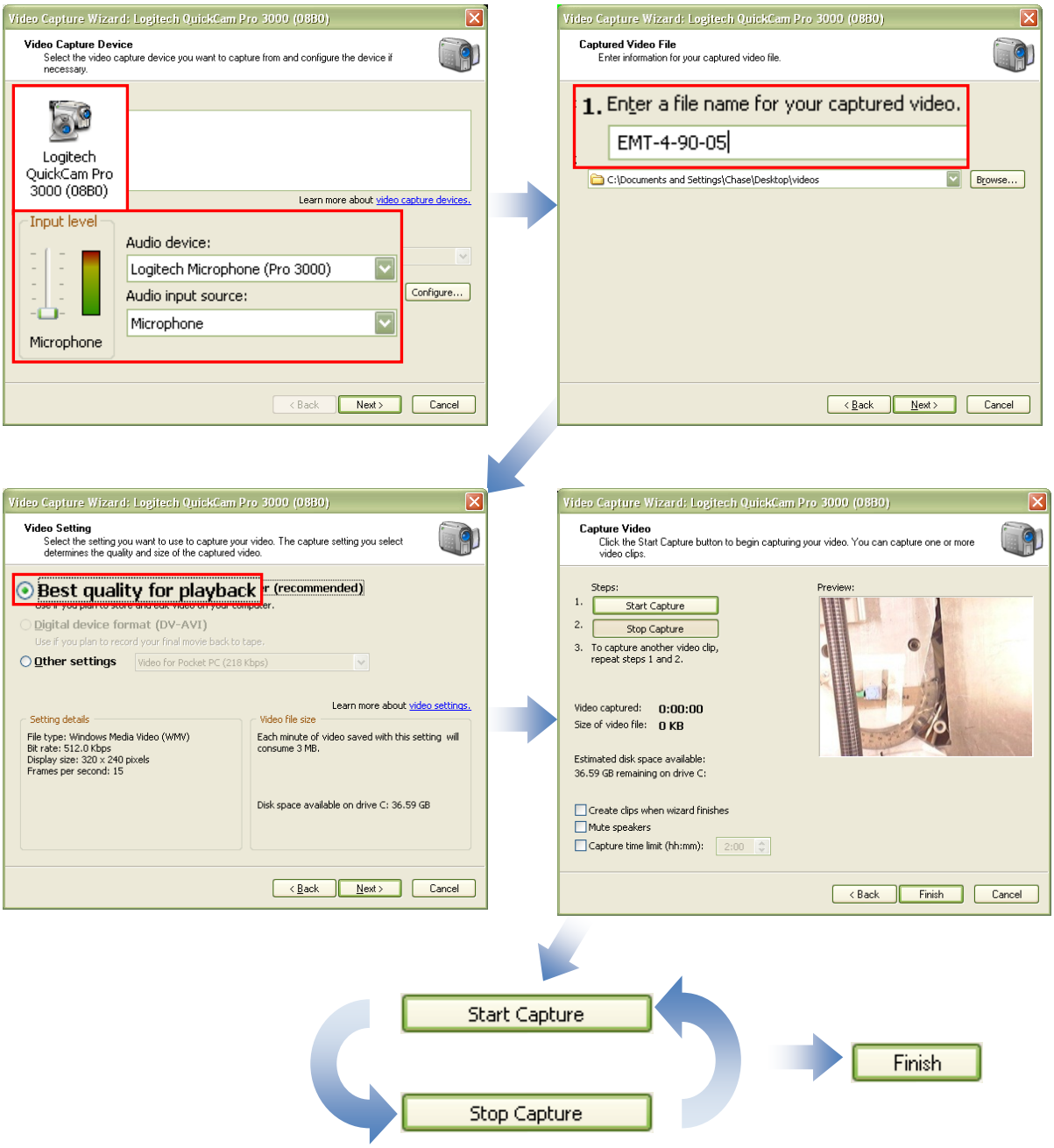

Figure 8: Capturing video in Windows Movie Maker

1. Select the video capture device. The current setup uses a Logitech QuickCam Pro 3000. The audio input can also be specified, but is largely unimportant.
2. The file names used indicate several of the test parameters. They follow the format [Material]-[Bend Radius]-[Bend Angle]-[Test Number]. EMT-4-90-05 is the fifth test of EMT bent in a four inch radius to 90°.
3. The default video setting is "Best quality." This is what has been used so far.
4. On the final screen, "Start Capture" starts recording video. You can start and stop several times, and all of the videos will be stitched together into one clip until you hit the "Finish" button. This allows you to stop recording if you need to take measurements of the tubing dimensions or if you need to stop the bend cycle for any other reason.

Reviewing Video Frame-by-Frame

Once the video has been saved, Windows Movie Maker also proves to be a good tool to view the videos and determine the buckling angle. It provides the option of moving the video forward and backward one frame at a time, thus allowing comparison of the tubing at every degree of bending angle. Finding the buckling angle while letting the video play or by trying to pause at the correct point in the video gives a resolution in the range of about ±5°, as shown in Figure 9. Moving frame-by-frame allows a resolution as fine as within 1° of buckling, as shown in Figure 10.

Figure 9: Determining buckling angle with "Play" and "Pause" alone
Simply watching the video and pausing it at the right time reveals that this copper sample buckled between 65° and 55° (protractor angle).

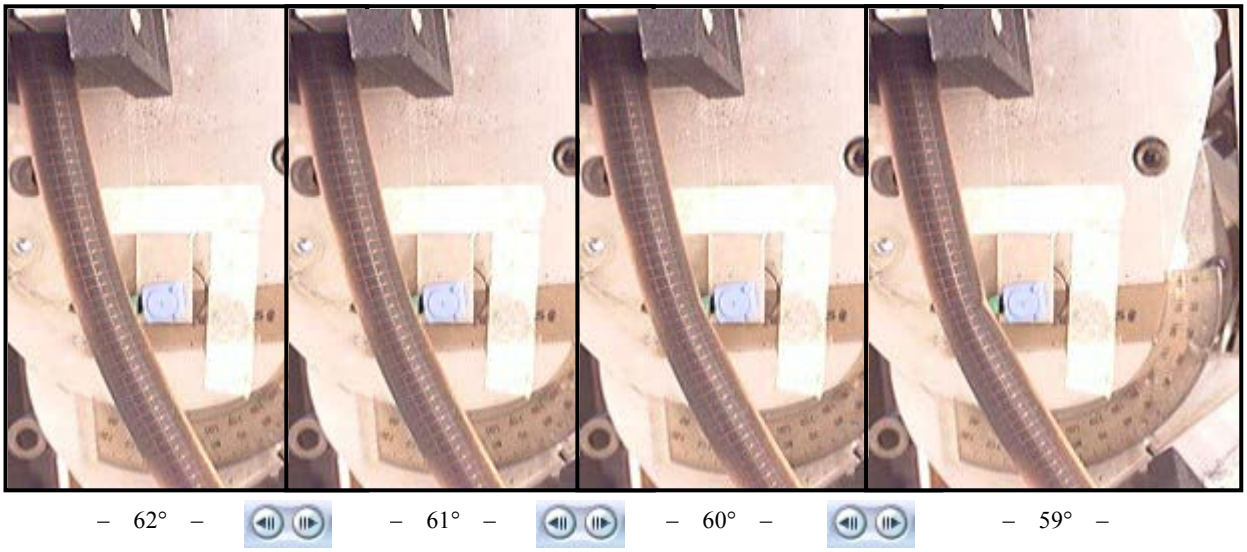

Figure 10: Determining buckling angle by viewing footage frame-by-frame

Using the frame-by-frame viewing available in Windows Movie Maker allows comparison of the sample at 62°, 61°, 60°, and 59° protractor angles, as shown above. Buckling has clearly occurred by 60° but is uncertain at 61°. I interpreted this sample as buckling at 61°.

Note that the angle shown on the protractor is the compliment angle to the bend angle. This means that when the protractor shows 90°, the bend angle is 0°, and when the protractor says 0°, the bend angle is 90°. For some samples, frame-by-frame viewing ensures that you can determine a buckling angle accurately to the degree. In other cases, the difficulty in determining the buckling angle is due to a very gradual buckling process. For the purposes of this experiment, buckling occurs as soon as the curve of the tubing goes from a uniform radius to a sharper radius near the middle of the sample. This is followed by a rapid decrease in tubing width at the buckling site, and finally by the formation of an obvious kink in the tube. In some cases, as with the copper tubing in Figure 10, these three stages of buckling occur almost simultaneously and the buckling angle is clear. For other samples, they occur so gradually that it is nearly impossible to decide at what angle they actually begin. This illustrated in Figure 11 and Figure 12.

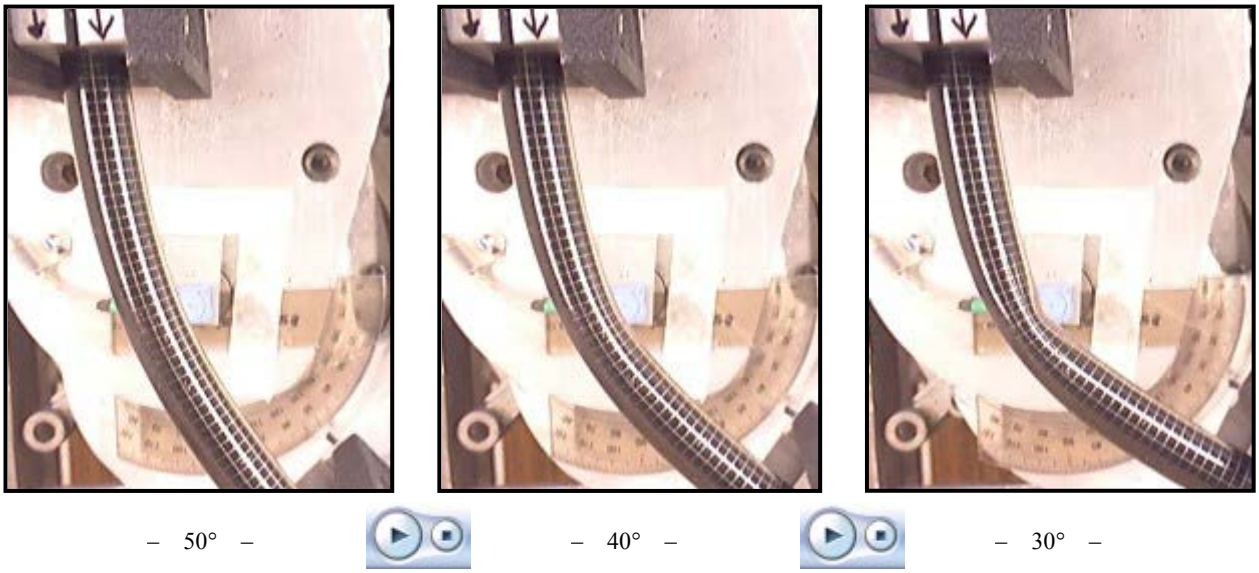

Figure 11: Using "Play" and "Pause" for a more ambiguous sample

Simply viewing the video and pausing it at the right time reveals that this EMT sample buckled between 50° and 30° (protractor angles). 40° looks like it's very close to the actual buckling angle, but there is no definite kinking point.

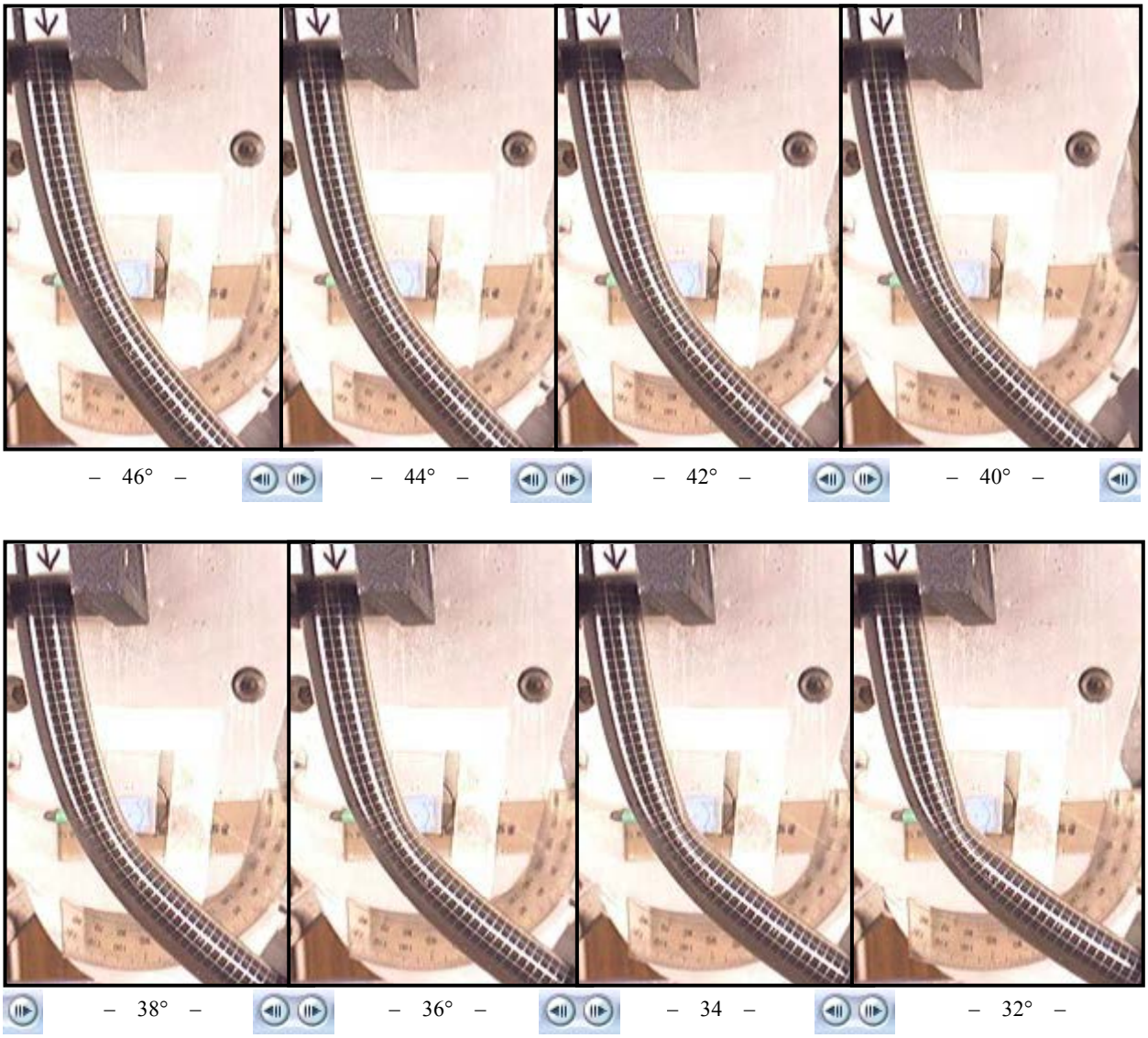

Figure 12: Stages of the buckling process viewed frame-by-frame

Using the frame-by-frame viewing available in Windows Movie Maker allows comparison of the sample at small increments from 46° to 32° (protractor angles). There seems to be a clear kinking point by about 36°. The sample has undergone a noticeable decrease in cross-section by 40° or 38°. The curve of the tube is no longer continuous somewhere around 42°. I interpreted this sample as buckling at 41°.

The examples shown in this section use the "protractor angle" to measure buckling. A pin on the moving arm of the bending machine points to a plastic protractor taped to the fixed arm of the machine during the bend cycle. When the tube is completely straight, this instrument reads 90°, and at the completion of a 90° bend cycle it reads 0°. A more meaningful measurement for analysis is the actual "bend angle," which is simply 90° minus the protractor angle.

Building Clamp Jaw Inserts for the Machine:

In order for the samples to bend consistently, they must be gripped properly in the bending machine clamp jaws. The clamp jaws themselves are flat, which would tend to flatten the tubing specimens and make them buckle prematurely right next to the clamp jaws. To prevent this, there are different sizes of clamp jaw inserts that are shaped to fully support and uniformly clamp the tubing specimens; these are shown in Figure 16. Using the best-fit clamp jaw will provide the most consistent experimental results.

Critical Dimensions:

When it becomes necessary to build new clamp jaw inserts, the critical features are: diameter, fixed-jaw offset, concentricity, leading-edge spacing, and bolt spacing.

Diameter:

Of course, the diameter of the channels in the vise jaw inserts should match the outside diameter of the tubing that you want to bend.

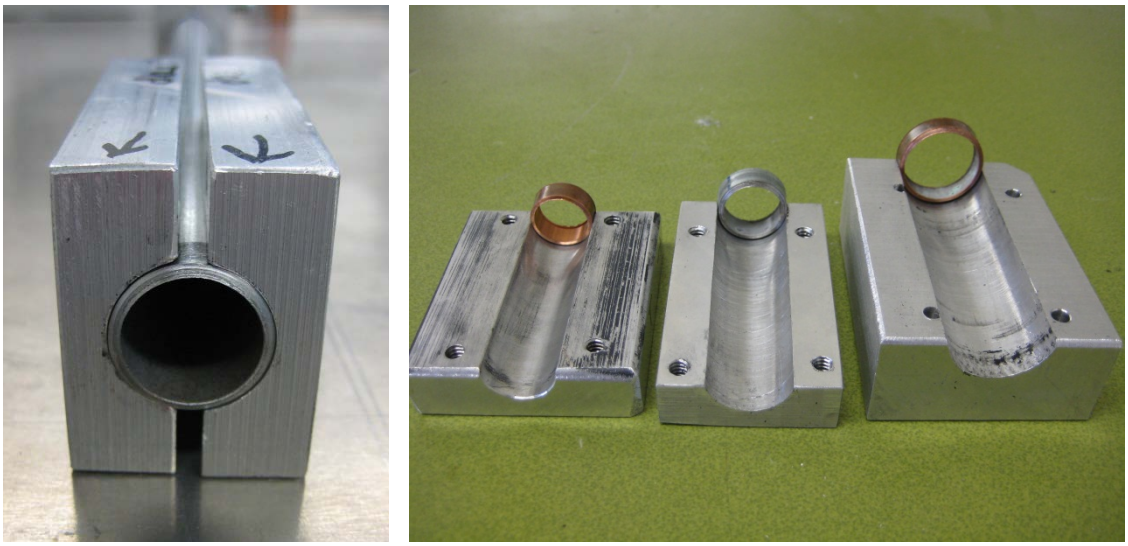

Figure 13: Various sizes of clamp jaw inserts
The curvature of the clamp jaw insert should match the tubing diameter. There are clamp jaws sized to fit tubing of three different diameters so far: ⅝", 0.7", and ⅞".

Fixed-Jaw Offset:

The offset on both clamps needs to be the same. That means that the thickness of the clamp jaw insert should be the same for the fixed side of the clamp jaw on both clamps. The thickness of the insert will not matter on the moving side of the clamps, because they can be moved in and out to accommodate variations in thickness. This fixed-jaw offset is the alignment of the inserted clamp jaws, not the offset from the centroidal radius to the rotational motor axis (u) used in the strain calculations.

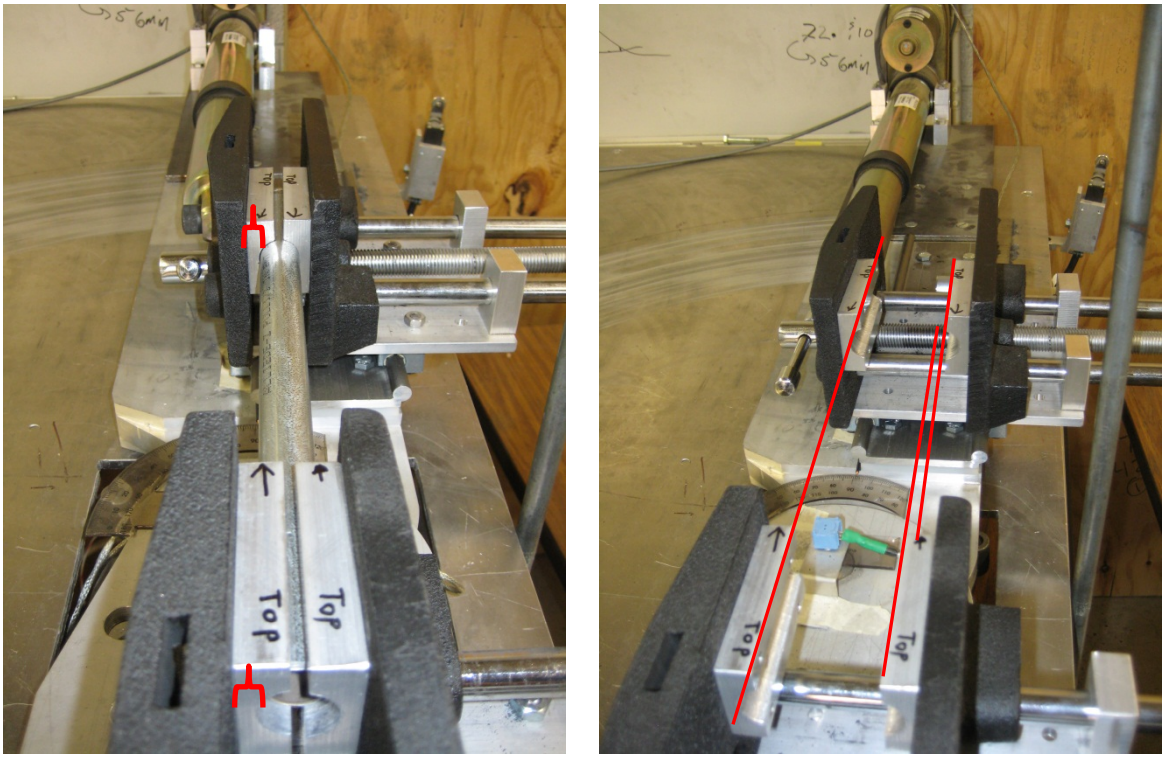

Figure 14: Aligning the tube in both vises.
Only the thickness of the fixed side (shown at left with red brackets) matters, as the moving side of each clamp can be moved to accommodate variations in thickness on that side.

Concentricity

The channels of the four vise jaw inserts have to line up with each other in order to hold one piece of tubing. Perhaps the easiest way to achieve this is to mark the position of the bolt holes in the four inserts (the holes that pass the bolt that connects the jaw to the clamp) while clamping a piece of tubing. This bolt pattern should be marked so that alignment will stay the same if the jaws are removed and then replaced.

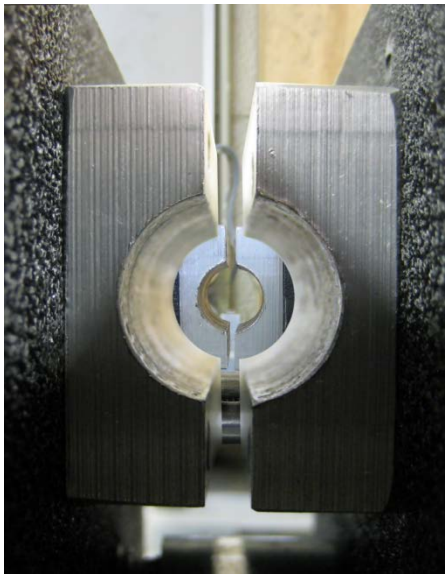

Leading-Edge Spacing:

Make sure that the space between the two clamps, *as measured from the leading edge of the vise jaw insert*, matches what the LabView program says it should be for a given bend radius.

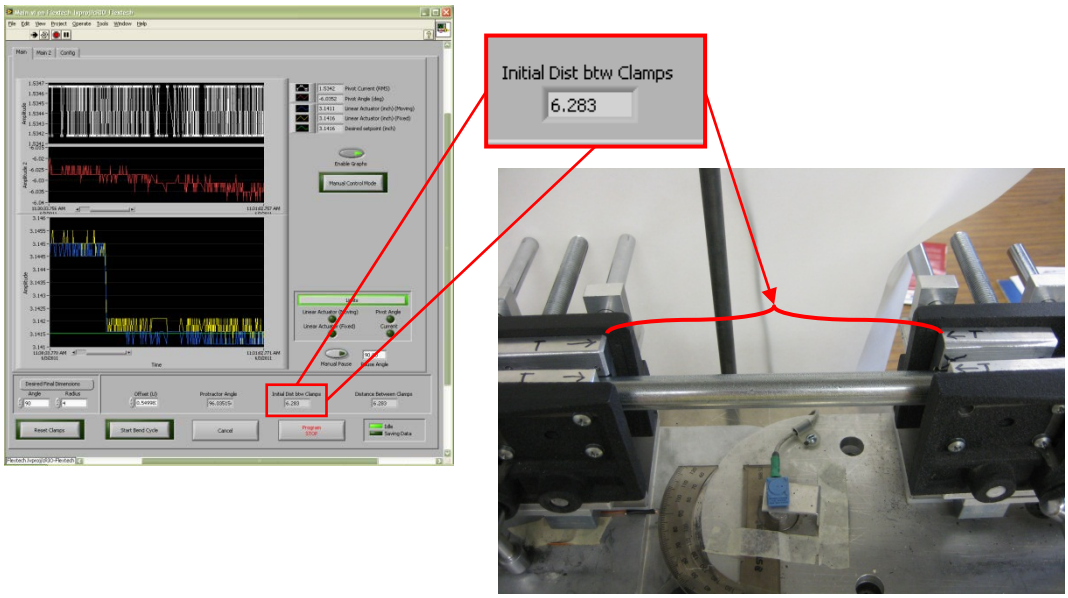

Figure 15: Initial Dist btw Clamps

The initial space between the vise jaw inserts should match the distance specified in the LabView program.

Bolt Spacing:

Each of the clamp jaws has a slightly different, irregular bolt pattern. The clamp jaw insert for each jaw must be drilled and tapped to match that specific clamp.

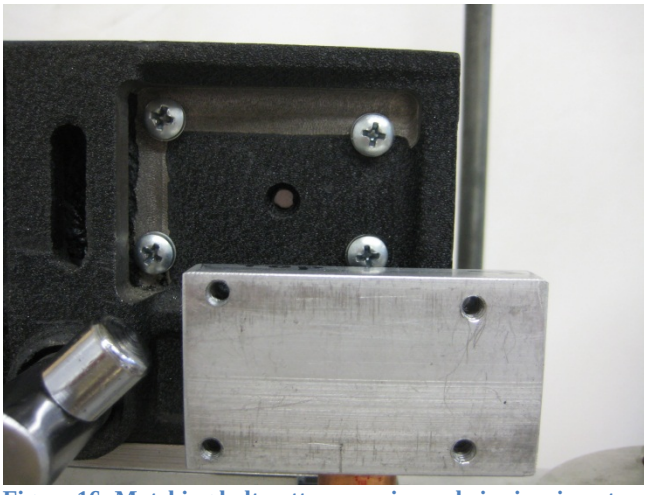

Figure 16: Matching bolt pattern on vise and vise jaw inserts

APPENDIX B: Derivations

This section includes derivations of different formulas that were derived by Joel Bloomer during his efforts with the project. Included are the following derivations:

- The area of the cross section of a tube cut along its length
- Clamp adjustments based on offset
- The shift in the neutral axis
- Neutral axis dimension for a tube with a hollow circular cross section
- Stress and strain due to large deflection bending
- Cross-sectional bending due to ovalization.

Contents

B.1 Deriving a formula for the cross-sectional area of a section of tubing cut normal to its tube axis.

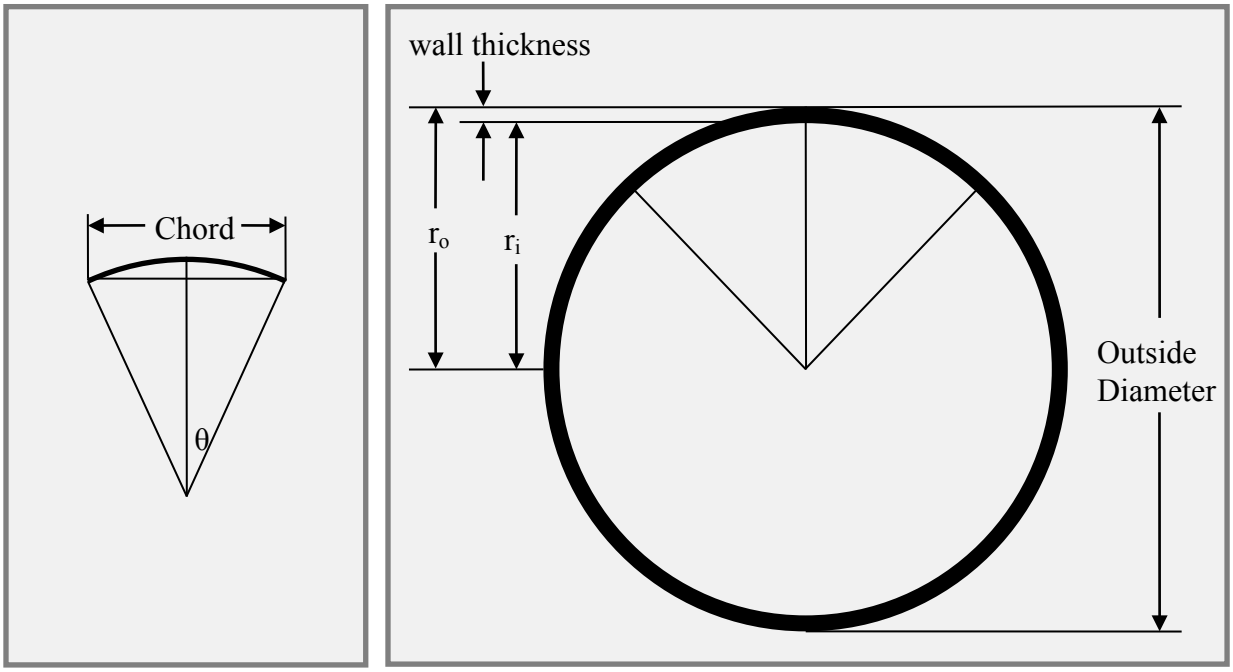

Figure 1—1: Chord and Cross-Section of a tube

B.1.1 Trigonometric relationships:

$$\sin(\theta) = \frac{opp.}{hyp.} = \frac{chord/_2}{outside\ diam./_2} = \frac{chord}{outside\ diameter}$$

$$\theta = \sin^{-1}\left(\frac{chord}{o.d.}\right)$$

B.1.2 Geometric relationships:

$$r_o = \frac{outside\ diameter}{2}$$

$$r_i = \frac{outside\ diameter}{2} - wall\ thickness$$

B.1.3 Derivation:

The area of the chord cross-section is a fraction of the area of a hoop. The hoop's area is given as the difference between the areas of two circles, and the fraction is the angle of the arc behind the chord over the angle covered by the entire hoop:

$$A_c = (\pi {r_0}^2 - \pi {r_i}^2)\frac{2\theta}{2\pi}$$

Simplify:

$$A_c = \pi({r_0}^2 - {r_i}^2)\frac{\theta}{\pi}$$

$$A_c = ({r_0}^2 - {r_i}^2) \times \theta$$

Substitute in the expressions for r_o and r_i:

$$A_c = \left(\left(\frac{outside\ diameter}{2}\right)^2 - \left(\frac{outside\ diameter}{2} - wall\ thickness\right)^2\right) \times \theta$$

Simplify:

$$A_c = \left(\frac{o.d.^2}{4} - \left(\frac{o.d.^2}{4} - 2\frac{o.d.}{2}wall + wall^2\right)\right) \times \theta$$

$$A_c = \left(\frac{o.d.^2}{4} - \frac{o.d.^2}{4} + (o.d.)(wall) - wall^2\right) \times \theta$$

$$A_c = wall(o.d. - wall) \times \theta$$

Substitute in the expression for θ:

$$\boxed{\boldsymbol{A_{cross\ sectional} = wall(o.d. - wall) \times \sin^{-1}\left(\frac{chord}{o.d.}\right)}}$$

B.2 Deriving the formula for clamp adjustment based on offset, etc.

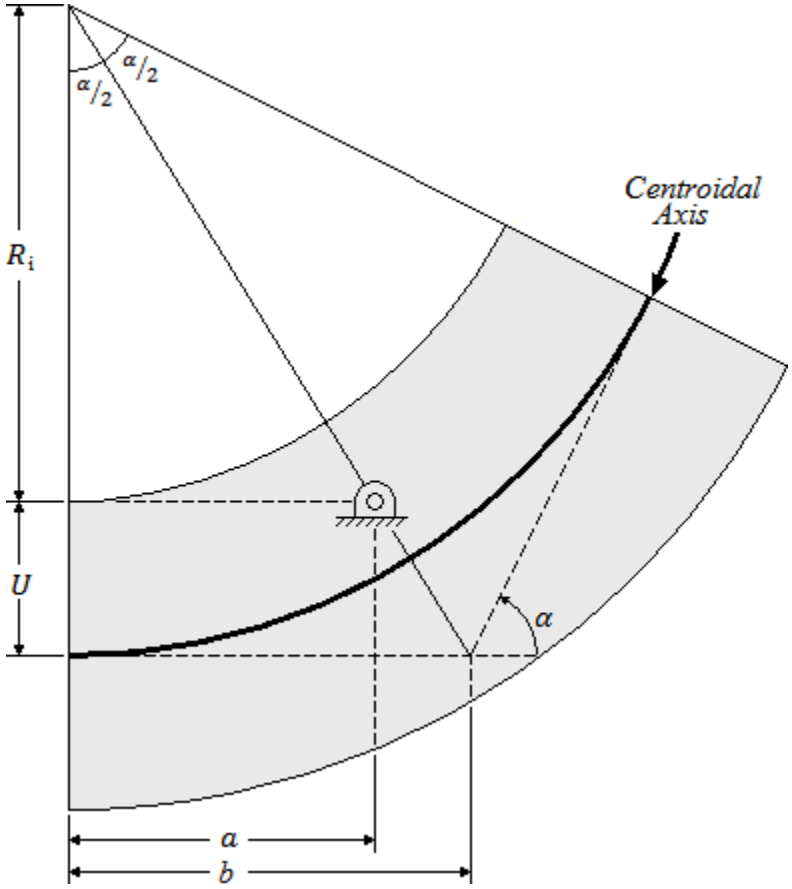

Figure 2—1: Tube in bending

B.1.4 Definitions:

R_i = inside bend radius
U = offset (From centroidal axis to pivot point)
α = current bend angle
$(U+R_i)$ = radius of centroidal axis at any angle α
L_c = length of centroidal axis
R_f = bend radius of the centroidal axis at α_f
α_f = final bend angle (before springback)
a = linear distance from clamp leading edge to the actual pivot point
b = linear distance from clamp edge to the ideal pivot point (projected)

B.1.5 Derivation:

Some basic trigonometry tells us that:

$$a = R_i \tan\left(\frac{\alpha}{2}\right)$$

$$b = (R_i + U) \tan\left(\frac{\alpha}{2}\right)$$

$$\frac{a}{b} = \frac{R_i}{R_i + U}$$

Before the bend cycle starts, α = 0 and $R_i = \infty$, but $a_0 = b_0$ = half the length of tube required to make the final bend:

$$a_0 = b_0 = \frac{R_f \alpha_f}{2}$$

At an arbitrary intermediate angle α during the bend cycle, the length of the centroidal axis (L_c) is:

$$L_c = (R_i + U)\alpha$$

At the beginning and end of the cycle, the length of L_c is fixed at $R_f\alpha_f$. Ideally, the neutral axis would be kept at a constant length throughout the bend cycle. However, to simplify the calculations, we will instead keep the centroidal axis (L_c) at a constant length throughout the cycle. In order to keep L_c constant, let:

$$L_c = R_f \alpha_f$$

This means that:

$$(R_i + U)\alpha = R_f \alpha_f$$

Solving for R_i gives:

$$R_i = \left(\frac{R_f \alpha_f}{\alpha} - U\right)$$

Substituting this value into the expressions for *a* and *b* gives:

$$a = \left(\frac{R_f \alpha_f}{\alpha} - U\right) \tan\left(\frac{\alpha}{2}\right)$$

$$b = \left(\frac{R_f \alpha_f}{\alpha} - U + U\right) \tan\left(\frac{\alpha}{2}\right)$$

$$b = \frac{R_f \alpha_f}{\alpha} \tan\left(\frac{\alpha}{2}\right)$$

B.1.6 Clamp Adjustment:

The clamps start out at a distance a_0 from the pivot point. Their position throughout the bend cycle must be adjusted so that:

$$a = \left(\frac{R_f \alpha_f}{\alpha} - U\right) \tan\left(\frac{\alpha}{2}\right)$$

The command given to the actuators that move the clamps will be a value for the change in a from a_0. This value, Δa, is determined by the following equation:

$$\boxed{\Delta \boldsymbol{a} = a - a_0 = \left(\frac{\boldsymbol{R_f \alpha_f}}{\boldsymbol{\alpha}} - \boldsymbol{U}\right) \tan\left(\frac{\boldsymbol{\alpha}}{\boldsymbol{2}}\right) - \frac{\boldsymbol{R_f \alpha_f}}{\boldsymbol{2}}}$$

B.3 Deriving the formula for neutral axis shift as the tube bends.

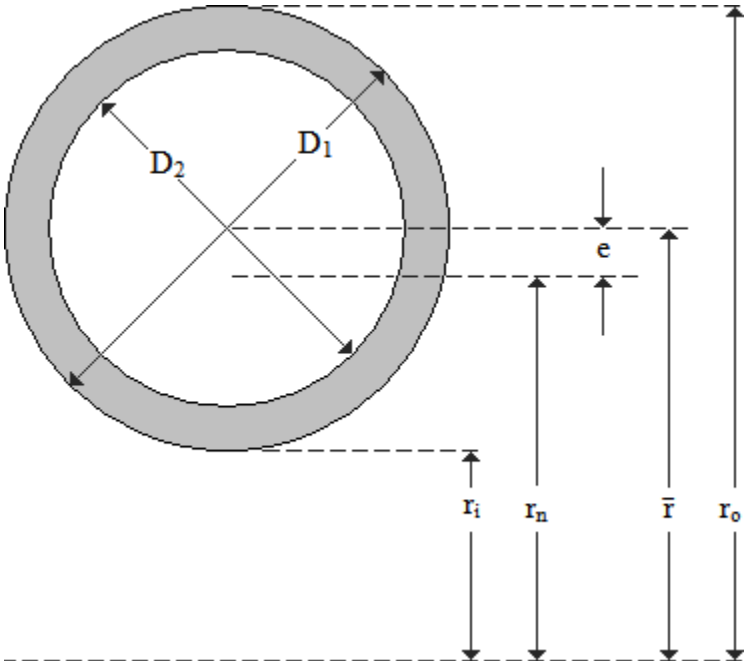

Figure 3—1: Reference figure for neutral axis shift equations

B.1.7 Definitions:

D_1 = outside diameter of tube
D_2 = inside diameter of tube
R_x = ½D_x
$\bar{r}$ = bend radius of the centroidal axis
r_n = bend radius of the neutral axis
r_i = inside bend radius
r_o = outside bend radius
e = neutral axis shift

B.1.8 Derivation:

For any shape with area A at a distance ρ from the bending axis, the general equation for the location of the neutral axis during bending is:

$$r_n = \frac{A}{\int \frac{\partial A}{\rho}}$$

For a solid circular cross-section with diameter D, the radius to the centroidal axis ($\bar{r}$) is related to the inner bend radius (r_i) by the following equation[1]:

$$\bar{r} = r_i + \frac{D}{2}$$

The neutral axis is located according to the following equation[2], where R = ½D:

$$r_n = \frac{R^2}{2\left(\bar{r} - \sqrt{\bar{r}^2 - R^2}\right)}$$

For a hollow circular cross-section the equation for the centroidal axis $\bar{r}$ is similarly:

$$\bar{r} = r_i + \frac{D}{2}$$

This can also be written as:

$$\bar{r} = r_i + R$$

The proposed equation governing the location of the neutral axis is:

$$r_n = \frac{A_2 - A_1}{\frac{A_2}{r_{n2}} - \frac{A_1}{r_{n1}}}$$

Substitute in the expressions for areas and neutral axes:

$$r_n = \frac{\pi\left(\frac{D_2}{2}\right)^2 - \pi\left(\frac{D_1}{2}\right)^2}{\left[\frac{\pi\left(\frac{D_2}{2}\right)^2}{\left(\frac{{R_2}^2}{2\left(\bar{r_2} - \sqrt{\bar{r_2}^2 - {R_2}^2}\right)}\right)} - \frac{\pi\left(\frac{D_1}{2}\right)^2}{\left(\frac{{R_1}^2}{2\left(\bar{r_1} - \sqrt{\bar{r_1}^2 - {R_1}^2}\right)}\right)}\right]}$$

[1] Budynas, Richard G. and J. Keith Nisbett. *Shigley's Mechanical Engineering Design, Eighth Edition*. (Table 3-4, "Formulas for Sections of Curved Beams") McGraw Hill Higher Education.
[2] Budynas, Richard G. and J. Keith Nisbett. *Shigley's Mechanical Engineering Design, Eighth Edition*. (Table 3-4, "Formulas for Sections of Curved Beams") McGraw Hill Higher Education.

Invert the bottom-most fractions:

$$r_n = \frac{\pi\left(\frac{D_2}{2}\right)^2 - \pi\left(\frac{D_1}{2}\right)^2}{\left[\frac{2\pi\left(\frac{D_2}{2}\right)^2\left(\bar{r_2} - \sqrt{\bar{r_2}^2 - {R_2}^2}\right)}{{R_2}^2} - \frac{2\pi\left(\frac{D_1}{2}\right)^2\left(\bar{r_1} - \sqrt{\bar{r_1}^2 - {R_1}^2}\right)}{{R_1}^2}\right]}$$

Substitute R in for $\frac{D}{2}$:

$$r_n = \frac{\pi {R_2}^2 - \pi {R_1}^2}{\left[\frac{2\pi {R_2}^2\left(\bar{r_2} - \sqrt{\bar{r_2}^2 - {R_2}^2}\right)}{{R_2}^2} - \frac{2\pi {R_1}^2\left(\bar{r_1} - \sqrt{\bar{r_1}^2 - {R_1}^2}\right)}{{R_1}^2}\right]}$$

Cancel π, ${R_1}^2$, and ${R_2}^2$:

$$r_n = \frac{{R_2}^2 - {R_1}^2}{2\left(\bar{r_2} - \sqrt{\bar{r_2}^2 - {R_2}^2}\right) - 2\left(\bar{r_1} - \sqrt{\bar{r_1}^2 - {R_1}^2}\right)}$$

Because the circles are concentric, $\bar{r_1} = \bar{r_2} = \bar{r}$. With this substitution, the equation becomes:

$$r_n = \frac{{R_2}^2 - {R_1}^2}{2\left(\bar{r} - \sqrt{\bar{r}^2 - {R_2}^2}\right) - 2\left(\bar{r} - \sqrt{\bar{r}^2 - {R_1}^2}\right)}$$

Finally, this simplifies to:

$$\boxed{\boldsymbol{r_n = \frac{{R_2}^2 - {R_1}^2}{2\sqrt{\bar{r}^2 - {R_1}^2} - 2\sqrt{\bar{r}^2 - {R_2}^2}}}}$$

B.4 Proving the equation used to derive the neutral axis shift for a hollow, circular cross-section:

B.1.9 Diagrams and basic equations:

In order to prove that the proposed equation $\left(r_n = \frac{A_2 - A_1}{\frac{A_2}{r_{n2}} - \frac{A_1}{r_{n1}}}\right)$ is correctly applied, we will use this same equation to derive a known formula for the neutral axis shift. For a hollow rectangular cross-section, the following diagram and accompanying equation have been published[3]:

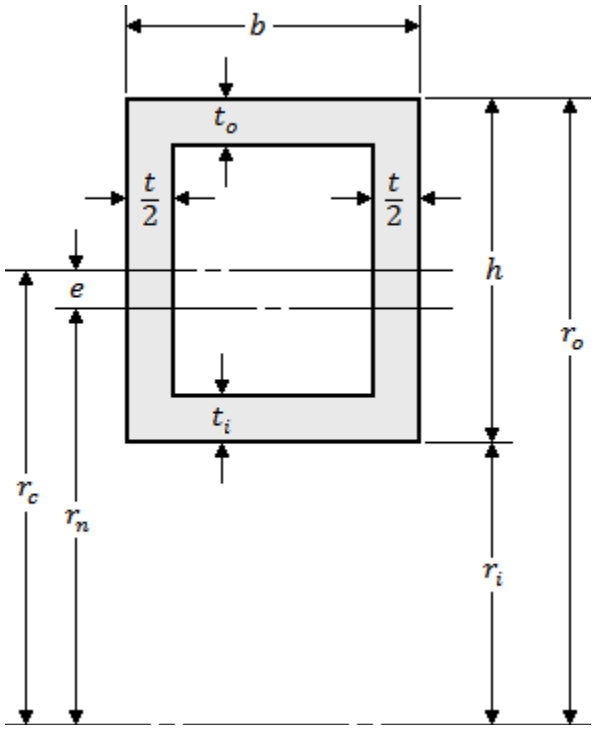

Figure 4—1: Reference figure for neutral axis equations for a square cross section

$$r_n = \frac{(b-t)(t_i + t_o) + ht}{b\left(\ln\frac{r_i + t_i}{r_i} + \ln\frac{r_o}{r_o - t_o}\right) + t\ln\frac{r_o - t_o}{r_i + t_i}}$$

In order to make this reflect the set-up of the hollow circular cross-section, we adapt this diagram and equation to represent a small rectangular area subtracted from a larger. We also simplify the scenario by giving the section a constant wall thickness.

[3] Budynas, Richard G. and J. Keith Nisbett. *Shigley's Mechanical Engineering Design, Eighth Edition*. (Table 3-4, "Formulas for Sections of Curved Beams") McGraw Hill Higher Education.

The adapted diagram and basic equation are as follows:

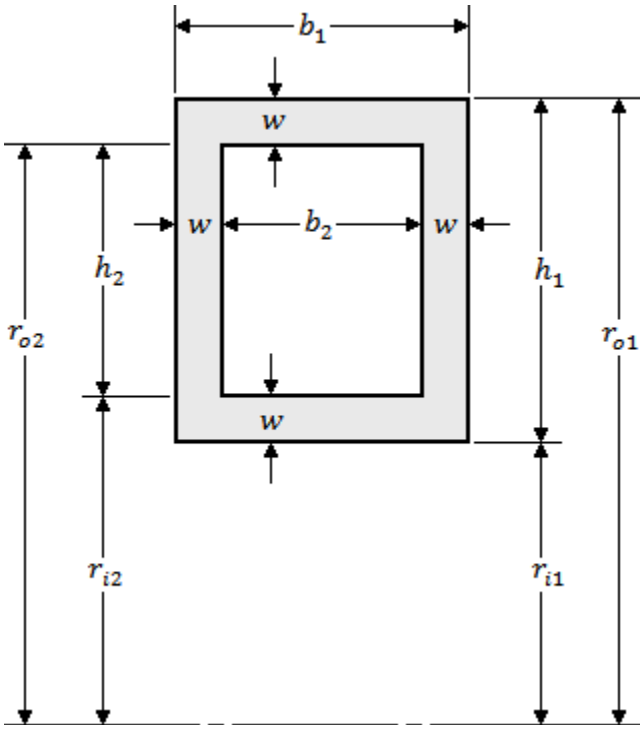

Figure 4—2: dimensions of a square tube cross section

$$r_n = \frac{A_2 - A_1}{\frac{A_2}{r_{n2}} - \frac{A_1}{r_{n1}}}$$

B.1.10 Derivation by subtraction:

For a rectangular cross-section *x*:

$$r_{nx} = \frac{h_x}{\ln \frac{r_{ox}}{r_{ix}}}$$

And:

$$A_x = b_x h_x$$

When these expressions are substituted into the equation for a hollow cross-section with areas *1* and *2*, it becomes:

$$r_n = \frac{b_2 h_2 - b_1 h_1}{\left(\frac{b_2 h_2}{\ln \frac{r_{o2}}{r_{i2}}}\right) - \left(\frac{b_1 h_1}{\ln \frac{r_{o1}}{r_{i1}}}\right)}$$

Invert the bottom-most fractions:

$$r_n = \frac{b_2 h_2 - b_1 h_1}{\frac{b_2 h_2 \ln \frac{r_{o2}}{r_{i2}}}{h_2} - \frac{b_1 h_1 \ln \frac{r_{o1}}{r_{i1}}}{h_1}}$$

Cancel h_x:

$$r_n = \frac{b_2 h_2 - b_1 h_1}{b_2 \ln \frac{r_{o2}}{r_{i2}} - b_1 \ln \frac{r_{o1}}{r_{i1}}}$$

By comparing the published (and more generalized) diagram of a hollow rectangular cross section to our more specific diagram with uniform wall thickness *w*, we see that:

$$r_{i2} = r_i + w$$
$$r_{i1} = r_i$$

$$r_{o2} = r_o - w$$
$$r_{o1} = r_o$$

Making these substitutions gives:

$$r_n = \frac{b_2 h_2 - b_1 h_1}{b_2 \ln \frac{r_o - w}{r_i + w} - b_1 \ln \frac{r_o}{r_i}}$$

This can be simplified with the following logarithm operations:

$$r_n = \frac{b_2 h_2 - b_1 h_1}{\ln \left(\frac{r_o - w}{r_i + w}\right)^{b_2} - \ln \left(\frac{r_o}{r_i}\right)^{b_1}}$$

$$r_n = \frac{b_1 h_1 - b_2 h_2}{\ln \left(\frac{r_o}{r_i}\right)^{b_1} - \ln \left(\frac{r_o - w}{r_i + w}\right)^{b_2}}$$

$$r_n = \frac{b_1 h_1 - b_2 h_2}{\ln \left(\frac{r_o}{r_i}\right)^{b_1} + \ln \left(\frac{r_i + w}{r_o - w}\right)^{b_2}}$$

$$\boxed{r_n = \frac{b_1 h_1 - b_2 h_2}{\ln \left[\left(\frac{r_o}{r_i}\right)^{b_1} \left(\frac{r_i + w}{r_o - w}\right)^{b_2}\right]}}$$

This is the equation for the neutral axis shift in a hollow rectangular cross-section as derived by subtracting one area from another.

B.1.11 Derivation by simplification:

Again, the published, generalized equation for the neutral axis of a rectangular cross section in bending is:

$$r_n = \frac{(b-t)(t_i+t_o)+ht}{b\left(\ln\frac{r_i+t_i}{r_i}+\ln\frac{r_o}{r_o-t_o}\right)+t\ln\frac{r_o-t_o}{r_i+t_i}}$$

We need to verify that this is equal to the equation derived by subtracting the two rectangular areas. Giving this equation a uniform wall thickness *w* allows us to make the following substitutions:

$$\frac{t}{2} = t_o = t_i = w$$

This changes the generalized equation to:

$$r_n = \frac{(b-2w)(w+w)+2hw}{b\left(\ln\frac{r_i+w}{r_i}+\ln\frac{r_o}{r_o-w}\right)+2w\ln\frac{r_o-w}{r_i+w}}$$

At this point, both the numerator and the denominator of the equation require some significant manipulation in order to complete the proof:

$$r_n = \frac{(b-2w)(2w)+2wh}{b\left(\ln\frac{r_i+w}{r_i}+\ln\frac{r_o}{r_o-w}\right)+2w\ln\frac{r_o-w}{r_i+w}}$$

$$r_n = \frac{2wh+(b-2w)(2w)}{b(\ln(r_i+w)-\ln r_i+\ln r_o-\ln(r_o-w))+2w(\ln(r_o-w)-\ln(r_i+w))}$$

$$r_n = \frac{(bh-bh)+2wh+(b-2w)(2w)}{\ln\frac{(r_i+w)^b}{(r_i+w)^{2w}}-b\ln r_i+b\ln r_o+\ln\frac{(r_o-w)^{2w}}{(r_o-w)^b}}$$

$$r_n = \frac{bh-bh+2wh+(b-2w)(2w)}{\ln(r_i+w)^{b-2w}-\ln {r_i}^b+\ln {r_o}^b+\ln(r_o-w)^{2w-b}}$$

$$r_n = \frac{bh-(b-2w)(h)+(b-2w)(2w)}{\ln(r_i+w)^{b-2w}-\ln {r_i}^b+\ln {r_o}^b-\ln(r_o-w)^{b-2w}}$$

$$r_n = \frac{bh-(b-2w)(h)-(b-2w)(-2w)}{\ln\frac{(r_i+w)^{b-2w}}{(r_o-w)^{b-2w}}+\ln\frac{{r_o}^b}{{r_i}^b}}$$

$$r_n = \frac{bh - (b-2w)(h-2w)}{\ln\left(\frac{r_i + w}{r_o - w}\right)^{b-2w} + \ln\left(\frac{r_o}{r_i}\right)^{b}}$$

$$r_n = \frac{bh - (b-2w)(h-2w)}{\ln\left[\left(\frac{r_o}{r_i}\right)^{b}\left(\frac{r_i + w}{r_o - w}\right)^{b-2w}\right]}$$

Again comparing the two diagrams,

$$b = b_1$$
$$b - 2w = b_2$$
$$h = h_1$$
$$h - 2w = h_2$$

Substituting these values in gives:

$$r_n = \frac{b_1 h_1 - (b_2)(h_2)}{\ln\left[\left(\frac{r_o}{r_i}\right)^{b_1}\left(\frac{r_i + w}{r_o - w}\right)^{b_2}\right]}$$

This is now identical to the equation for the neutral axis shift of a hollow rectangular cross-section based on subtracting one area from another.

$$\boxed{r_n = \frac{b_1 h_1 - b_2 h_2}{\ln\left[\left(\frac{r_o}{r_i}\right)^{b_1}\left(\frac{r_i + w}{r_o - w}\right)^{b_2}\right]}}$$

This supports our use of the same method to derive an equation for the neutral axis shift of a hollow circular cross-section.

B.5 Determining Stress and Strain Due to Large Deflection Bending.

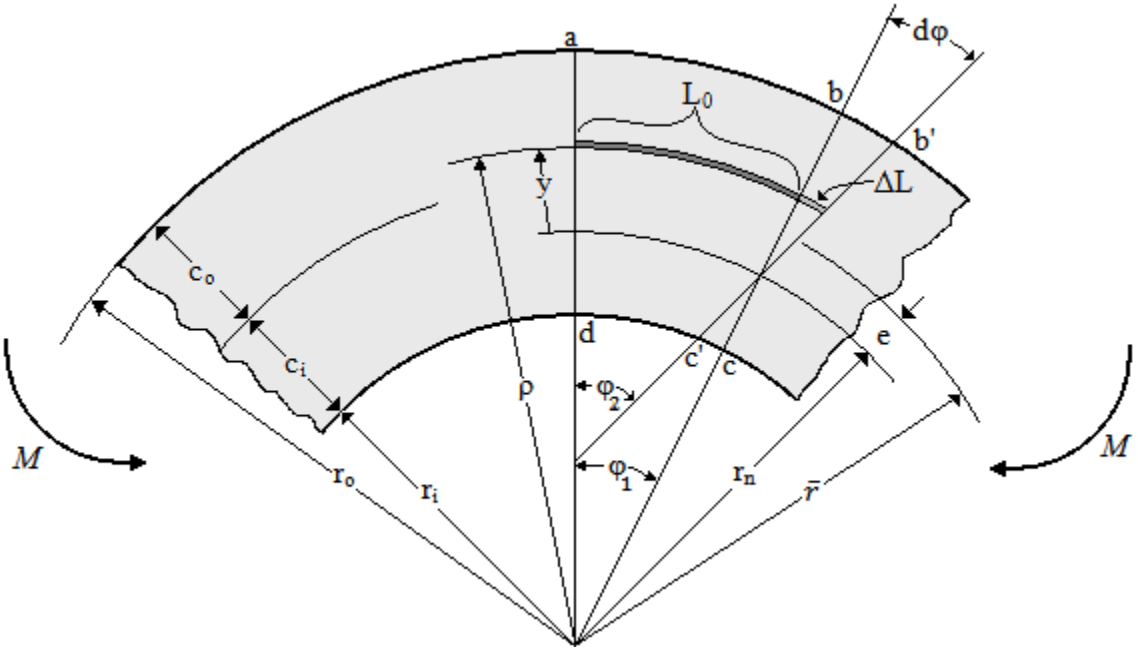

Figure 5—1: Reference figure for large deflection bending

B.1.12 Definitions:

r_o = radius of curvature of the outer surface
$\bar{r}$ = radius of curvature of the centroid
r_n = radius of curvature of the neutral axis
r_i = radius of curvature of the inner surface
M = applied bending moment
e = neutral axis shift with respect to the centroid
ρ = distance from the center of bending to any given point on the curved beam
y = distance above the neutral axis to any given point on the curved beam
φ = angle used to define the wedge-shaped element *abcd* for analysis
L_0 = initial length of a differential area on element *abcd*
c_i = distance from the inner surface of the beam to the centroidal axis
c_o = distance from the outer surface of the beam to the centroidal axis
dφ = differential bending angle due to bending moment M
ΔL = change in length of the differential area as it changes from *abcd* to *ab'c'd*
t = wall thickness (not shown)
ϵ = strain (not shown)
σ = stress (not shown)

B.1.13 Derivation:

In order to determine the strain, it is necessary to find both L_0 and ΔL, because:

$$\epsilon = \frac{\Delta L}{L_0}$$

This linear equation only works for small values of ΔL. In order to use it in the context of a large-angle bend, it is necessary to perform the calculation over several smaller increments during the bend, re-defining L_0 each time. The result of each calculation will be the change in strain over that increment; the summation of all of them will be the total strain. For these reasons, the strain equation is perhaps better given as:

$$\Delta\epsilon = \frac{\Delta L}{L}$$

Because the angles are defined in radians, *L* is simply the product of the angle φ and the distance ρ from the center of bending:

$$L = \rho\varphi$$

Assuming that the neutral axis does not change length and that plane sections remain plane during bending, it can be seen that the line *bc* simply rotates about a point on the neutral axis as it moves into position *b'c'*. In this case, the length ΔL is simply the product of the angle $d\varphi$ and the distance *y* from the neutral axis:

$$\Delta L = yd\varphi$$

Substituting these expressions into the original strain equation gives:

$$\Delta\epsilon = \frac{yd\varphi}{\rho\varphi_1}$$

Interestingly enough, because this equation will be used repeatedly at constant intervals, the numerator $y \times d\varphi$ will show only small changes as the neutral axis shifts, while largest changes will occur as the denominator goes through each increment.

There are six points at which we need to calculate the stress. They are located on the inside bend radius, outside bend radius, and centroidal axis of the tube with respect to the bend radius; three are at these points on the outside wall of the tube, and the other three are located at these points on the inside of the tube. This will allow us to examine the tube in tension, in compression, and have an idea of what is going on in between the two. These points are labeled in Figure 5—2.

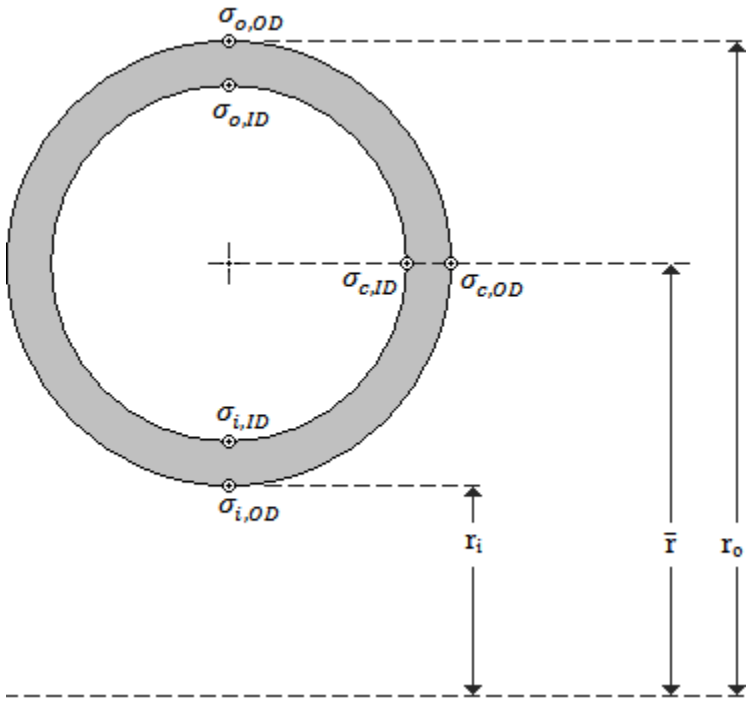

Figure 5—2: Critical points in a tube cross section

Normal stress is related to strain by Young's Modulus (E) as $\sigma = \epsilon E$. At a distance y from the neutral axis,

$$\sigma = E\left(\frac{yd\varphi}{\rho\varphi_1}\right)$$

Along the outside edge of the beam, $y = (e + c_o)$ and $\rho = (r_n + y) = r_o$. Substituting these into the stress equation gives:

$$\boxed{\sigma_{o,OD} = E\left(\frac{(e + c_o)d\varphi}{r_o\varphi_1}\right)}$$

To get the stress at the inside diameter of the tube at this outer bend radius, subtract the wall thickness t from the relevant parts of the equation; $y = (e + c_o - t)$ and $\rho = r_o - t$. Substituting these into the stress equation gives:

$$\boxed{\sigma_{o,ID} = E\left(\frac{(e + c_o - t)d\varphi}{(r_o - t)\varphi_1}\right)}$$

Following the same process in the other four locations gives the following equations:

$$\boxed{\sigma_{c,OD} = \sigma_{c,ID} = E\left(\frac{ed\varphi}{\bar{r}\varphi_1}\right)}$$

$$\boxed{\sigma_{i,OD} = E\left(\frac{(e - c_i)d\varphi}{r_i\varphi_1}\right)}$$

$$\boxed{\sigma_{i,ID} = E\left(\frac{(e - c_i + t)d\varphi}{(r_i + t)\varphi_1}\right)}$$

B.6 Analyzing Cross-Sectional Bending Due To Ovalization.

B.1.14 Diagrams:

As the tubing is bent, its cross-section in the bending region changes from circular to elliptical, as seen in the figure below. To avoid confusion, areas of the tube wall that will be analyzed have been labeled as North, South, East, and West.

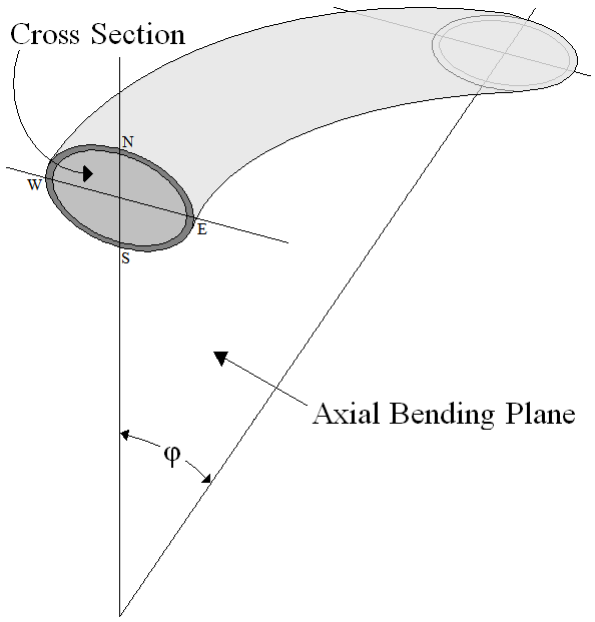

Figure 6—1: Orientation of critical points N, S, E, and W

This change in shape gets more pronounced as the bend angle increases up until the tube buckles. The major axis is stretched out and the minor axis is shortened.

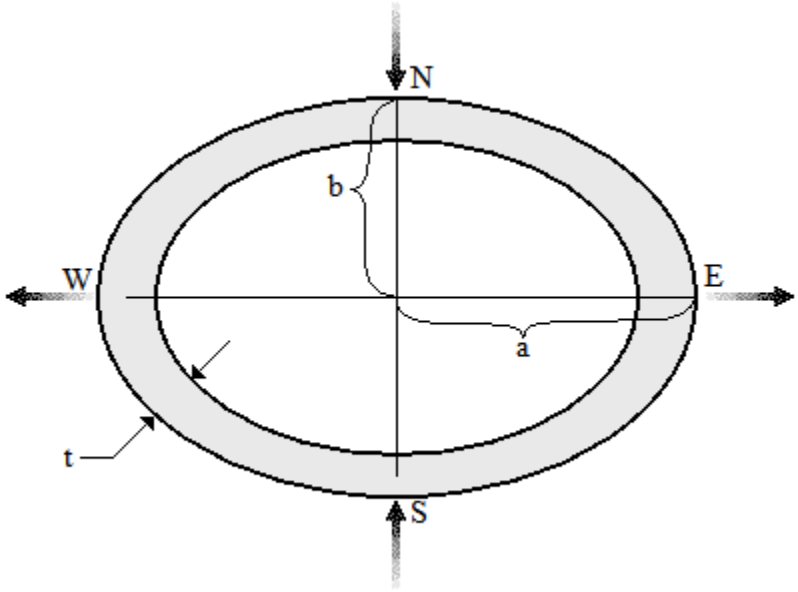

Figure 6—2: Orientation of a and b dimensions along major and minor axes

If the portion of the cross-section along either axis is examined, the bending process *of the cross-section* is very similar to that of a curved beam subject to a simple bending moment. At the

North and South locations of the cross section, the moment tends to straighten the beam (as illustrated in Figure 6—3), whereas the moment tends to make the beam curve more at the East and West locations (as in Figure 6—4).

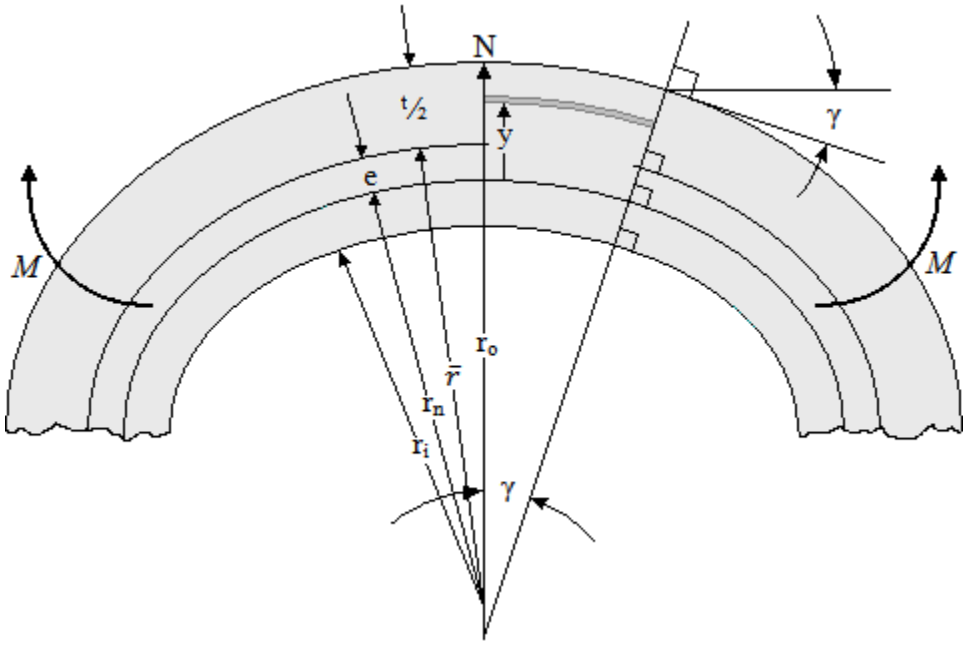

Figure 6—3: Reference figure for cross sectional strain calculations at the North point

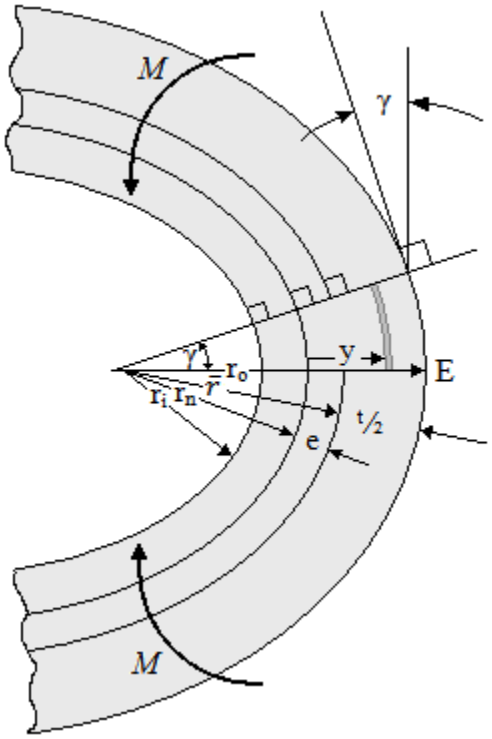

Figure 6—4: Reference figure for cross sectional strain calculations at the South point

B.1.15 Definitions:

a = semi-major axis of the cross-section (half of the outside major diameter)
b = semi-minor axis of the cross-section (half of the outside minor diameter)
t = wall thickness of the cross-section
r_N, r_S = radii of curvature at the North and South locations, on the major axis
r_W, r_E = radii of curvature at the West and East locations, on the minor axis
r_o = radius of curvature of the outer surface
$\bar{r}$ = radius of curvature of the centroid
r_n = radius of curvature of the neutral axis
r_i = radius of curvature of the inner surface
e = neutral axis shift with respect to the centroid
γ = angle used to define a wedge-shaped element for analysis
y = distance above or past the neutral axis
ϵ = strain
σ = stress

B.1.16 Derivation:

There are four general locations for which we need expressions for stress, σ. We start with the basic equation for stress:

$$\sigma = E\epsilon$$

Again, this is a linear equation that will have to be applied to small increments of the overall bending motion, so each calculation of σ is actually a calculation of Δσ, and they will all have to be added together in order to get a value for the overall stress:

$$\Delta\sigma = E\Delta\epsilon$$

$\Delta\epsilon$, strain, is simply $\Delta L/L$:

$$\Delta\sigma = E\frac{\Delta L}{L}$$

Similar to the equation for ΔL due to macro-scale stress and strain, ΔL in this case is the distance y from the neutral axis times the angle of rotation $d\gamma$. L (in the denominator) is the distance from the center of bending multiplied by the initially picked angle γ. The distance from the center of bending to any point being examined is ρ:

$$\Delta\sigma = E\frac{yd\gamma}{\rho\gamma}$$

For each of these steps, Δσ is going from an initial position *1* to a final position *2*. At this point it will be important to delineate at which position each of these values is taken. The expression $\rho\gamma$ is for the initial length L, so these variables will be given the subscript *1*. y will also receive the *1* subscript, because the distance of the differential element is measured before the plane rotation due to bending has begun, as in the previous derivations:

$$\Delta\sigma_{(1\to2)} = E\frac{y_1 d\gamma_{1\to2}}{\rho_1\gamma_1}$$

The variable y_1 is simply the distance from the neutral axis to the point being examined, which means that $r_n + y = \rho$. We can therefore substitute in the expression $(\rho - r_n)$ for *y* in the stress equation.

$$\Delta\sigma_{(1\to2)} = E\frac{(\rho_1 - r_{n1})d\gamma_{1\to2}}{\rho_1\gamma_1}$$

Next we need an expression for *d*γ. For small changes in curvature, we assume that the neutral axis does not change length. Based on this assumption the following equation holds true as it changes from position *1* to position *2*:

$$r_{n1}\gamma_1 = r_{n2}\gamma_2$$

Solving for γ_2 gives:

$$\gamma_2 = \frac{r_{n1}}{r_{n2}}\gamma_1$$

By definition:

$$d\gamma_{1\to2} = \gamma_2 - \gamma_1$$

Substituting the expression for γ_2 into the *d*γ equation gives:

$$d\gamma_{1\to2} = \frac{r_{n1}}{r_{n2}}\gamma_1 - \gamma_1 = \gamma_1\left(\frac{r_{n1}}{r_{n2}} - 1\right) = -\gamma_1\left(1 - \frac{r_{n1}}{r_{n2}}\right)$$

This can then be substituted back into the stress equation, which becomes:

$$\Delta\sigma_{(1\to2)} = E\frac{(\rho_1 - r_{n1})\left(-\gamma_1\left(1 - \frac{r_{n1}}{r_{n2}}\right)\right)}{\rho_1\gamma_1} = -E\frac{(\rho_1 - r_{n1})\left(1 - \frac{r_{n1}}{r_{n2}}\right)}{\rho_1}$$

$$\boxed{\Delta\sigma_{(1\to2)} = -E\left(1 - \frac{r_{n1}}{\rho_1}\right)\left(1 - \frac{r_{n1}}{r_{n2}}\right)}$$

This is the most generalized form of the equation for stress due to ovalization. In this equation, ρ_1 can represent r_i or r_o at any one of the compass points, and r_{n1} and r_{n2} can then be calculated from the values of r_i and r_o at that same compass point. To illustrate the point, we will examine first the North location at the outside of the tubing.

The radius, ρ, of the location in question is based on the measured values for *a* and *b* and on the assumption that the deforming cross-section takes the shape of an ellipse:

$$\rho = r_{N,outer} = \frac{a^2}{b}$$

The inner radius at that point is different from the outer radius only by the wall thickness:

$$r_{N,inner} = r_{N,outer} - t = \frac{a^2}{b} - t$$

The neutral axis is based on both the inner and outer radii of curvature and on the wall thickness:

$$r_{N,neutral} = \frac{t}{\ln \frac{r_{N,outer}}{r_{N,inner}}}$$

Plugging these expressions into the equation for ovalization stress, keeping careful track of the subscripts, and simplifying eventually gives the following equation:

$$\Delta\sigma_{o,1\to2} = -E\left(1 + \frac{t}{\left(\frac{{a_1}^2}{b_1}\right)\ln\left(1 - t\frac{b_1}{{a_1}^2}\right)}\right)\left(1 - \frac{\ln\left(1 - t\frac{b_2}{{a_2}^2}\right)}{\ln\left(1 - t\frac{b_1}{{a_1}^2}\right)}\right)$$

However, this is unnecessarily complicated. With the aid of a spreadsheet program, it is much easier to simply use the following equations, each one depending on the previous equations:

$$r_{N1,outer} = \frac{{a_1}^2}{b_1}, \qquad r_{N2,outer} = \frac{{a_2}^2}{b_2}$$

$$r_{N1,inner} = r_{N1,outer} - t_{N1}, \qquad r_{N2,inner} = r_{N2,outer} - t_{N2}$$

$$r_{N1,neutral} = \frac{t_{N1}}{\ln \frac{r_{N1,outer}}{r_{N1,inner}}}, \qquad r_{N2,neutral} = \frac{t_{N2}}{\ln \frac{r_{N2,outer}}{r_{N2,inner}}}$$

$$\rho_{N1,outer} = r_{N1,outer}$$

$$\Delta\sigma_{N(1\to2),outer} = -E\left(1 - \frac{r_{N1,neutral}}{\rho_{N1,outer}}\right)\left(1 - \frac{r_{N1,neutral}}{r_{N2.neutral}}\right)$$

These steps can be repeated at each point of the compass at both the inner and outer radii. For the East and West locations, $r_o = \frac{b^2}{a}$ rather than $\frac{a^2}{b}$.

B.7 Analyzing the change in thickness due to both macro bending and ovalization:

As the tube bends, it changes thickness due to the Poisson effect. This is affected by both the strains of macro bending and ovalization. These strains combine differently at each of the compass points on the tube. It will be the least confusing if we examine one compass point at a time. We will start with the North point.

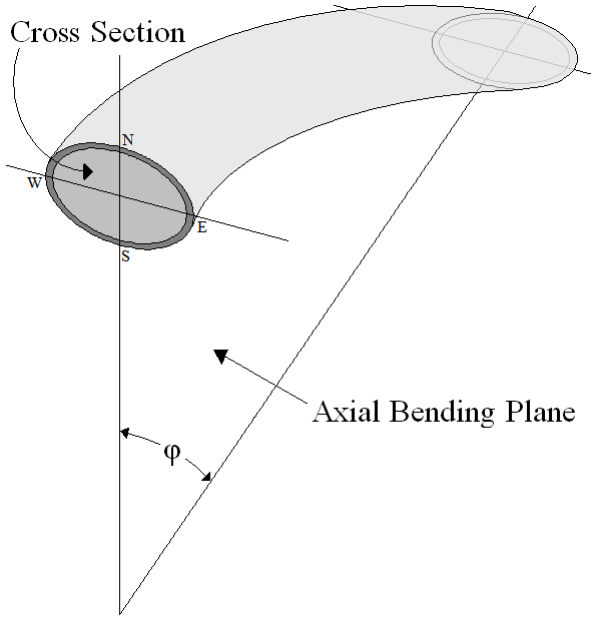

Figure 6—1 (repeated)

The strain due to bending within the North wall of the tubing has the following general distribution:

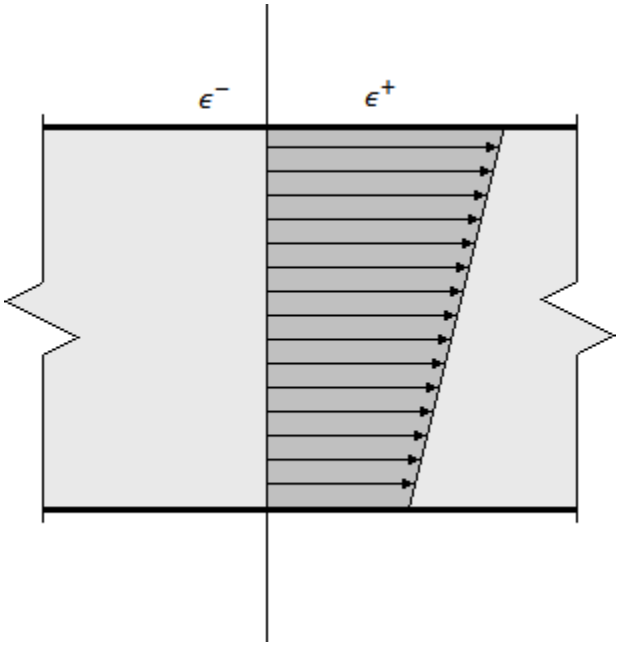

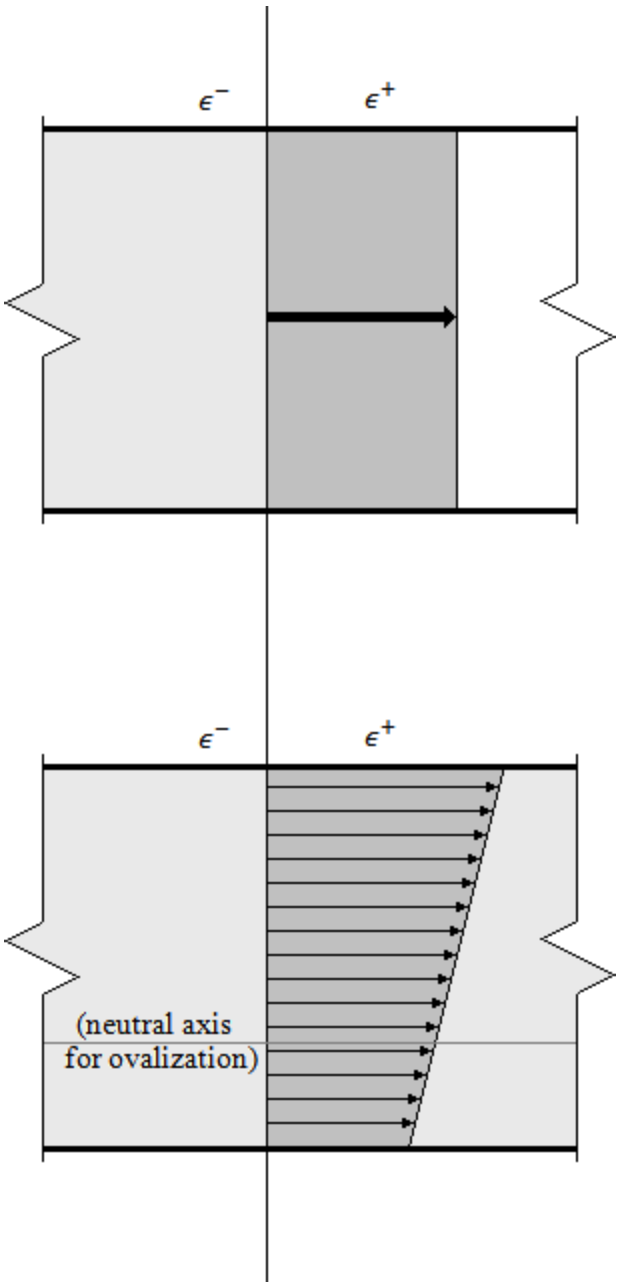
ϵ^-
ϵ^+
ϵ^-
ϵ^+
(neutral axis
for ovalization)

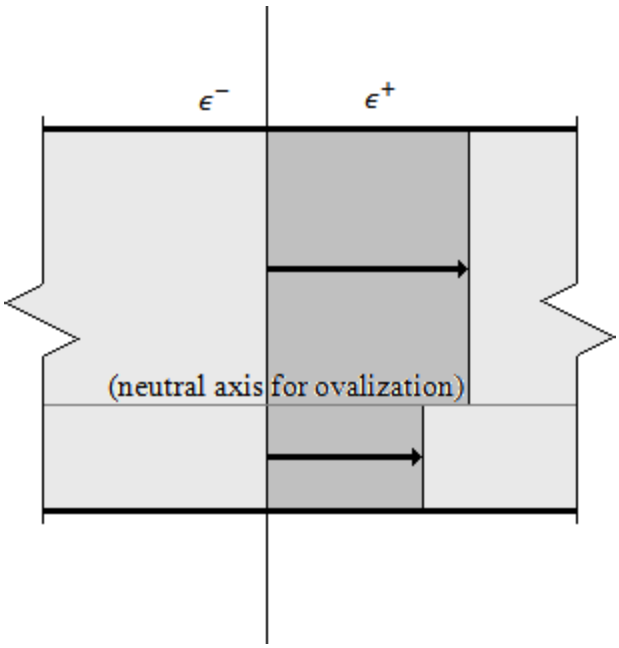

The Poisson effect of this strain on wall thickness can be easily approximated by using an average strain through the cross section. However, the strain due to cross-sectional ovalization is not nearly as simple. Its shape is closer to the following:

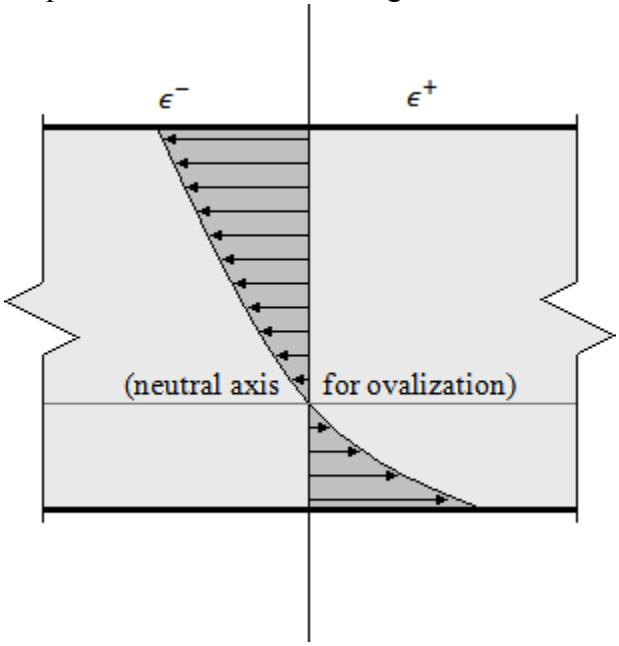

A simple average across the entire wall will not accurately reflect the actual strains

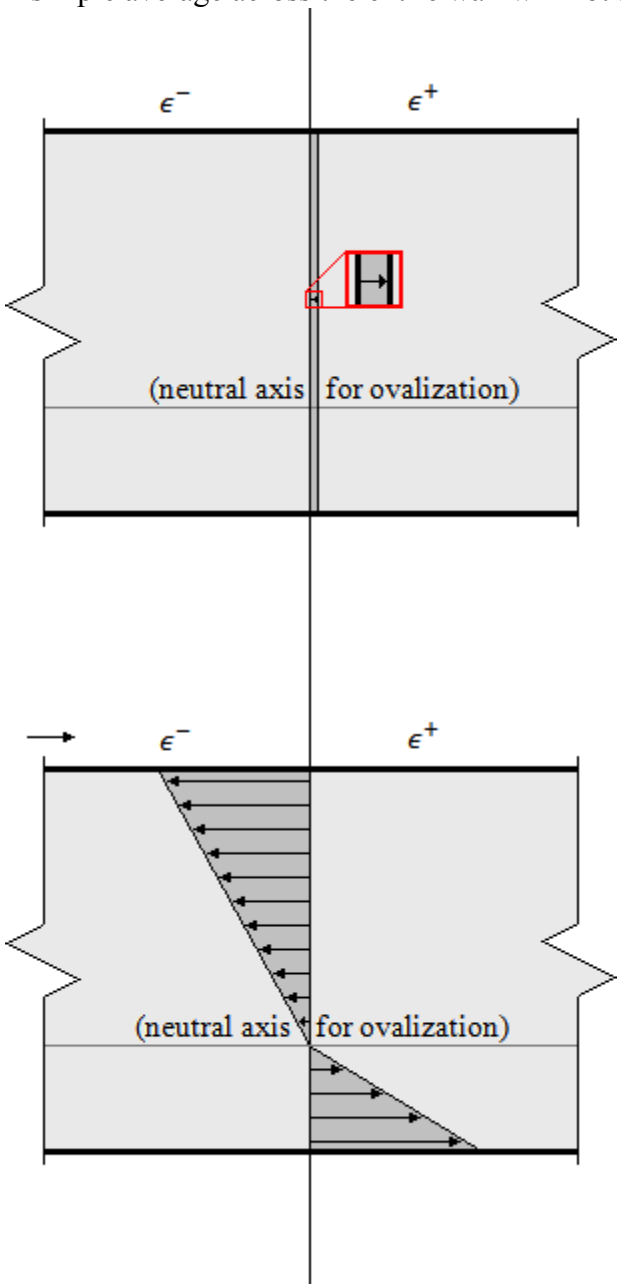

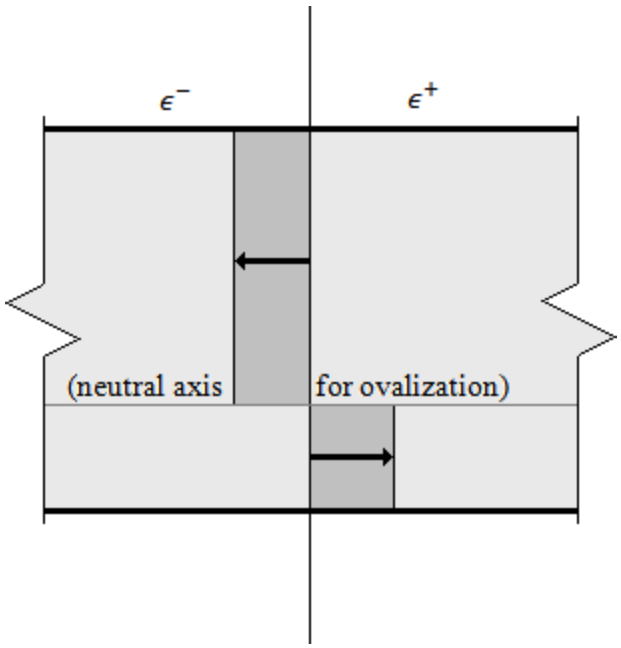
ϵ^-
ϵ^+
(neutral axis
for ovalization)

APPENDIX C: Statistical Analysis of Buckling Angles by Material

The following plots relate to Section 5.4, the linearity tests. This statistical analysis was completed for each of the different materials and dimension configurations as shown below. For each material the failure angle is plotted versus the intended bend angle first. Then these values are fitted with a best fit line. This line acts as our predicted value based on our empirical data.

The residual value for each point is then calculated based on this line using the equation

$$Residual = f(x) - f(\bar{x})$$

where $\bar{\boldsymbol{x}}$ is the expected value based on the line and $\boldsymbol{x}$ is the failure angle. These values are then plotted versus the intended bend angle. These values can show us if our curve fit line is a good fit for the data. If there is a visible curve to the residual data points, then the curve is not accounting for all the sources of variation. The range of the data should stay about the same throughout the plot. This means that there is equal variance throughout the failure angles. Finally, they should look random, ensuring the reader that there are no points that are biasing the results.

The residual plots for aluminum and EMT show some trends that would hopefully disappear with more tests. The failure angles were harder to see on the video, causing a larger error in the way they were recorded. The residual plots for copper show very good randomness, no trends, and equal variance, ensuring a good fit to the data.

The normal distribution probability plots are calculated using the residuals data. To find these points, the data is first put in order, smallest to largest, based on the residual value. These

points are then plotted versus what we would expect to see if the curve had a normal distribution. The function in Excel to see this is "normsinv(z)" where the z-value is calculated for each point ***I*** from 1 to n using the equation

$$z_i = \frac{i - .5}{n}$$

Normal probability plots show how normal the distribution of the data is around the curve fit line. If the data is normally distributed, the normal probability distribution curve will follow a straight line. The slope of this line is not important, but it will be positive. Also, it will go through the origin. The closer it follows this curve fit line, the more normal the distribution. If there is a curve to the data, then the data is either right or left-skewed.

The aluminum data looks normal based on the normal probability plot, but the EMT data looks skewed. The copper data looks like it fits the normal distribution well, and so it can be said that the data for the copper tubes is normally distributed about the expected failure angle based on the curve fit line.

Material	Residual Plot	Curve Fit Quality	Normal Probability Plot
Aluminum	Curve is visible Range changes	Poor	Has some skew, R^2=0.9095 Nearly normal probability
EMT	Curve clearly visible Range changes	Poor	Has fat tails, but otherwise nearly normal probability, R^2=0.9148
Copper ¾ M	No visible curve Fairly constant range Looks random	Good	Very near a normal distribution, R^2=0.9719
Copper ½ M	No visible curve Constant range Looks random	Great, one outlier	Normal with a few outlier R^2=0.9488
Copper ¾ L	No visible curve Fairly constant range Looks random	Good	Normal distribution R^2=0.9473
Copper ½ L	No visible curve Range is acceptable Looks random	Good	Normal distribution R^2=0.9706

A.1 Aluminum

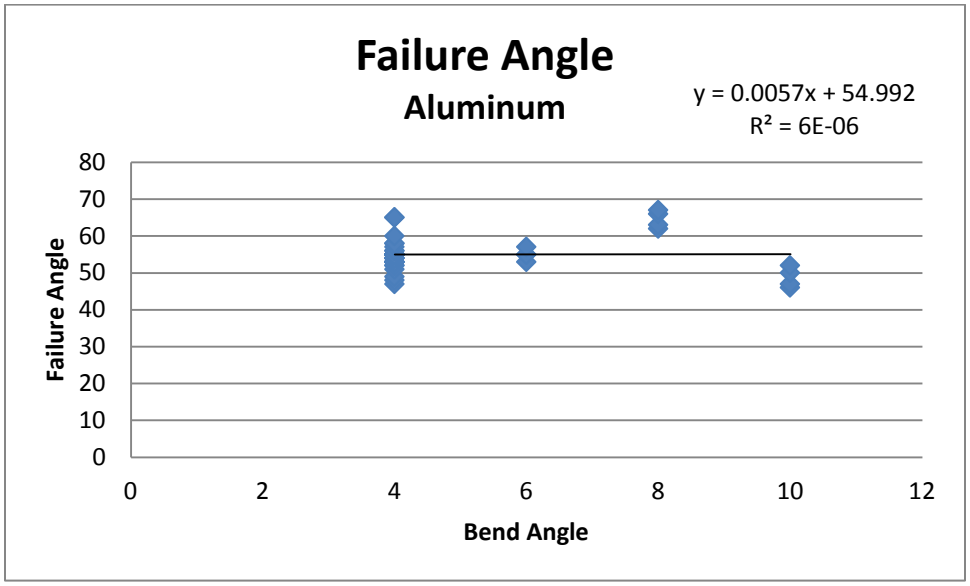
Failure Angle
Aluminum
y = 0.0057x + 54.992
R² = 6E-06
Failure Angle
Bend Angle
80
70
60
50
40
30
20
10
0
0
2
4
6
8
10
12

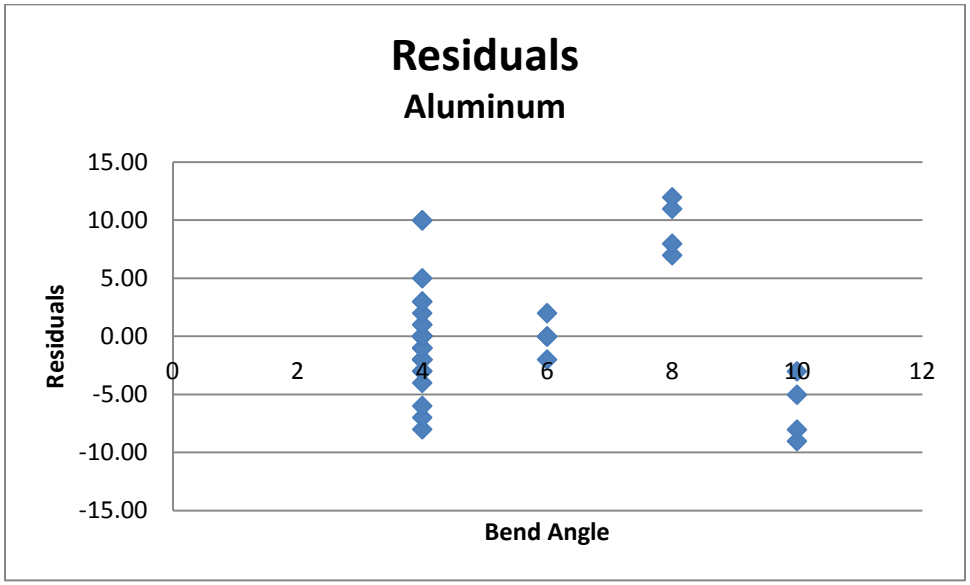
Residuals
Aluminum
Residuals
Bend Angle
15.00
10.00
5.00
0.00
-5.00
-10.00
-15.00
0
2
4
6
8
10
12

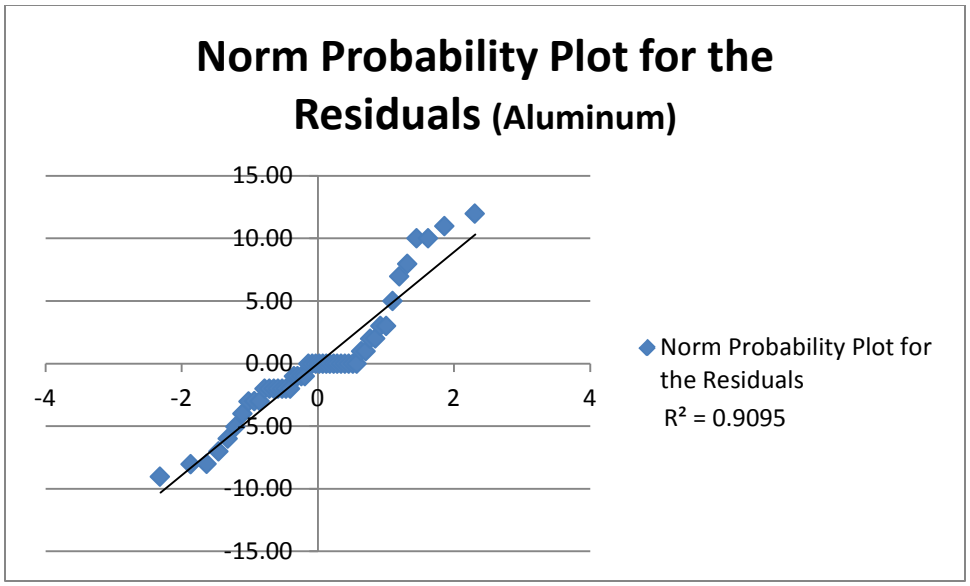
Norm Probability Plot for the Residuals (Aluminum)
15.00
10.00
5.00
0.00
-5.00
-10.00
-15.00
-4
-2
0
2
4
Norm Probability Plot for the Residuals
R² = 0.9095

A.2 EMT

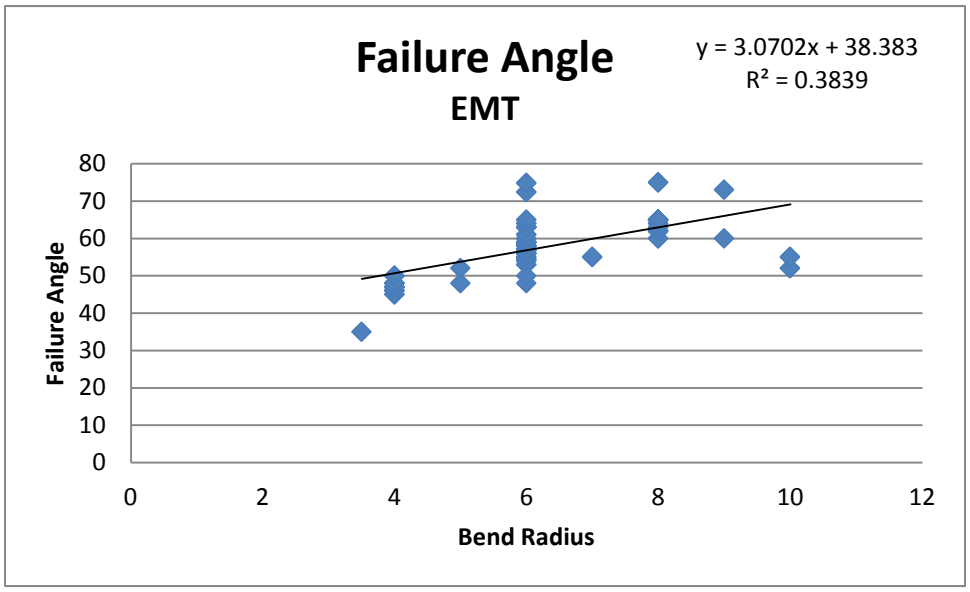
Failure Angle
EMT
y = 3.0702x + 38.383
R² = 0.3839
Failure Angle
80
70
60
50
40
30
20
10
0
0
2
4
6
8
10
12
Bend Radius

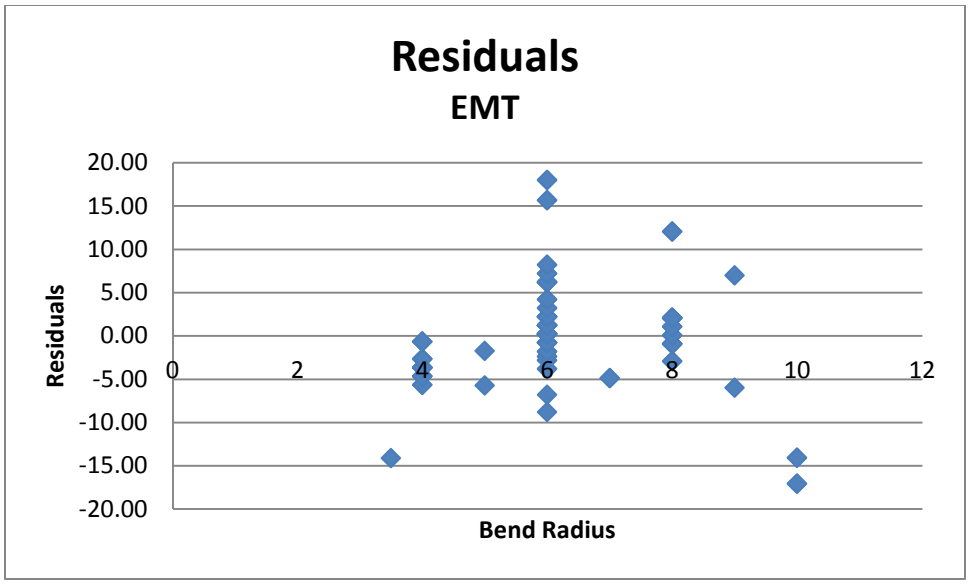
Residuals
EMT
20.00
15.00
10.00
5.00
0.00
-5.00
-10.00
-15.00
-20.00
Residuals
0
2
4
6
8
10
12
Bend Radius

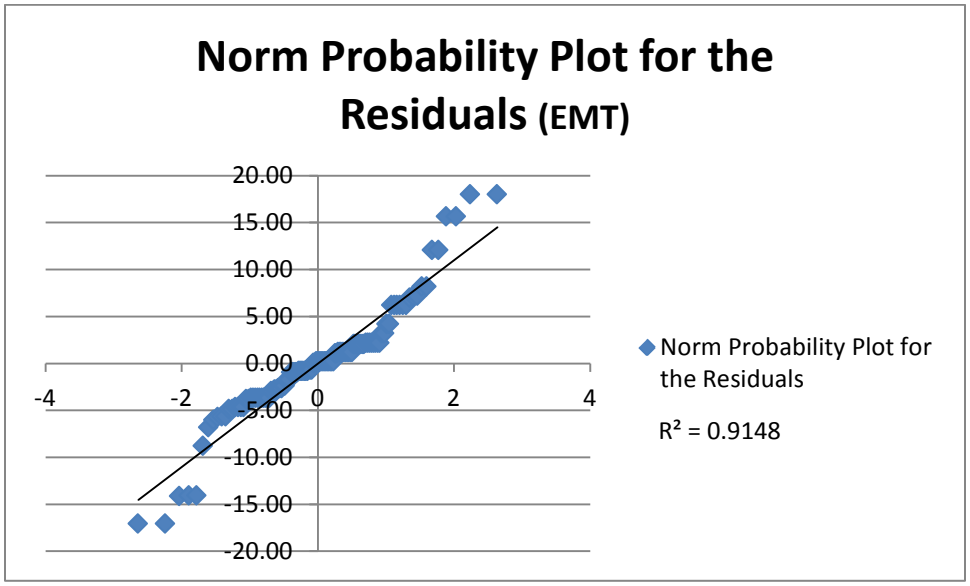
Norm Probability Plot for the Residuals (EMT)
20.00
15.00
10.00
5.00
0.00
-5.00
-10.00
-15.00
-20.00
-4
-2
0
2
4
Norm Probability Plot for the Residuals
R² = 0.9148

A.3 Copper alloy 122

A.3.1 Copper alloy 122, ¾ Type M

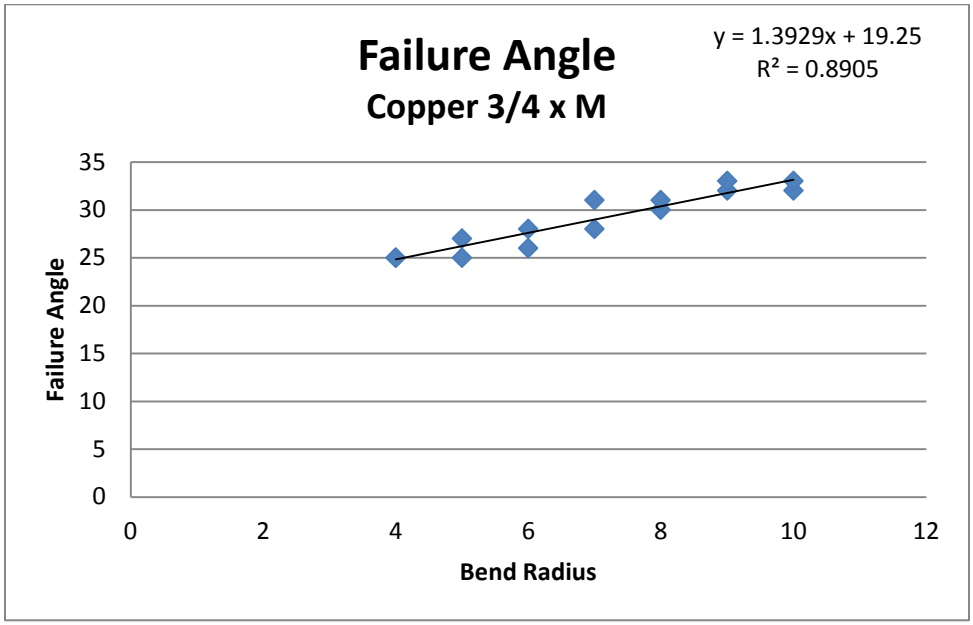

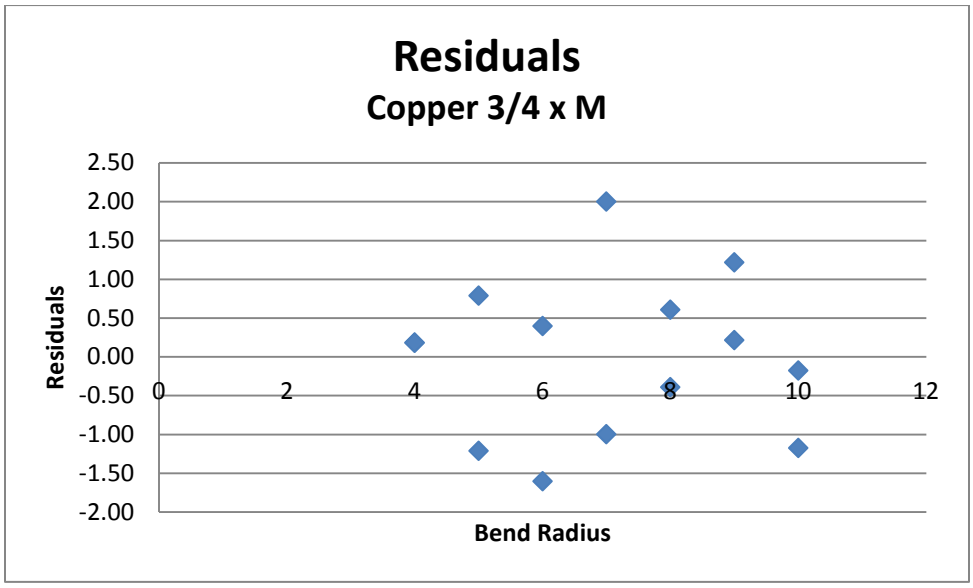

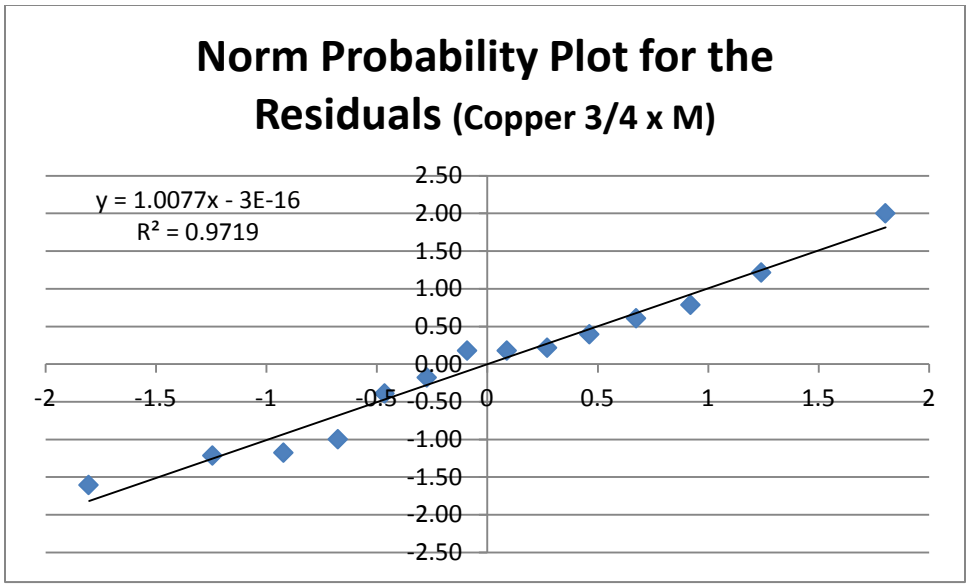

A.3.2 Copper alloy 122, ½ Type M

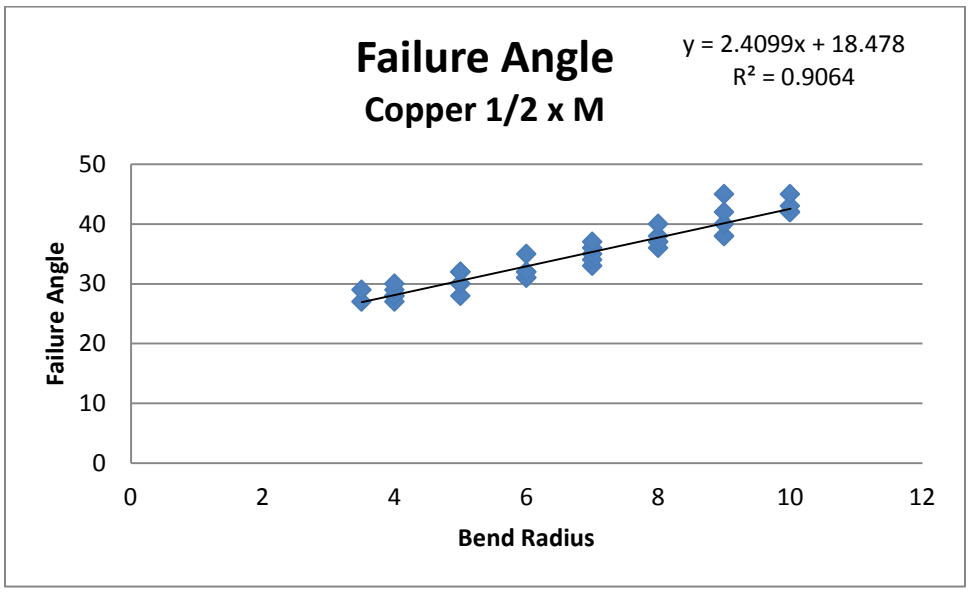

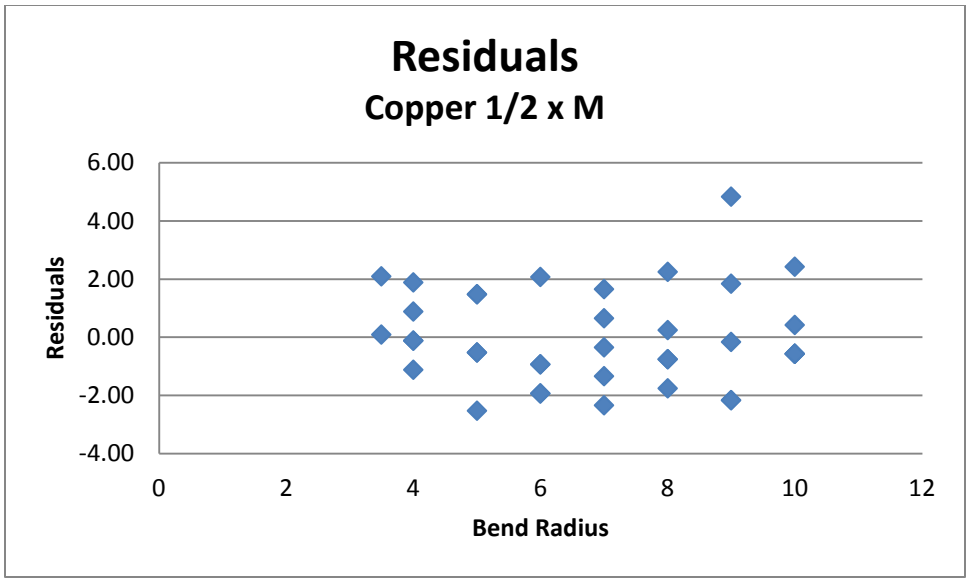
Residuals
Copper 1/2 x M
6.00
4.00
2.00
0.00
-2.00
-4.00
Residuals
0
2
4
6
8
10
12
Bend Radius

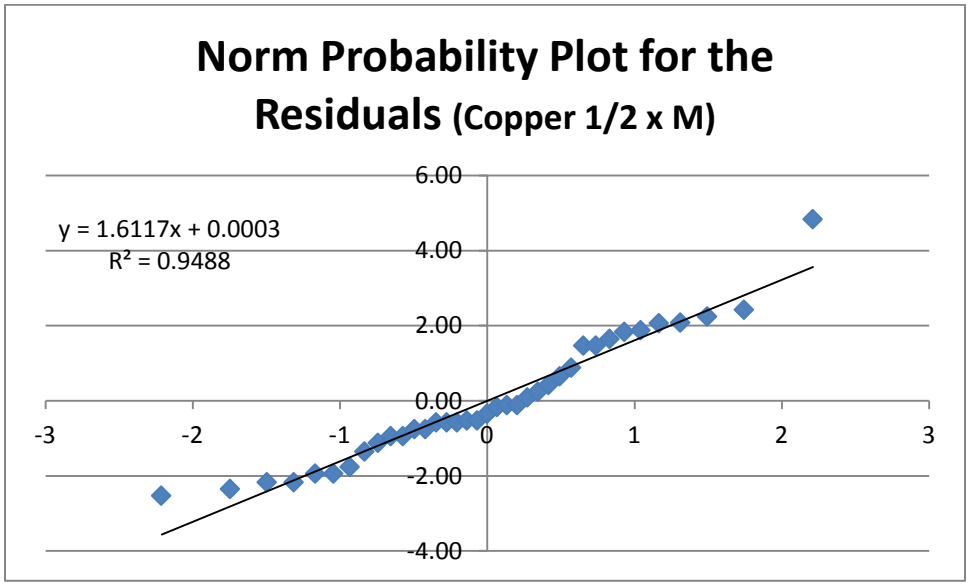
Norm Probability Plot for the Residuals (Copper 1/2 x M)
y = 1.6117x + 0.0003
R² = 0.9488
6.00
4.00
2.00
0.00
-2.00
-4.00
-3
-2
-1
0
1
2
3

A.3.3 Copper alloy 122, ¾ Type L

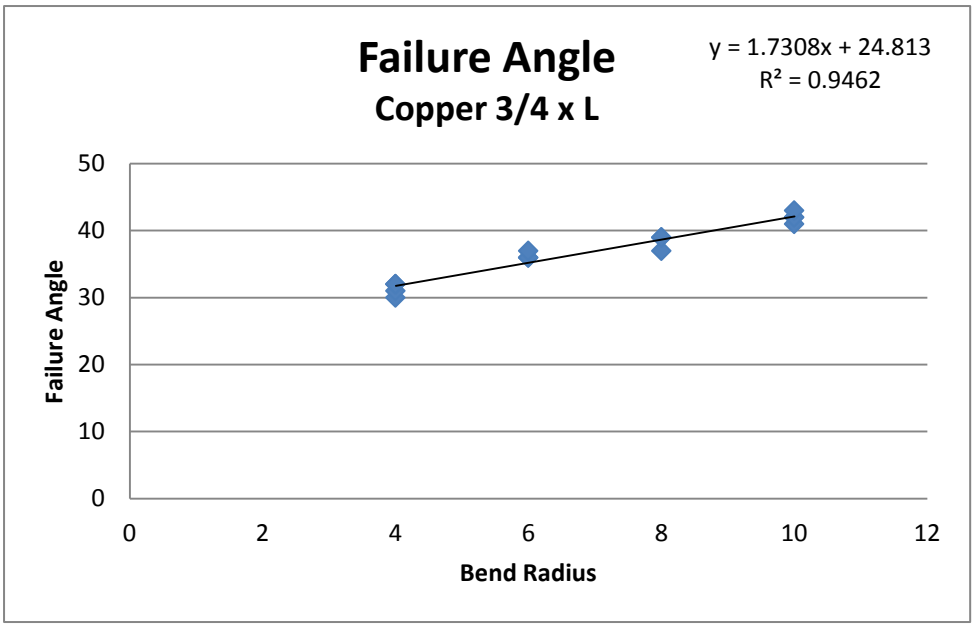

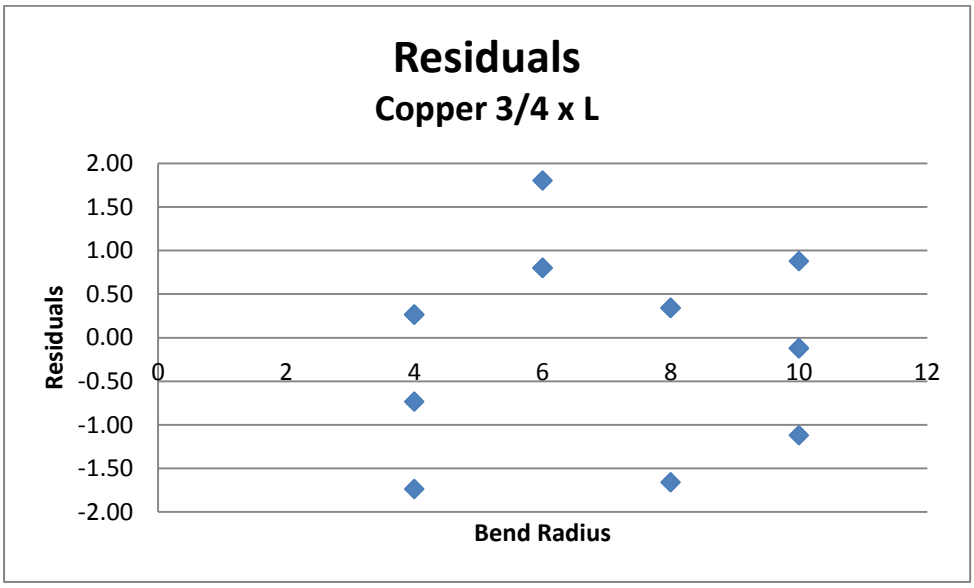

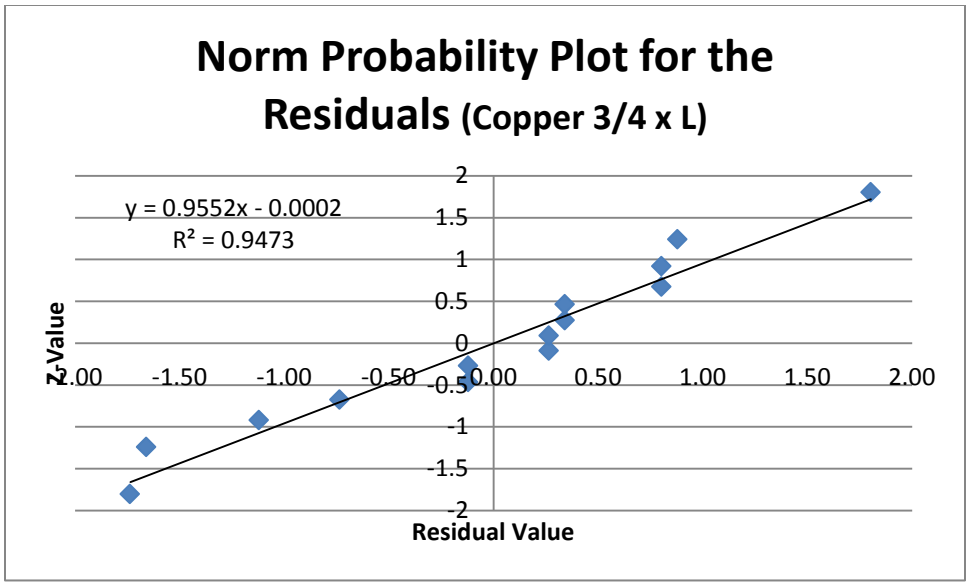

A.3.4 Copper alloy 122, ½ Type L

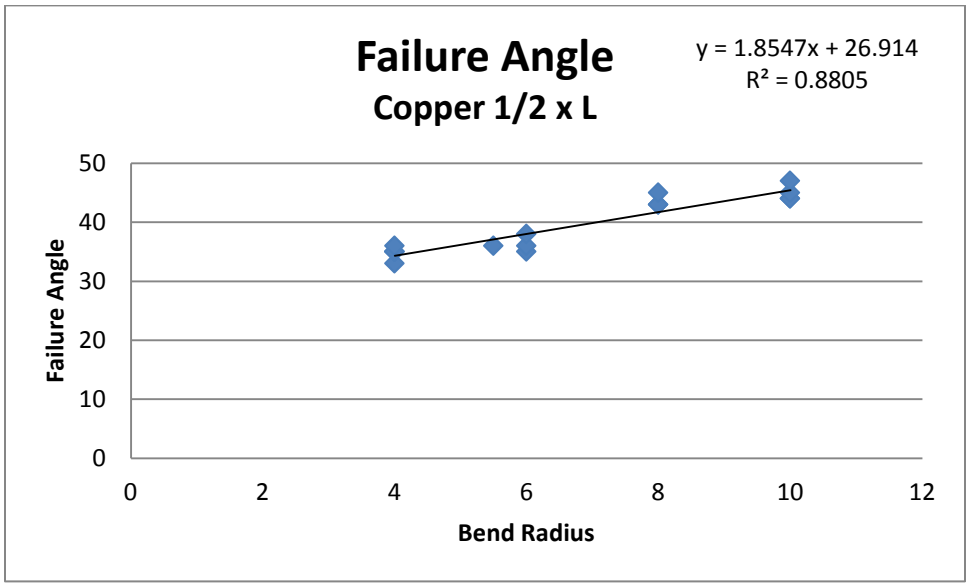

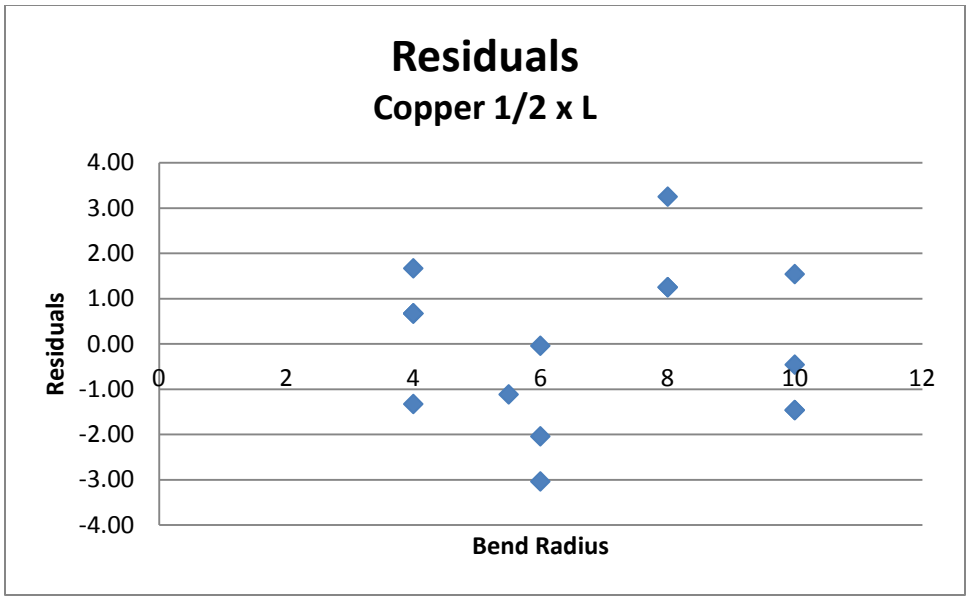
Residuals
Copper 1/2 x L
4.00
3.00
2.00
1.00
0.00
-1.00
-2.00
-3.00
-4.00
Residuals
0
2
4
6
8
10
12
Bend Radius

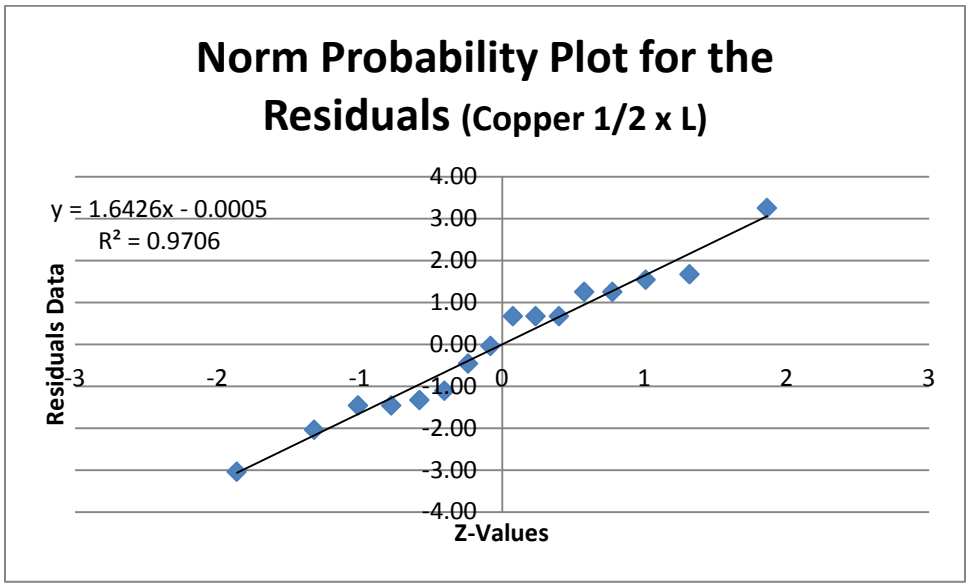
Norm Probability Plot for the Residuals (Copper 1/2 x L)
y = 1.6426x - 0.0005
R² = 0.9706
Residuals Data
4.00
3.00
2.00
1.00
0.00
-1.00
-2.00
-3.00
-4.00
-3
-2
-1
0
1
2
3
Z-Values